Elisabeth Strunz

Synthesis and modification of $CuInS_2$ nanoparticles for the application in nanocomposite solar cells

DIPLOMARBEIT

zur Erlangung des akademischen Grades einer Diplom-Ingenieurin der technischen Wissenschaften

erreicht an der

Technischen Universität Graz

Betreuer:
Assoc. Prof. DI Dr.Gregor Trimmel

Institut für Chemische Technologie von Materialien
Technische Universität Graz

2011

STATUTORY DECLARATION

I declare that I have authored this thesis independently, that I have not used other than the declared sources / resources, and that I have explicitly marked all material which has been quoted either literally or by content from the used sources.

Graz, August 16th, 2011 Elisabeth Strunz

To my family

ABSTRACT

Synthesis and modification of $CuInS_2$ nanoparticles for the application in nanocomposite solar cells

In recent years nanocomposite solar cells gained considerable high interest. This type of solar cell consists of a material combination of organic, conjugated polymers and inorganic nanoparticles, which reveals several advantages. The optical and electronic properties of the nanoparticles, which act as the acceptor phase, can be tuned by the size and shape. In addition the nanoparticles contribute to the absorption of light and higher current densities are expected compared to fullerene/polymer solar cells. Within this thesis $CuInS_2$ nanoparticles were investigated because they provide a high absorption coefficient and a band gap of 1.5 eV.

In the first chapters the main focus was set on the synthesis of $CuInS_2$ nanoparticles with a narrow size distribution and a homogeneous crystal modification. Oleylamine was used as capping agent and solvent. Various reaction conditions and their influence on the fabrication of the nanoparticles were investigated. It was found that with short reaction times (under 1 hour) favourably wurtzite as crystal modification was formed, whereas prolonged reaction times (1-5 hours) leads to chalcopyrite. The materials were characterized by transemission electron microscopy, X-ray diffraction, optical spectroscopy and dynamic light scattering.
Further the surface properties of the $CuInS_2$ nanoparticles were modified. Therefore nanoparticles underwent size-selective precipitation, acid washing treatment and capper exchange methods.

Finally the $CuInS_2$ nanoparticles were incorporated into nanocomposite solar cells. As donor material poly[[9-(1-octylnonyl)-9H-carbazole-2,7-diyl]-2,5-thiophenediyl-2,1,3-benzothiadiazole-4,7-diyl-2,5-thiophenediyl] and poly[2,1,3-benzothiadiazole-4,7-diyl-2,5-thiophenediyl(9,9-dioctyl-9H-9-silafluorene-2,7-diyl)-2,5-thiophenediyl were used. In order to optimize the performance of the solar cells various inorganic and organic concentrations, annealing steps and solvents mixture were investigated. The solar cells were characterized by I-V characteristics, profilometer measurements and optical microscopy.

KURZFASSUNG

Synthese und Modifizierung von $CuInS_2$ Nanopartikeln für den Einbau in Nanocomposit Solarzellen

Während der letzten Jahre wurde das Interesse an Nanocomposit Solarzellen immer stärker. Solarzellen dieser Art bestehen aus einer Materialkombination von organisch, leifähigen Polymeren und anorganischen Nanopartikeln, welche einige Vorteile aufweisen. Die optischen als auch die elektrischen Eigenschaften der Nanopartikel, welche als Akzeptormaterial eingesetzt werden, können durch Größe und Form dieser beeinflusst werden. Darüber hinaus tragen diese zur Absorption des Lichtes bei, wodurch eine höhere Stromdichte im Vergleich zu rein organischen Solarzellen zu erwarten ist. Im Rahmen dieser Arbeit wurde $CuInS_2$ Nanopartikeln untersucht, da dieses Material einen hohen Absorptionkoeffizienten und einen Bandgap von 1.5 eV besitzt.

Zunächst lag das Hauptaugenmerk auf der Synthese der $CuInS_2$ Nanopartikeln mit einer geringen Größenverteilung und einer einheitlichen Kristallmodifikation. Hierfür wurde Oleylamin als Capper und Lösungsmittel verwendet. Unterschiedliche Reaktionsbedingungen und deren Einfluss auf die Herstellung der Nanopartikel wurden untersucht. Die Ergebnisse zeigten, dass kürzere Reaktionszeiten vorwiegend Wurtzit als Kristallmodifikation ausbildeten, wohingegen längere Reaktionsdauern zu Chalkopyrit führten. Anschließend wurden die Partikel mittels Transmissionselektronenmikroskopie, Röntgendiffraktometrie, optischer Spektroskopie und dynamischer Lichtstreuung analysiert.
In einem weiteren Schritt wurde die Oberfläche der $CuInS_2$ Nanopartikel modifiziert. Dafür wurden diese einer größenabhängigen Fällung, einer Säure Behandlung oder einem Capper Austausch unterzogen.

Zuletzt wurden die $CuInS_2$ Nanopartikeln in Nanocomposit Solarzellen eingebaut. Als Donormaterial wurden entweder Poly[[9-(1-octylnonyl)-9H-carbazol-2,7-diyl]-2,5-thiophenediyl-2,1,3-benzothiadiazol-4,7-diyl-2,5-thiophenediyl] oder Poly[2,1,3-benzothiadiazol-4,7-diyl-2,5-thiophenediyl(9,9-dioctyl-9H-9-silafluoren-2,7-diyl)-2,5-thiophenediyl verwendet. Für die Optimierung der Solarzellen wurden zunächst verschiedene Verhältnissen von Anorganik und Organik sowie Temperaturprogramme

und Lösungsmittelgemische untersucht. Die Charakterisierung erfolgte mittels I-V Kennlinien, Profilometermessungen und optischer Mikroskopie.

ACKNOWLEDGEMENTS

I would like to thank Univ. Prof. DI Dr. Franz Stelzer, head of the Institute for Chemistry and Technology of Materials (ICTM) at Graz Technical University, and especially Assoc. DI Dr. Gregor Trimmel, who was my supervising tutor, for giving me the opportunity to write this diploma thesis. Thank you all for your help and support during my work. I am deeply grateful to you.

Furthermore I would like to thank all the members of this institute, in special the ones of the nanocomposite solar cells working group. A very special thank goes to DI Dr Andreas Pein, who was a great support and huge help during my time at the institute. I am deeply grateful for your help and the things you taught me. Moreover I want to thank Christopher Fradler for the help and the enjoyable atmosphere. Also I want to thank DI Dr Thomas Rath who helped with his experience. In addition I want to thank the girls in my working room, DI Elisabeth Ziegler and Eva Haberfellner for the good working atmosphere and a special thank goes to DI Verena Kaltenhauser, thank you for your friendship.

I also wish to thank the following persons who contributed to the content of this work:
DI Wernfried Haas, for the TEM images, DI Dr Thomas Haber, for support in questions concerning crystal modification, Josephine Hobisch for the TGA measurements, Univ. Doz. DI Dr. Franz-Andreas Mautner for the XRD measurements,

Financial support of this work was provided by the Bundesminesterium für Wirtschaft, Familie und Jugend (BMWFj) and Isovoltaic AG within the Christian Doppler Laboratory for Nanocomposite Solar Cells.

Last, and most of all, I wish to express my deepest gratitude to my parents, who were supporting me throughout my entire life in every imaginable situation. Thanks for being understanding but being motivating and encouraging at the same time. Last but for sure not least I want to thank Michael for motivating me in difficult times and just listening. This would not have been possible without any of you.

TABLE OF CONTENTS

1 Introduction

1.1 World energy demand

The world energy demand has been growing since 200 years, driven by industrialization, starting in the middle of the 18th century in Europe and North America and in the last decades spreading to Asia and South America. Additionally the increasing population and use of technology have dramatically increased energy consumption. Figure 1 shows the primary energy consumption of the world in correlation with the energy usage of each country.

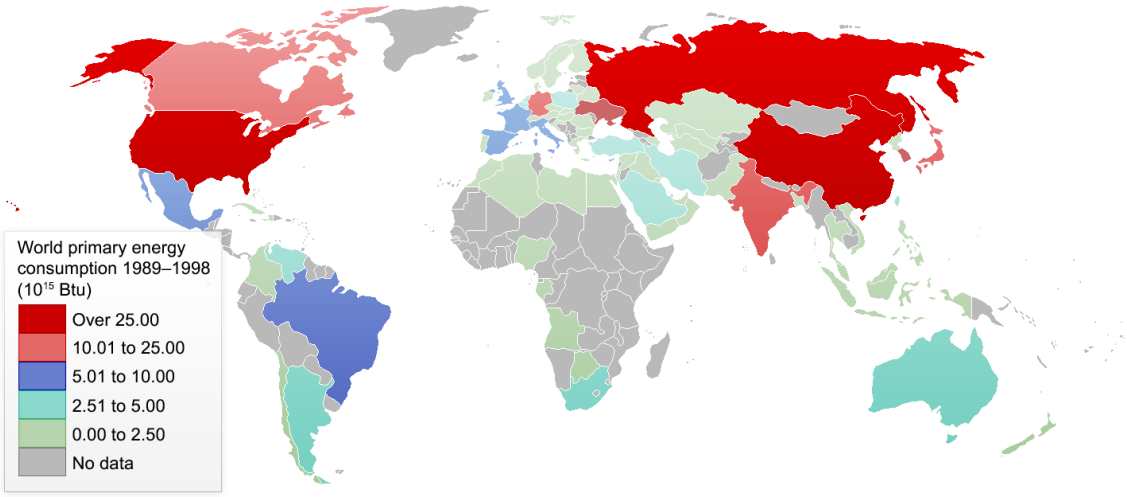

Figure 1 World primary energy consumption of the world[1]

In the last century fossil fuels, coal and natural gas were the most dominate source for energy production. Within the last few decades the awareness of renewable resources, such as wind, geothermal, rain, tidal and solar power are growing, on the account that fossil fuels will deplete during the next century. In addition to high oil prices but also concerns about environmental impacts force people and governments to think about renewable resources and support the research in this sector of energy production. The use of fossil fuels contributes to air pollution throughout the whole world. Gases like carbon dioxide have a harmful effect on the environment.

---

[1] Data of the International Energy Agency (IEA), created by User:SG(en.wiki), http://en.wikipedia.org/wiki/File:Energy-consumption-World2.png, accessed on 9th August 2011

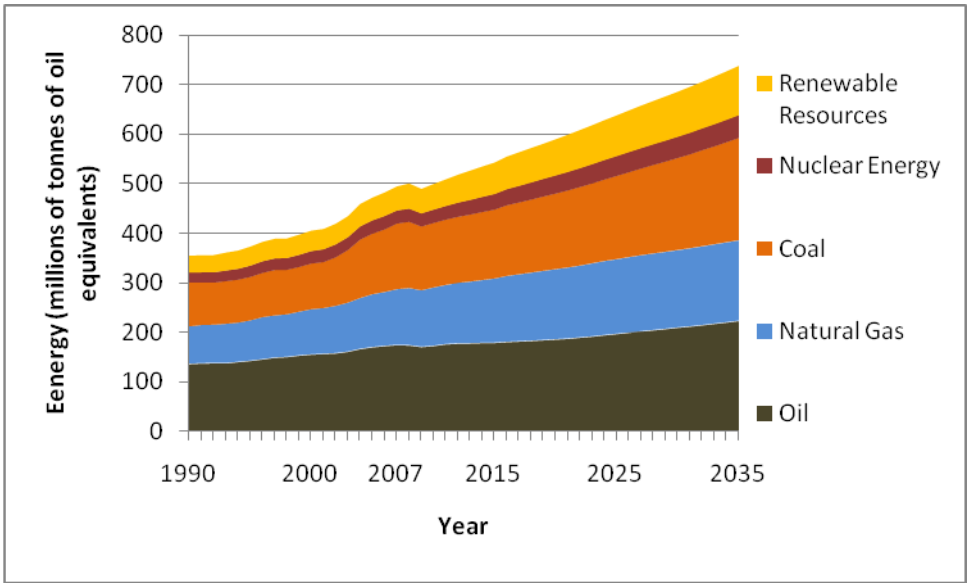

Figure 2 Energy demand and its projection for the next decades (data taken from EIA[2])

Figure 2 displays the energy demand and its projection for the next decades. According to a 2010 report by EIA[2] fossil fuel is meant to be the slowest growing source of energy with an annual rate of 0.9 percent from 2007 to 2035, whereas the energy consumption will increase by 1.4 percent. Renewable resources are the fastest growing energy source with 2.6 percent increase per year. Nonetheless most of today's energy demand is produced by fossil fuels. Only about 12% comes from renewable resources.[3]

With the increase in awareness of the need of renewable resources, it will be one of the challenges of the 21st century to cover the world's energy demand and protect the environment. Since the middle of the 20th century the interest and research of renewable resources grew.

1.2 Renewable resource: Solar energy

In an effort to address the world energy demand, which will rise up to 30 terawatts per year by 2050, sunlight offers an huge advantage, due to the fact that it is sustainable. The energy provided by the sun per year correlates to an amount of about 3*1024 joules per year, which is significantly more than the predicted energy consumption of the world by 2050.

---

[2] U.S. Energy Information Administration, "*International Energy Outlook"*, **2010**, DOE/EIA-0484

[3] http://www.eia.gov/cneaf/electricity/pub_summaries/renew_es.html, accessed 4th July 2011

Generating electricity from sunlight is one of the most promising alternatives to replace energy sources like fossil fuels or nuclear energy. The necessity for off grid power supplies together with the huge potential of photovoltaics have resulted in increasing activities during the last decades.

Since the first realization of a current generating device in 1954 at Bell laboratories[4] much effort has been devoted to a better understanding of the related photo physical processes and to enhance efficiency. Ever since the 50s, "classical" PV technology was based on inorganic semiconductors like Si or GaAs, the 1st generation, profiting from technological improvements in the semiconductor industry.

Over time different inorganic materials evolved (materials like $CuInSe_2$) leading to 2nd generation thin-film solar cells, which were market-available for some years. Enhanced absorption properties of the materials reduced device thickness from about 200 µm (crystalline silicon) to a few microns, lowering material consumption dramatically. Third generation inorganic PV-materials make use of advanced absorption concepts in intermediate-band gap semiconductors, multi-junctions as well as quantum well structures.[5] Another development of photovoltaic cells brings us to organic photovoltaic cells, which can be dated back to 1959. There as single crystals anthracene was used. But this approach did not bring enough efficiency (below 0.1%). In 1979 C.W.Tang showed the improvement of the performace of such solar cells when bringing two organic semiconductors into contact.[6] In 1986 Kodak laboratories built an all organic small molecule device with an efficiency of 1% and C.W.Tang demonstrated first the bilayer heterojunction photovoltaic cell, which was the key for the success.[7] Up till now these solar cells reached an efficiency of 7.7%.

During the last three decades much research was done on organic photovoltaics. In 1993 Sariciftci et al.[8] fabricated the first polymer/C_{60} heterojunction solar cells. 1994 Yu et al.[9] introduced the bulk heterojunction assembly. With this knowledge very thin layers could be applied on plastic layers, which made the photovolatics flexible and broadened the application for these types of devices. Although photovolatics reveal more advantages than disadvantages, more research has to be done so that the devices can compete with Si based solar cells. Today the market is dominated by Si

---

[4] Chapin, D.; Fuller, C.; Pearson, G*. J. Appl. Phys*. **1954**, 25, 676-677

[5] Conibeer, G. *Materials Today*, **2007**, 10, 42-50

[6] Tang C.W. *In US Patent* **1979**, p 4,164,431

[7] Tang, C.W. *Appl. Phys. Lett*. **1986**, 48, 183-185

[8] Sariciftci, N.S.; Braun, D.; Zhang, C.; Srdanov, V.I.; Heeger, A.J.; Stucky, G.; Wudl, F. *Applied Physics Letters* **1993**, 62, 585-587

[9] Yu, G.; Pakbaz, K.; Heeger, A.J. *Applied Physics Letters* **1994**, 64, 3422

based solar cells, because of their long term stability and high efficiencies. The disadvantage of silicon based technology is the high cost production.
In Table 1 the advantages and disadvantages of photovoltaic devices are shown. The three most substantial and crucial factors for the future of organic photovoltaic's will be the increase in efficiency and stability and further lowering in the costs of fabrication.[10]

Table 1 Advantages and disadvantages of photovoltaics[11, 12]

Advantages	**Disadvantages**
Sun currently deposits 4000x the total energy used today	Efficiency
Pollution free	Stability
Maintenance simple	Daylight, climate, weather cycle
No costs after the installation	
With further research higher efficiencies are possible	
Renewable	
Available for generations	

In recent years nanocomposite solar cells gained considerable high interest. This type of solar cell consists of a material combination of organic, conjugated polymers and inorganic nanoparticles, which reveals several advantages. The optical and electronic properties of the nanoparticles, which act as the acceptor phase, can be tuned by the size and shape. In addition the nanoparticles contribute to the absorption of light and as a consequence higher current densities are expected compared to PCBM/polymer solar cells. More detailed information can be found in chapter 2.2.

1.3 Aim of the work

The aim of this thesis is to synthesize $CuInS_2$ nanoparticles in a narrow size distribution, preferring wurtzite as crystal modification and its resulting shape for the

[10] Brabec, C.J. *Solar Energy Materials & Solar Cells* **2004**, 83, 273-292
[11] Dr. Lee, R. *Lecture: Chemistry for consumers*, CHEM-1030-003 **2010**
[12] Dr Mathis, D. *Lecture: Energy and Environment*, EST-4810-001 **2010**

nanoparticles. These nanoparticles should then be modified and optimized for the assembly in nanocomposite solar cells. This modification is focused towards the surfactant which is coordinated on the nanoparticles. The surface characteristics were changed using different approaches by ether reducing the cappers sphere or exchanging the capping agent. In a further step the nanoparticles were incorporated into the solar cells and the influence on the performance was investigated.
The following chapter deals with the basic theory of nanoparticles and their synthesis. Moreover it will be shown why $CuInS_2$ nanoparticles are suitable for the assembly in solar cells. The operating principles of a solar cell works are described. Afterwards an insight in the setup of a solar cell is given and finally the characteristic parameters are explained.

Chapter 3 obtained the results. The synthesis of $CuInS_2$ nanoparticles are characterized primarily by transmission electron microscopy and X-ray powder diffraction measurements as well as absorption and emission spectra. Afterwards the results of the modification of the nanoparticles are displayed. The solar cells are analyzed mainly by the I-V characteristics. Comparisons between the different experiments of varying parameters for the incorporation into the solar cell regarding an improvement of the performance are drawn.

Chapter 4 contains the experimental work in detail. The used materials, equipment and characteristic methods are listed. The synthesises of the $CuInS_2$ nanoparticles and the variation in the experiments are described as well as the modification procedures for the nanoparticles. Last all important facts about the variations in experiments for the fabrication of the solar cells are described.

A summary of the completed work and an outlook are written in chapter 5.

2 Theory

2.1 Nanoparticles

2.1.1 Synthesis methods

In recent years different synthesis methods to fabricate nanoparticles have been introduced, as there were for example the precipitation out of a liquid phase[13,14], hydrothermal and solvothermal methods[15,16], gas phase synthesis of semiconductor nanoparticles[17,18], colloidal solvent reaction method[19,20] or the reaction of single source precursors[21]. The interest of research in this master thesis lies in low cost routes to produce solar cell materials. Therefore, the fabrication of stable nanoparticles through solvent based routes are very attractive. The nanoparticles could be used in a broad technological field, since the dispersed nanoparticles could be applied on large areas.[22] Moreover, with a solvent based route the production is not energy intensive, due to the fact that vacuum techniques are avoided. This is another advantage when thinking of producing in an up scaling process.

During this work $CuInS_2$ nanoparticles were synthesized with a colloidal solvent reaction method. Therefore, a colloidal synthesis route using a capping agent was investigated. Using the colloidal solvent reaction method leads to well-defined and monodispersed nanoparticles. The initial point was found in the popular oleylamine

---

[13] Rossetti, R.; Ellison, J. L.; Gibson, L. M.; Brus, L. E. *J. Chem. Phys.* **1984**, 80, 4464.

[14] Baral, S.; Fojtik, A.; Weller, H.; Henglein, A. *J. Am. Chem. Soc*. **1986**, 108, 375

[15] Sheldrick, W.; Wachhold, M. *Angew.Chem.***1997**, 109, 204-234

[16] Cabanas, A.; Darr, J. A.; Lester, E.; Poliakoff, M. *J. Chem. Soc., Chem. Commun*. **2000**, 901

[17] Raab, C.; Simkó, M.; Fiedeler, U.; Nentwich, M.; Gazsó, A., *Nano trust dossiers* **2008**, 006, 1-4

[18] Kaito, C.; Fujita, K.; Shiojiri, M. *J. Crystal Growth* **1983**, 62, 375

[19] Younan X.; Yujie X.; Byongkwon L.; Skrabalak S. *Angew. Chem.* **2009**. 121, 62-108

[20] Kwon, S.; Hyeon T. *Accounts of chemical research* **2008**, 41, 12, 1696-1709

[21] Castro, S. L.; Bailey, S.G.; Banger, K. K.; Hepp, A. F. *Chem. Mater*. **2003**, 15, 3142

[22] Service, R.F. *Science* **2005**, 309, 548-551

route by Joo et al.[23], which describes the preparation of binary metal sulfide nanoparticles. It uses oleylamine and trioctylphosphine oxide (TOPO) as solvents and stabilizers and elemental sulfur as sulfur source.

2.1.2 Nucleation and growth

The formation of nanoparticles involves two main processes: nucleation and growth. In recent years the interest in nanocrystals grew, leading to an increased research effort in the field of nanoparticle synthesis. One of the difficulties in studying nucleation lies in the quantification of the size and concentration of the formed particles.[24,25] The primary crystallite size depends on the monomer concentration. Following the literature nomenclature, the term monomer is used to describe the precursors of the nanoparticles. As nucleation begins the precursors decompose or react and form a supersaturated monomer solution.[26] Hereafter more and more educts, which are still available in the solvent, are incorporated into the particle. The particles grow to a certain size at which they are stable. This size is called critical size. The higher the monomer concentration is in the solution the smaller are the nanoparticles. As soon as the concentration of the metal ions in the reaction solution gets below a certain concentration the nucleation is prevented. The growth rate passes through a maximal point which is caused by two processes. The monomer concentration decreases consequently the growth rate gets slower. Additionally a geometrical reason occurs. Considering two particles, in which one is bigger than the other, less time and less monomer concentration is needed in order to increase the size of the smaller particle provided that the same monomer flow and concentration are available. As to increase the size of the bigger particle more time and more monomer concentration is needed to obtain a bigger particle. Hence, the growth rate get slower the bigger the particle grow. When the growth rate passes through this point it comes to an increase in the critical size. At this point particles smaller than this new shifted critical size, decompose. Therefore, more monomer concentration is available. So the particles start to grow at the cost of smaller particles. As a result it comes to a broadening and therefore a more regular particle size distribution at costs of having bigger particles. The growth of

---

[23] Joo, J.; Na, H.; Yu. T.; Yu, J. H.; Kim, Y. W.; Wu, F.; Zhang, J. Z.; Hyeon, T. *J. Am. Chem.Soc.* **2003**, 125, 11100

[24] Yin, Y.; Alivisatos A. *Nature* **2005**, 437, 664

[25] Xie. R.; Li Z.; Peng X. *J. Am. Chem. Soc*. **2009**, 131, 15457-15466

[26] Cushing B.L.; Kolesnichenko V.L.; O'Connor C.J. *Chem. Rev.* **2004**, 104, 3893-3946

particles at costs of smaller particles is known as Ostwald ripening.[27,28] The most noted model of nucleation and growth of nanoparticles was described by LaMer and Dinegar.[29]

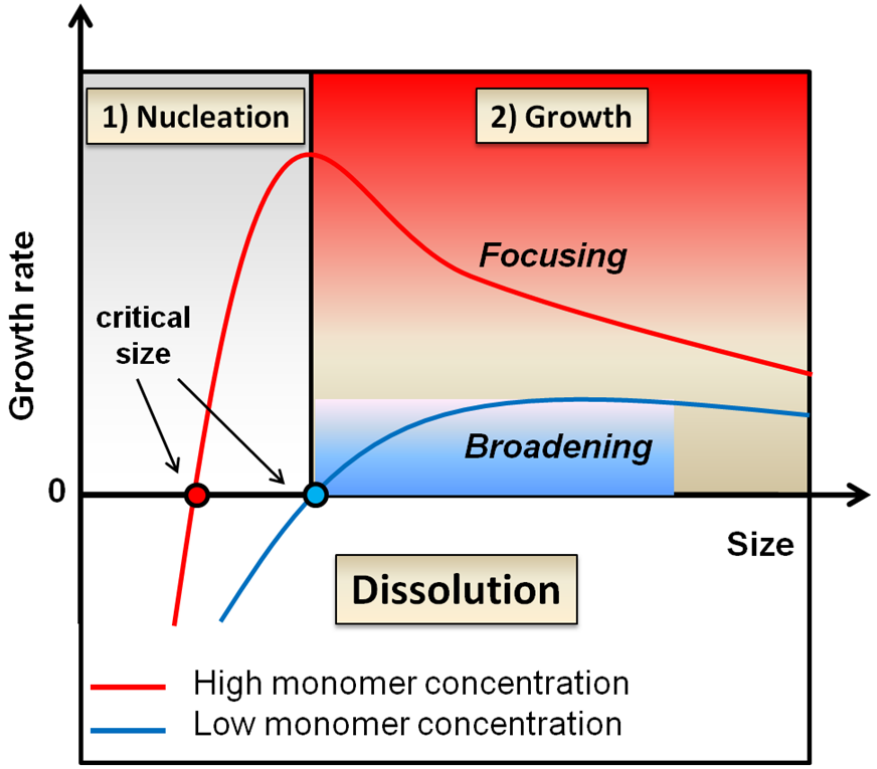

Figure 3 Nanoparticle synthesis: Nucleation and growth process [30]

2.1.3 Capper

A capping agent is one component which coordinates to the surface of the particle and also possesses another part facing opposite. In this thesis the second part is a long bulky organic tail. This organic tail is responsible for the solubility of the particles and at the same time because of the steric effect it prevents the particles of agglomeration. The capping agent is very important in this synthesis method due to the fact that it controls the nucleation as well as the particle growth and therefore the size and morphology.[24] Another advantage is that the capping agent binds to the surface of the nanoparticles and as a consequence it reduces the traps. Traps are defects on the

[27] Younan X.; Yujie X.; Byongkwon L.; Skrabalak S. *Angew. Chem*. **2009**. 121, 62-108

[28] Nose, K.; Soma, Y.;Omata,T.; Otsuka-Yao-Matsuo, S. *Chem.Mate.* **2009** ,21, 2607-2613

[29] LaMer V.K.; Dinegar R.H. *J. Am. Chem. Soc*. **1950**, 72 4847-4854

[30] Pein, A. *Dissertation: Synthesis and Characterization of Materials for Optoelectronic Devices*, **2011**

surface of the nanoparticle. Having traps on the surface of the nanoparticles mean additional energy levels, which cause the decrease of the effective band gap.

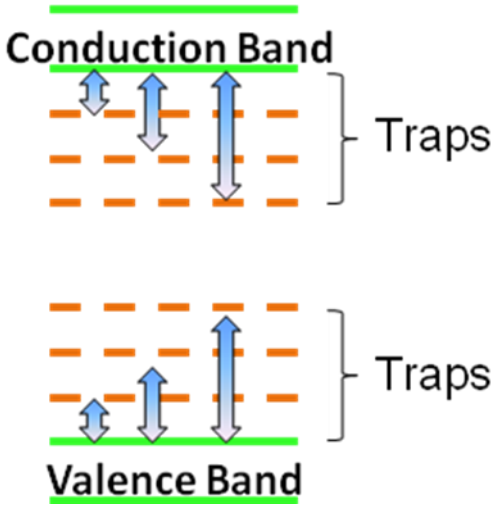

Figure 4 Energy diagram for a donor and acceptor material, showing the additional energy levels of traps on the surfaces of nanoparticles

By occupying the traps with the coordinating capping agent it principally leads to an increase of the current density and the voltage. If a capping agent with a long bulky organic tail is used, as is the case with oleylamine, the disadvantage is that it operates as an electric barrier.

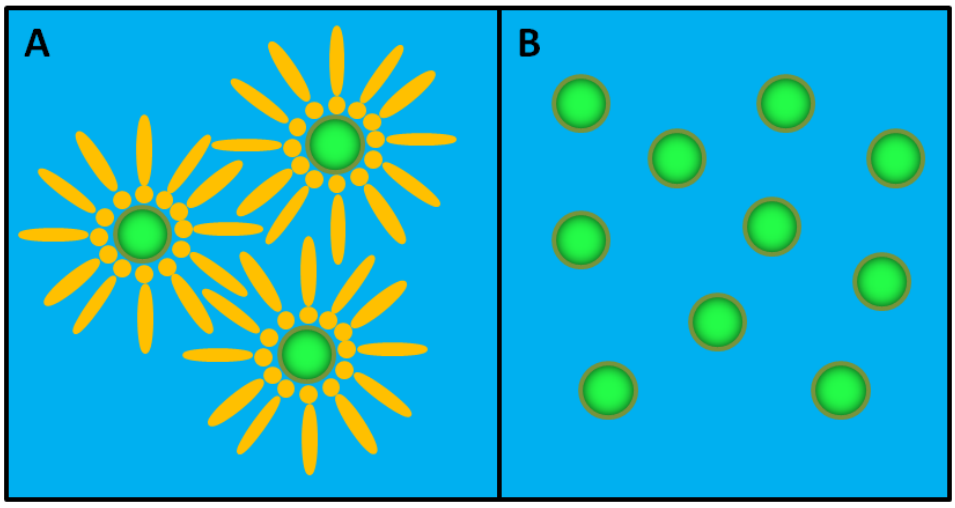

Figure 5 Schematic illustration of nanoparticles with capping agent (A) coordinating on their surface and without capping agent (B)

In Figure 5 the schematic illustration of nanoparticles with and without capping agent are displayed. Considering the fact that the capper sphere can be seen as a barrier around the nanoparticles, case a, it can be assumed that in case B the electrons could be transported easier if the capping agent would not be coordinated to the surface.

This effect and its impact on the performance of a solar cell will be shown and described in chapter 3.3.

2.1.4 $CuInS_2$ nanoparticles

Copper indium disulfide, $CuInS_2$, became an attractive alternative as an absorber material in photovoltaic cells. It is a I-III-VI_2 semiconductor, which normally crystallizes as chalcopyrite. The other interesting crystal modification is wurtzite. The chalcopyrite structure crystallizes tetragonal, where the side length A is B and not equal to C . (A=B: 5.5 Á; C= 11.1 Á; α=β=γ=90°)[31]. The density of chalcopyrite is in the range between 4.1-4.3 g/cm^3.[32] Moreover chalcopyrite has a band gap of 1.5 eV.[33,34] The wurtzite structure crystallizes in a hexagonal system and consists of tetrahedral coordinated anions and cations. Its stacking pattern is ABAB, in which it differs to the similar crystal modification of the zinc blende. The side length A equals B with a value of 3.90 Á and is different to C with a value of 6.43 Á. (α=β=90°; γ=120°) [35] It possesses a density of around 4.0-4.08 g/cm^3. [36, 37] It was reported that chalcopyrite is the thermodynamically stable phase and wurtzite is the kinetically favoured phase.[28] This can be explained by the crystal structure. Wurtzite is build out of alternating cation side and an anion side, where the cations are not strictly ordered whereas chalcopyrite consists out of a layer, where one cation is dominant, followed by an anion-layer. Therefore, chalcopyrite has a higher order in its crystal structure which needs more time to form.

---

[31] Reference data: ICSD 42127; *http://icsd.fiz-karlsruhe.de/viscalc/jsp/sliderDetailed.action*; accessed 8th July **2011**

[32] Okrusch, M.; Matthes, S. Mineralogie*: Eine Einführung in die spezielle Mineralogie, Petrologie und Lagerstättenkunde*; Springer Verlag **2005**

[33] He, Y.; Kramer, T.; Polity A.; Gregor R.; Kriegseis W.; Osterreicher I.; Hasselkamp D.; Meyer B. *Thin Solid Films* **2003**, 431, 231

[34] Tell, B., Shay, J. L., Kasper, H. M. *Physical Review B* **1971**, 4, 2463

[35] Refereence data: ICSD 163489; *http://icsd.fiz-karlsruhe.de/viscalc/jsp/sliderDetailed.action*; accessed 8th July **2011**

[36] http://www.geodz.com/deu/d/Wurtzit; accessed 7th July 2011

[37] http://webmineral.com/data/Wurtzite.shtml, accessed 7th July 2011

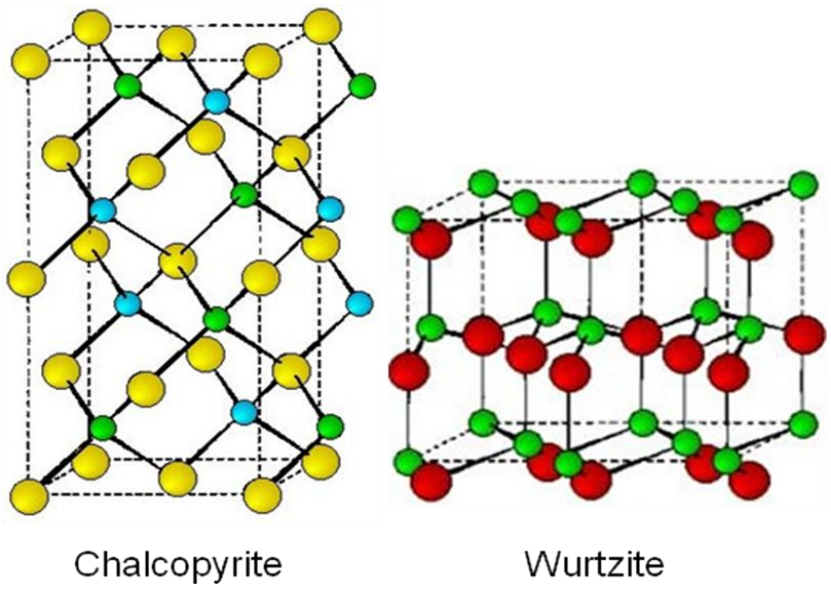

Figure 6 Crystal modification: chalcopyrite (Cu green balls, In blue balls, S yellow balls) and wurtzite (Cu and In green balls, S red balls)[38]

The favored crystal structure for the incorporation into solar cells in this work was wurtzite. In the wurtzite crystal structure there exists a lattice plane occupied by Cu and In, which are randomly distributed. Therefore, the possibility of a stoichiometric exchange of Cu and In exists. This flexibility can lead to a tuning of the Fermi energy and as a consequence to a tuning of the band gap.[39]

All in all $CuInS_2$ provides all requirements for the incorporation into a solar cell. It possesses a direct band gap of 1.5 eV, which is suitable, due to the fact that it matches with the solar spectrum. Moreover $CuInS_2$ has a high absorption coefficient ($>10^4$ cm^{-1}) and consistst of non-toxic components which are easily available. Additionally it possesses high radiation stability and a good efficiency is possible.[39] Its applicability for incorporation into solar cells was already demonstrated.[40]

[38] Barron, A. *Lecture: CHEM 360 Inorganic chemistry* **2007**

[39] Kruszynska, M.; Borchert, H.; Parisi, J.; Kolny-Olesiak, J. *J.Am.Chem.Soc*. **2010**; 132,15976-15986

[40] Nanu, M.; Schoonman, J.; Goossens, A. *Nano Lett*. **2005**,5,1761

2.2 Nanocomposite solar cells

Up until today classical silicon based technologies dominate the photovoltaic market. High efficiencies and good stability are the advantages of this technology. Nevertheless, in recent years the interest into alternatives is increasing, especially towards low-cost photovoltaic's. Nanocomposite solar cells provide the possibility of easy and cost-effective production technologies. Moreover these solar cells can be produced on plastic foils using cheap printing techniques. Another advantage of nanosomposite solar cells lies in the thickness of the device. Silicon, an indirect semiconductor, based solar cells need at least a layer thickness of 100 µm in order to absorb enough photons, whereas the thickness of the nanocomposite solar cell devices is around 200 nm or less. Disadvantages of this technology are the comparably low efficiencies and lower stability.

In general nanocomposite solar cells should exhibit a better performance than organic bulk heterojunction solar cells. In nanocomposite solar cells organic, conjugated polymers and inorganic nanoparticles are in direct contact. The high absorption coefficient as well as the optical and electronic properties of the nanoparticles, which act as the acceptor phase, contribute to the performance and as a consequence higher current densities are expected.[41]

In the synthesis of nanoparticles capping surfactants are commonly applied to prevent agglomeration. Non conductive surfactants, such as oleylamine, are coordinated to the surface and with its long alkyl chain it reduces the performance of the solar cell.[42] Therefore the chemical modification of the surface of nanoparticles is proven to be important, as soon as nonconductive surfactants are bond to the surface of the nanoparticle[43].

2.2.1 Functional principles in nanocomposite solar cells

Nanocomposite solar cells are mainly build in two different assemblies: first the bulk heterojunction assembly, described in the next chapter and second the bilayer heterojunction assembly. The difference is that within the bulk heterojunction assembly the donor and acceptor material is mingled in the photoactive layer and builds one

[41] Yu, W.; Qu, L.; Gui, W; Peng, X. *Chem. Mater*. **2003**, 15, 2854-2860

[42] http://www.lookchem.com/oleylamine/, accessed on 30th of June 2011

[43] Owen, J.; Park, J.; Trudeau, P.; Alivisatos, A. *J. Am. Chem. Soc*. **2008**,130, 12279-12281

layer in contrast to the bilayer heterojunction assembly where the donor and acceptor material are applied as one thin film upon the other and consists of two layers.

The conversion of solar radiation into direct current electricity, which happens in a nanocomposite solar cell, involves several fundamental steps. In Figure 7 the principal processes of a nanocomposite solar cell are displayed. Here the fundamental processes are separated in 4 main parts.

The process starts with the absorption of light which creates an exciton in the photoactive layer (Step 1 in Figure 7). An excition is defined as electron-hole pairs, which are bond through electrostatic interactions. In order to create an exciton, an incoming photon needs at least the energy of the band gap of the absorbing material, so that an electron gets excited from the highest occupied molecule orbital (HOMO) to the lowest unoccupied molecule orbital (LUMO). One advantage of nanocomposite solar cells is that the process can occur in the donor as well as in the acceptor phase. As a consequence the materials can be chosen in a way so that the wide range of the solar spectrum is covered.

Next the generated exciton diffuses towards the donor/acceptor interface. Two main events can happen during the exciton diffusion: either the exciton reaches the donor/acceptor interface and charge separation takes place or the exciton recombines. Excitons have a limited life time due to radiative or non radiative decays. As a consequence excitons can only diffuse a certain distance before they recombine again. Normally the distance an exciton can diffuse are in a range of a few nanometers up to 10 nanometers, which is depending mostly on the nature of the polymer. This fact already shows the advantages of the bulk heterojunction assembly due to the enlarged donor/acceptor interface (Figure 8). However, the bulk hetero-junction concept does not entirely create continuous pathways throughout the materials to the electrodes, which is necessary for electron transport. Therefore recombination can take place.

If the exciton reaches the donor/acceptor interface, charge separation happens (step 3 in Figure 7). The exciton dissociation takes place due to the energetically different LUMO levels of the donor and acceptor material. While the electron transfer from the LUMO of the donor to the LUMO of the acceptor, the hole stays in the HOMO of the donor material. The charge separation is promoted by an enlarged contact area, which is also given when using nanoparticles as acceptor material, out of the reason that their surface to volume ratio is rather high. (Figure 8)

The last process of converting photons to photocurrent involves the charge transport to the corresponding electrodes. The electric field caused by the use of two different electrodes with different work functions is the reason for the transport to the electrodes. The transport of the charges can only occur if continuous pathways are available. As a

result it can be noticed that charges generated on an isolated part with no access to the electrode cannot contribute to the resulting photocurrent density.

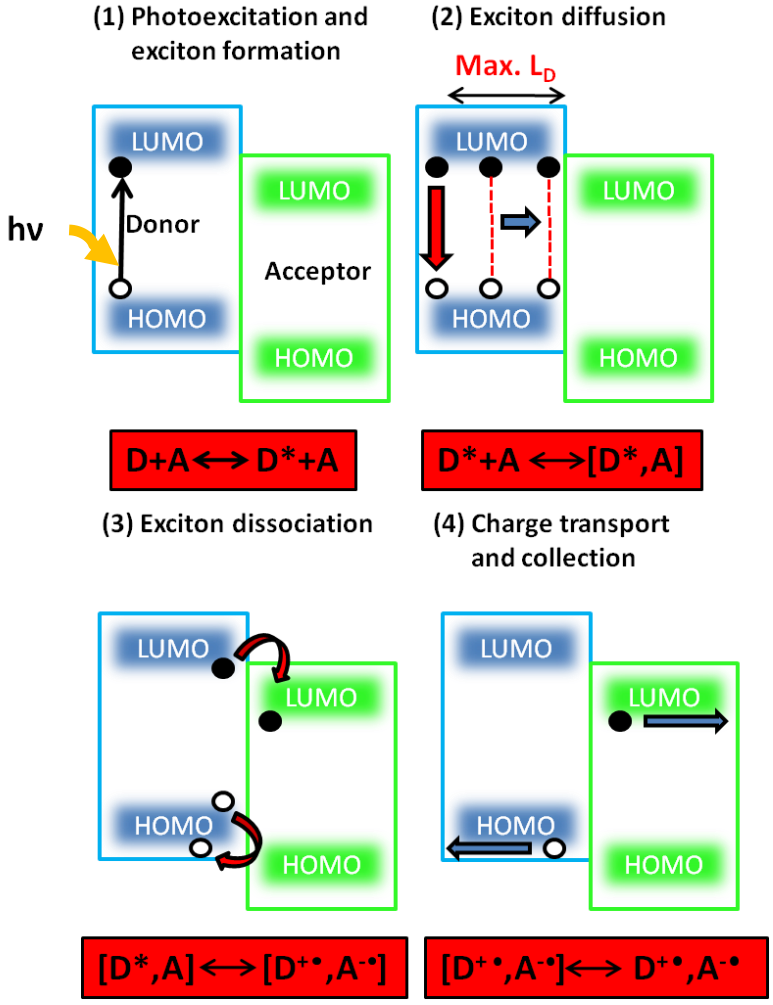

Figure 7 Functional principles in a nanocomposite solar cell (D stands for donor material, A stands for acceptor material)[30]

2.2.2 Bulk hetero-junction assembly

The acceptor/donor interface plays a major part for the efficiency of a solar cell. An enlarged contact area between the two materials is favourable. This can be provided by a bulk hetero junction assembly. With a homogeneous mixing of the inorganic and organic substances more interaction between the materials can be realized compared to bilayer hetero junction assemblies. In order to increase the donor/acceptor interface different strategies were investigated, for instance the incorporation of nanoparticles into the active layer. This can improve the efficiency. As stated before the diffusion of the excitions is limited, as a consequence the size of the nanoparticles can contribute to the performance of the solar cell. If a nanoparticle is just a few nanometers in size, the possibility of charge separation is higher due to the reduced distance to the contact

area of the polymer. As described in chapter 2.1.3, nanoparticles are surrounded by a stabilizing capper sphere, which prevents the particles for agglomeration. Thus it is an indication that the nanoparticles are not in direct contact with each other. However, the capper sphere is only one to a few nanometers thick and in due consideration of the tunnel probability, electrons can tunnel through this layer.

Based on strategies to increase the overall performance of a solar cell, another possibility to reach a continuous conductive pathway of electrons throughout the photoactive layer is to fabricate even thinner films. The disadvantage is that the thinner a layer is the less absorbing material is available in which excitions can be generated. An optimal thickness of the photoactive layers is in the range between 100-225 nm.[67]

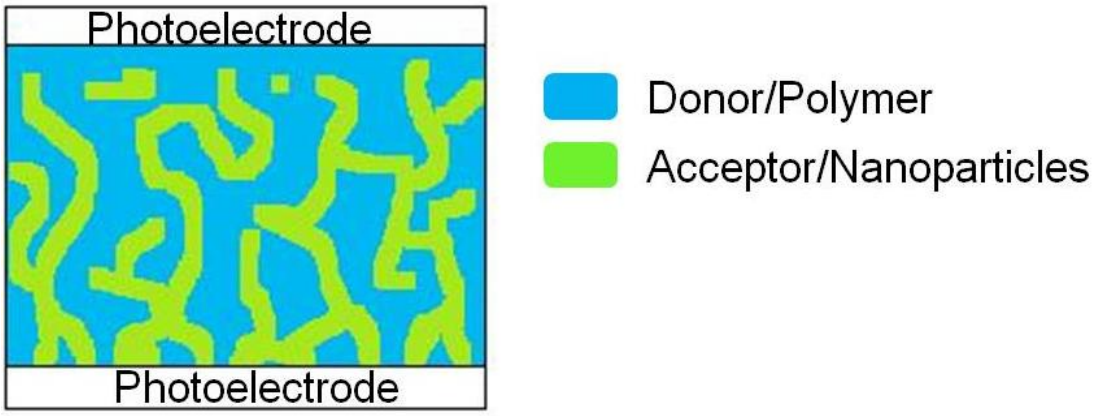

Figure 8 Schematical illustration of a bulk hetero-junction assembly

2.2.3 Characteristic Parameters

The performance of a solar cell is mainly described by its I-V characteristic. This curve is measured both in dark and illuminated conditions. The most important paramteres, which can be figured out in the I-V characteristics, are the open circuit voltage (V_{oc}, [V]), the short circuit current ($I_{sc,}$ [mA/cm^2]), the fill factor (FF, [%]) and the efficiency (PCE, [%]). All these parameters and the corresponding curve of an I-V characteristic are displayed in Figure 9.

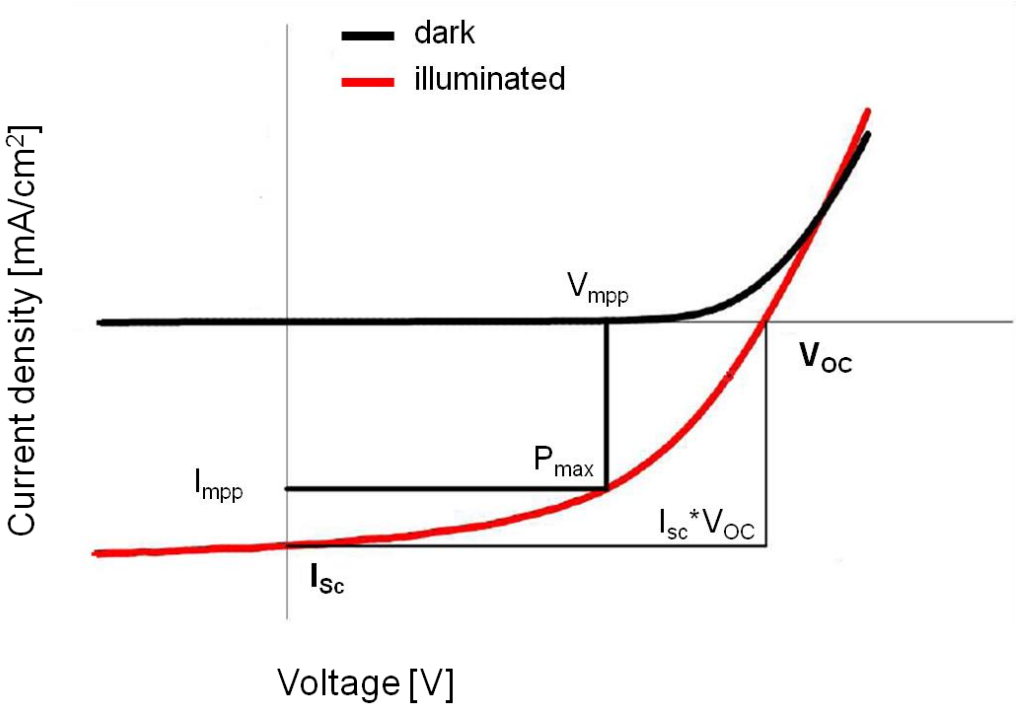

Figure 9 I-V characteristic of a solar cell, dark condition (black line), illuminated condition (red line)

The value at a current density of zero is the V_{oc}. It can be figured out at the interception point of the x-axis and the curve. The V_{oc} is mainly depending on the difference of the energy between the HOMO level of the donor material and the LUMO level of the acceptor material. It is also called and will be referred as “effective band gap”.

The value for the I_{sc} is at zero voltage. Therefore the value can be read out of the I-V characteristic on the y-axis at the interception point with the curve. The I_{sc} is depending on the number of absorbed photons and the absorbing properties of the materials including the band gap, the efficiency of the charge separation, the charge transportation through the material, the interface between active layer and the electrode and the morphology of the active layer.

A solar cell can be generally operated between V=0 and $V=V_{oc}$. Its corresponding current values are $I=I_{sc}$ and I=0. In Figure 9 the parameter P_{max} is shown. P_{max} stands for maximal power point. The electric power is defined as the product of voltage and current. If the corresponding current and voltage values are multiplied, one value will lead to a maximum, which is the maximal power point with V_{mmp} and I_{mmp} as its correlating values on the x and y axis. The maximal power point is important due to the fact that per definition the power output of a solar cell is the power at the maximum power point under an illumination of 100 mW/cm^2 and a temperature of 25 °C. It should be obvious that P_{max} aims to be as high as possible, which would be a perfect rectangle. Hence, the fill factor is an important parameter, because it describes the

relation between the ideal and the real power output. The fill factor is a characteristic factor for the degree of efficiency of the solar cells and is influenced by the cells serial and shunt resistance.[44]

$$FF = \frac{I_{mpp} * V_{mpp}}{I_{sc} * V_{oc}} \quad \textbf{(1)}$$

Another important parameter to describe a solar cell is the power conversion efficiency (η_e), which shows the relation between the maximal power point (P_{max}) and the incident light power (P_{in}).

$$\eta_e = \frac{P_{\max}}{P_{in}} * 100\% = \frac{V_{oc} * I_{sc} * FF}{P_{in}} * 100\% \quad \textbf{(2)}$$

The last parameter mentioned in this work, which describes the performance of a solar cell, is the external quantum efficiency (EQE) or incident photon to current efficiency (IPCE). It describes the ratio of the external current to the incident photons. This parameter can be obtained through experiments and is defined in two ways as followed:

$$EQE(IPCE) = \frac{1240 * I_{sc}}{\lambda * P_{in}} * 100\% = \eta_A \eta_{diff} \eta_{diss} \eta_{tr} \eta_{cc} \quad \textbf{(3)}$$

η_A…photon absorption efficiency
η_{diff}...exciton diffisuion yield
η_{diss}…exciton dissociation yield
$\eta_{tr.}$...charge carrier transport yield
η_{cc}…charge carrier yield

These are the most important parameters to describe the performance of a solar cell.

.

[44] Nunz,i J.-M. *C R. Physique* **2002**, 3, 523-542

3 Results and discussion

3.1 $CuInS_2$ nanoparticles

The basis for this investigation is found in the oleylamine route published for binary metal sulphide nanoparticles by Joo et al.,[23] describing the synthesis of ZnS, CdS and MnS nanocrystals in oleylamine as a solvent. This method was recently applied for the production of $CuInS_2$ nanoparticles. [45,46]

In this study, the reaction conditions, such as the reaction time frame and the reaction atmosphere, were varied as well as the sulfur source and the purity of the solvent/capping agent. Those variances were investigated on the account of having a major influence on the crystal phase and growth of the nanoparticles.
For the synthesis of $CuInS_2$ nanoparticles a modified synthesis route was used based on the methods described by Joo et al. and Panthani et al.[45] for the reaction conditions. CuI and $InCl_3$ were dissolved in oleylamine, which functioned as a solvent and as a capping agent. The metal salt solution was heated to 170 °C until all the salts were dissolved. The sulfur source was prepared separately by dissolving in oleylamine. The solutions were combined and heated to 220 °C and samples were taken after several stages during the reaction. The nanoparticles were separated by precipitation in methanol. The experimental information is described in detail in chapter 4.

3.1.1 Influence of inert gas and prolonged reaction time

In this experiment (V1) the effect of atmospheric oxygen on the reaction solution was investigated. Therefore the capping agent, which functions additionally as solvent, was degassed. The degasification of the solvent/capping agent should prevent two possible effects: first the oxidation of Cu^{1+} to Cu^{2+}. If Cu^{2+} is incorporated into the crystal lattice, it is possible that changes within the crystal lattice can occur. The stoichiometry of particle composition can be influenced. For example more sulfur could be incorporated

[45] Panthani, M.; Akhavan, V.; Goodfellow, B.; Schmidtke, J.; Dunn, L.; Dodabalapur, A.; Barbara, P..; Korgel, B. *J. Am. Chem. Soc*. **2008**, 130, 16770
[46] Kwon, S.; Hyeon T. *Accounts of chemical research* **2008**, 41, 12, 1696-1709

into the crystal lattice or the formation of CuS is possible. Furthermore vacancies of indium within the crystal lattice are possible. A second effect could be a concurrent incorporation of oxygen instead of sulfur. Nevertheless many other effects can have an impact on the growth of nanoparticles.

In order to investigate the influence of inert gas conditions while synthesising the nanoparticles, two separate batches were prepared. One batch was performed under strict inert gas condition (IG) with using the degassed oleylamine. The other batch was performed under atmospheric conditions (AC) and samples were taken after 5, 15 and 40 minutes.

This experiment was repeated (V2), nevertheless some changes were introduced. Due to the results of the first experiment, this time the oleylamine was not degassed for the batch under atmospheric conditions, which should result in a slightly higher oxygen concentration. Samples were taken after 60, 180 and 300 minutes.

At last one more experiment (V3) was done using degassed oleylamine and working under inert gas conditions but taking more samples at intermediate reaction times. Samples were taken after 60, 90, 120, 150 and 180 minutes.

Table 2 Overview of the experiments (V1-3), prepared under inert gas conditions (IG) or atmospheric conditions (AC) with different reaction times in minutes (digits)

V1		V2		V3
IG-5	AC-5	IG-60	AC-60	IG-60
IG-15	AC-15	IG-180	AC-180	IG-90
IG-40	AC-40	IG-300	AC-300	IG-120
				IG-150
				IG-180

TEM/XRD results of experiment V1

The results of the particles obtained in experiment V1 are discussed first. Considering the TEM images, shown in Figure 10, one can see that in both sets of experiments particles of defined shape were formed and only slight differences can be observed between the batches prepared under inert gas or atmospheric conditions. An explanation could be that for both batches degassed oleylamine was used. Therefore it is possible that not enough oxygen was available to have a major influence on the experiment. Still other reasons can have their impact on that observation. It may be attributable to the heating ramp of the metal precursors.[28] Compared to results of

earlier works done before in the workgroup[30], in the study at hand it took longer to reach the final end temperature, due to a higher amount of reactants.

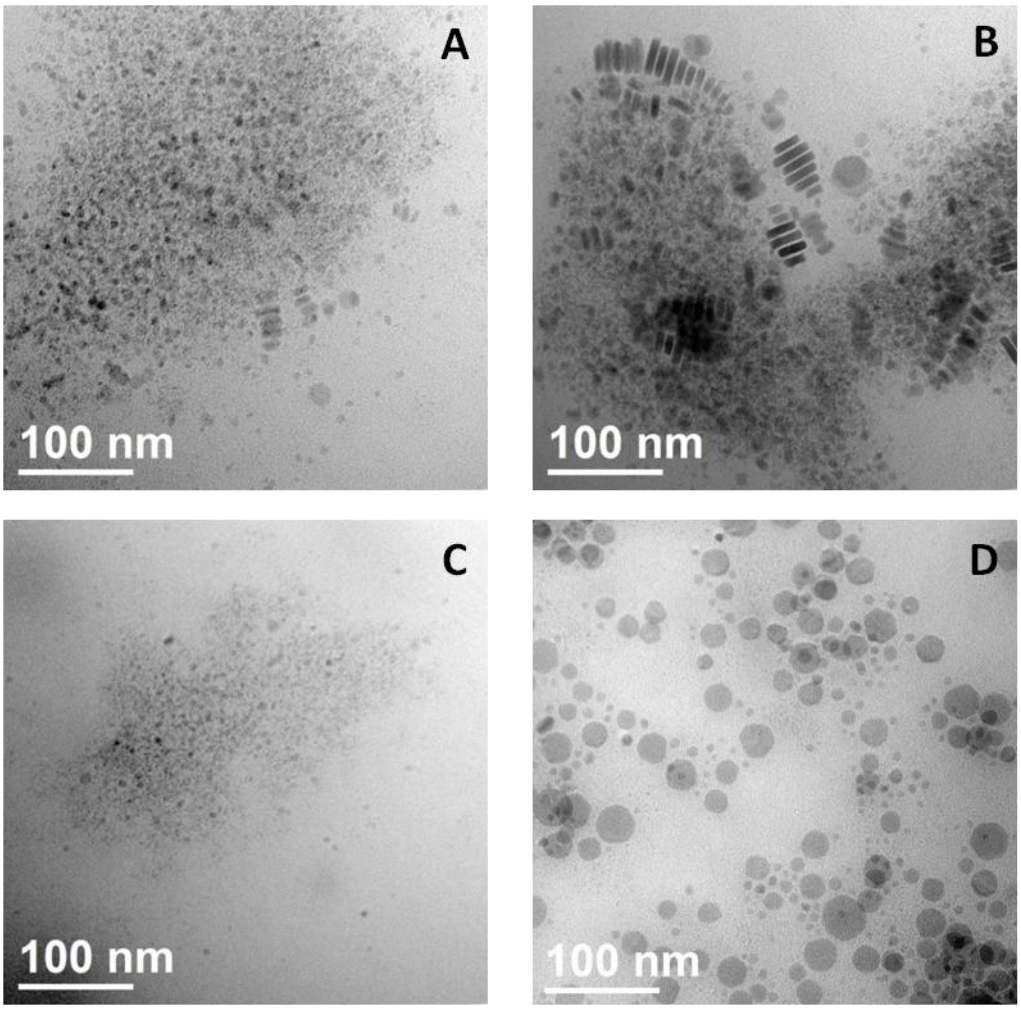

Figure 10 TEM images of samples from V1, $CuInS_2$ nanoparticles synthesized under inert gas condition after 15 minutes (A) and after 40 minutes (B), particles synthesized under atmospheric condition after 15 minutes (C) and after 40 minutes (D)

The particles displayed in Figure 10 are taken after 15 and 40 minutes out of the two batches. The sizes of the nanoparticles can be measured from the TEM image, but one has to remember that the image shows only an extract of the overall particles. A crystal size of 4-5 nm was read out for the particles obtained after 15 minutes under inert gas conditions. As can be seen in Figure 10 some particles have the shape of rods, which will be discussed in the next paragraph. The rods posses a lenght of 15-20 nm and a thickness of 8 nm. The bulk nanoparticles have a size between 1-4 nm. After 40 minutes the particles under inert gas condition reach a size of 5-10 nm. The bulk nanoparticles have a size under 5 nm. The discs have a diameter of 20-35 nm and a thickness of 8 nm after 40 minutes. The particles obtained after 15 minutes under

atmospheric condition reach a size of 2-4 nm. After 40 minutes there are particles with a size between 5-7 nm in the sample as well as hexagonal discs with a diameter of 8-33 nm. The particles under inert gas conditions reveal already bigger particles after 15 minutes, which is supposedly attributable to the absence of oxygen. It is assumed that the oxygen cannot interfere with the reaction and therefore no counter reactions, such as for instance the oxidation of Cu^{1+} or an assembly of oxygen, can occur. In order to get proof for this assumption, analytical investigations could be done to see the assembly of oxygen into the crystal lattice.

In order to prove that those particles, which reveal a shape of rods in the TEM image, are hexagonal discs, the TEM image was turned 20°. In Figure 11 it can be seen that the discs are overlapping and not only stabled next to each other. Therefore the rods are attributable to hexagonal edged on discs. Hexagonal discs indicate wurtzite.

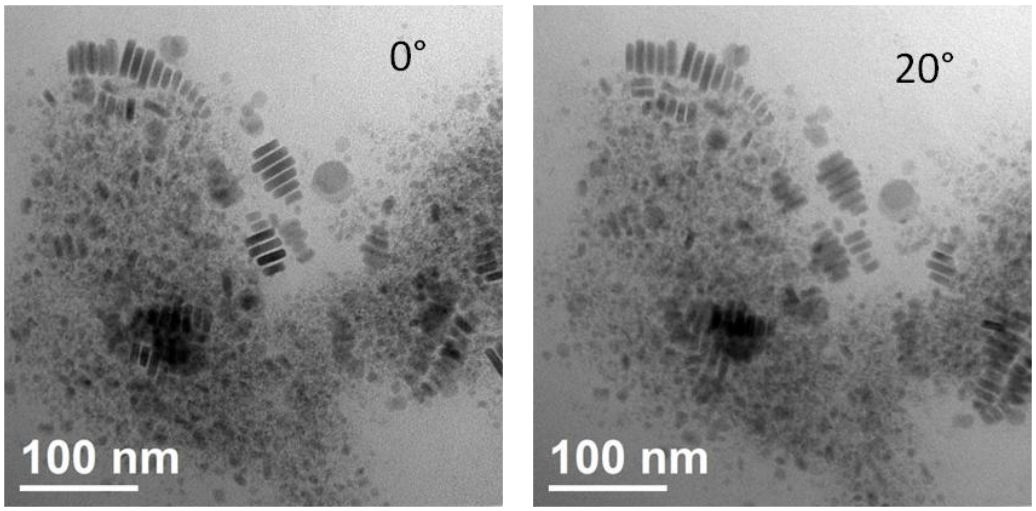

Figure 11 TEM image of sample V1 IG-40, taken at an angle of 0° and 20°

The hexagons are assigned to wurtzite, which is the kinetically favoured crystal modification.

The XRD results of the nanoparticles of experiment V1 are discussed in the next paragraphs. The corresponding XRD patterns are compared with the reference data for $CuInS_2$ of chalcopyrite (ICSD 42127) and wurtzite (ICSD 163489) in Figure 12. The most prominent reflections of chalcopyrite and wurtzite are depicted in the following figure.

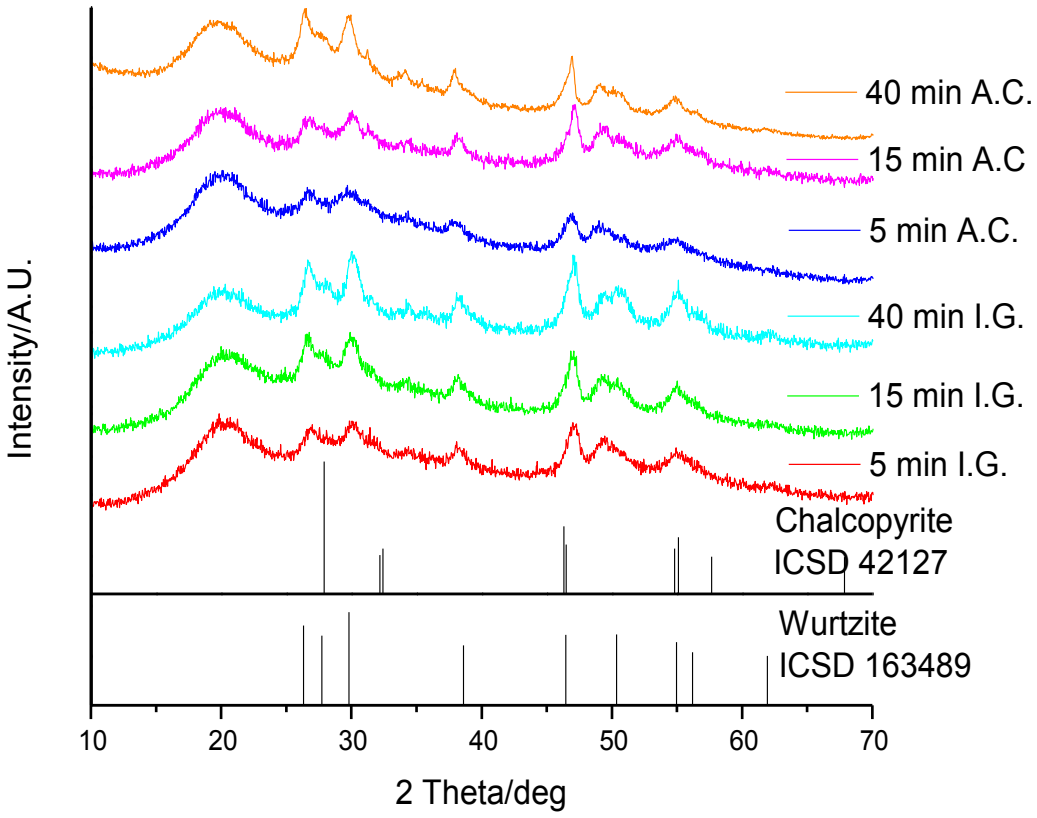

Figure 12 XRD patterns of $CuInS_2$ nanoparticles prepared under inert gas condition (I.G.) and atmospheric condition (A.C.) after different reaction times. The peaks are compared to the reference data of wurtzite and chalcopyrite shown on the bottom (sharp lines)

The corresponding Miller indices of the most dominate reflections, which are also shown in Figure 12, can also be found in Table 3.

Table 3 Miller Indices for chalcopyrite and wurtzite

Chalcopyrite: 2θ/deg	Miller Index	Wurtzite: 2θ/deg	Miller Index
27.9	112	26.3	100
32.1	200	27.7	002
46.3	204/220	29.8	101
54.8	116	38.6	102
55.1	312	46.5	110
57.6	224	50.4	103
67.8	400/008	54.9	112
74.6	316	56.2	201
		61.9	202
		70.9	203
		75.8	211

The peak at 2θ=20° can be assigned to the solvent and capping molecule oleylamine (Figure 12), which stabilizes the nanoparticles. The signals are noisy and broad which can be attributed to the reduced particle size.

The exact phase analysis is difficult due to the peak broadening of the XRD patterns. However, it can be assumed that the crystal modifications seen and compared to the reference data are chalcopyrite and wurtzite. This assumption can be confirmed by the TEM images, in which the hexagons could be noticed, which indicate wurtzite. Moreover, the reflections at 2θ= 29.8°(101) and 38.6°(102) can be attributed to wurtzite in the XRD patterns. The growth of chalcopyrite in this early stage of the reaction could not be definitely determined. It is very likely that polytype crystals were formed. This implies, that as soon as stacking fault occur the other modification is growing.[47]

TEM/XRD results experiment V2

Due to the fact that different reaction conditions have an influence on the growth, morphology and crystal modification of the nanoparticles, the experiment was repeated with prolonged reaction times but all other experimental conditions were the same. As mentioned before in this experiment the oleylamine was degassed for the one set and for the other batch it was left untreated. Once again in both batches defined particles

[47] Koo.B.; Patel, R.N.; Korgel, B. *Chem. Mater*. **2009**, 21, 1962-1966

are present. However, the influence of a prolonged reaction time on the nanoparticles could be shown as follows in the next paragraphs.

The appearance of tetrahedron after prolonged reaction time can be observed. The tetrahedrons indicate chalcopyrite as a crystal modification. The corresponding XRD results are displayed later.

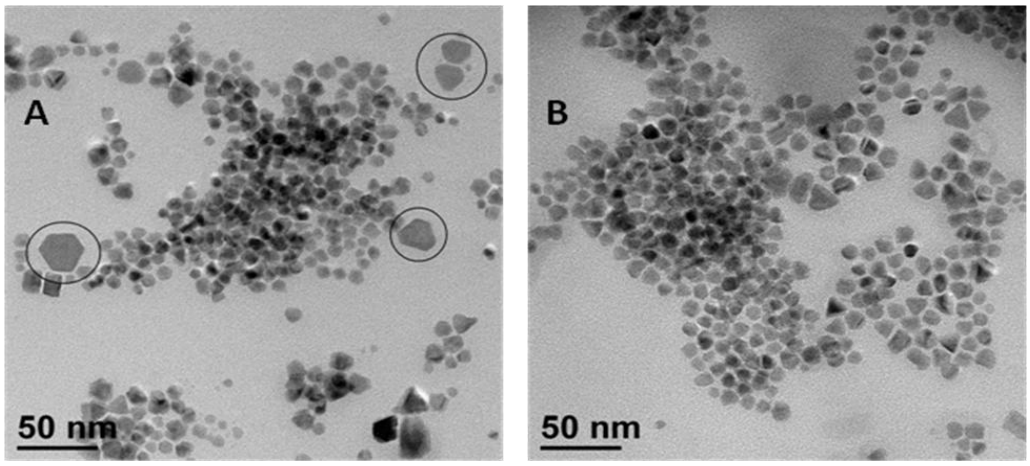

Figure 13 TEM images of $CuInS_2$ nanoparticles with a reaction time of 60 minutes, nanoparticles under inert gas condition(A) with deformed hexagons(black circled), nanoparticles under atmospheric condition (B)

As Figure 13 shows, already the prolonged reaction time of 60 minutes leads to a tendency of chalcopyrite formation, in both cases of the experiment (V2-IG-60 and V2-AC-60). The generation of chalcopyrite can be explained through the fact that this modification is more thermodynamically stable than wurtzite and resulting in a phase transformation probably induced by the influence of time.[28]

Also the TEM images (Figure 14) with a prolonged time frame of 180 minutes exhibit the characteristic shapes of chalcopyrite.

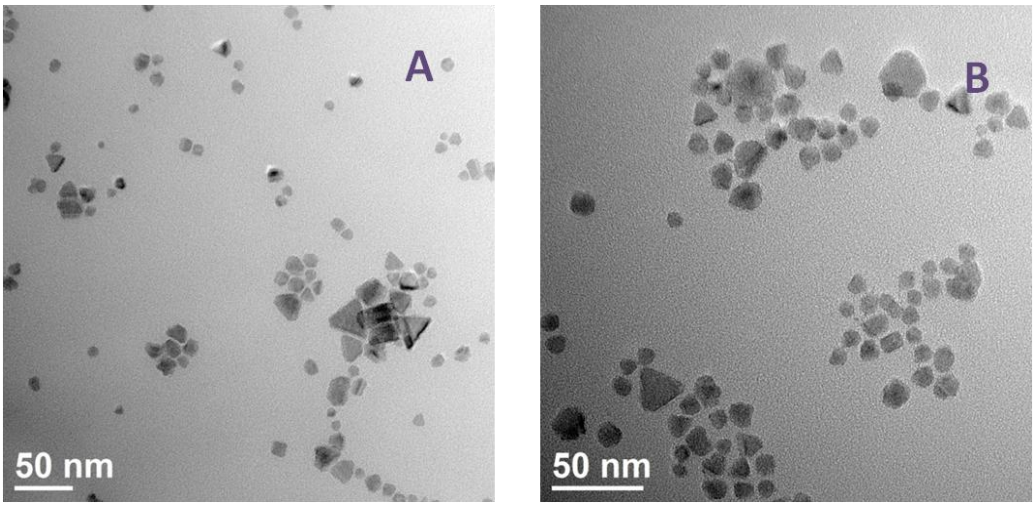

Figure 14 TEM images of samples of V3, $CuInS_2$ nanoparticles with prolonged reaction time of 180 minutes, prepared under inert gas condition (A), prepared under atmospheric conditions (B)

It can be noticed that there is no big difference between the sample taken after 60 minutes and the sample after 180 minutes, concerning the crystal structure, when comparing Figure 13 and Figure 14. It can be assumed that after 60 minutes the dominate crystal structure is chalcopyrite due to the crystal structures observed in the TEM image. The sizes, which were read out of the TEM images for the prolonged reaction time of 60 minutes, were determined to be 9-12 nm for the bulk and 22-25 nm for the bigger nanoparticles prepared under inert gas condition. Under atmospheric condition the particles grew up to a size of 8-10 nm with a few bigger ones with 15 nm.
The nanoparticles with a reaction time of 180 minutes revealed a particle size of approximately 30 nm for the tetrahedrons, 15x30 nm for the hexagons and around a value of 8-16 nm for the smaller particles prepared under inert gas conditions. A particle size of around 15-25 nm for the tetrahedrons was determined. The particles of hexagonal structure were slightly bigger with approximately 32 nm. The smaller particles were measured between 5-13 nm.

TEM investigations show that the crystallite shapes are significantly different when longer growth times are applied. Mainly triangular, quadrangular and hexagonal crystallites are observed. That is because different faces are formed to minimize the surface energy as described by the Wulff construction[48]. The observed shapes fit well with the crystal structure of chalcopyrite, which is in fact the energetically favoured

[48] Wulff, G. *Zeitschrift für Kristallographie und Mineralogie* **1901**, Band 34, 440-530

structure. However, rarely pentagonal crystallites are observed (Figure 15), which can neither be assigned to wurtzite nor to chalcopyrite based on their crystal shape only. Therefore, high resolution TEM images are analyzed to unambiguously determine the crystal structure. A first look at the pentagon shows, that there are five single crystalline domains rotated to each other, separated by distinct grain boundaries. The evaluation is thus performed for each domain separately. A Fourier transform of a single domain is shown in Figure 15 and reveals net plane distances as well as their orientations. The actual values are 3.2 Å, 3.9 Å and 5.5 Å which can be assigned to the chalcopyrite net planes {112}, {012} and {100}, respectively. Furthermore, the orientations of these planes with respect to each other (35° and 65°) fit to the crystal structure of chalcopyrite. Additionally, based on the identified planes and the crystal structure of chalcopyrite, the net plane parallel to the surface can be determined, which is (102).

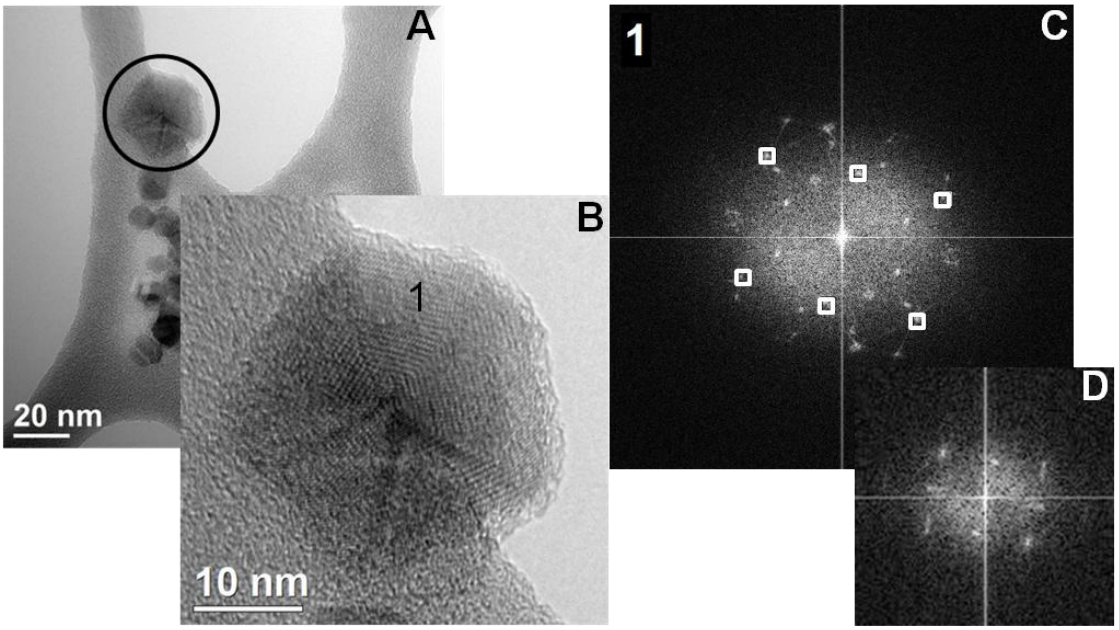

Figure 15 HRTEM of a pentagonal chalcopyrite structure of the experiment V2-IG-180 (A,B), Fourier transform of the particle (C) circled white the net plane distance of the area 1 (D)

XRD measurements for the experiment V2 were recorded as well.

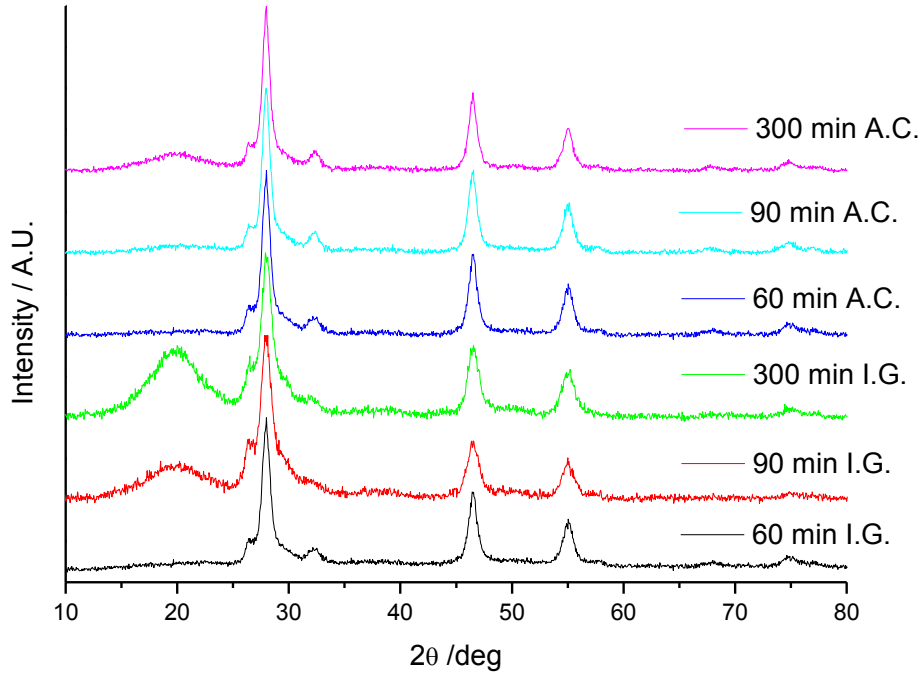

Figure 16 XRD patterns of particles prepared under inert gas condition (I.G.) and atmospheric condition (A.C.) after different reaction times.

When comparing the XRD patterns with the reference data, it can be noted that it shows chalcopyrite as the dominant crystal modification. The peak at 2 θ=32° (200) and the peak at 2θ=27.9°(112) are an indication of chalcopyrite. It can be speculated that a minor fraction of wurtzite is also existing due to the peak at 2θ=26.3°(100) but if it exists it has to be a small fraction due to the loss of signals of the characteristic reflections especially at 2θ=38.6°(102) and 50.4°.These results coincide with the TEM images(Figure 13 and Figure 14), which showed also chalcopyrite as the main crystal modification.

In summary, longer growth times lead to chalcopyrite crystallites, which is in line with XRD measurements and is a reasonable conclusion, since chalcopyrite is the thermodynamically favourable and thus the more stable crystal structure. Contrary to expectations no notable difference in shape and size between the particles prepared under inert gas condition and the particles under atmospheric oxygen could be observed.

XRD results of the experiment V3

More detailed observations were done in terms of intermediate reaction times between 60 and 180 minutes. Therefore the experiment V2 was repeated under inert gas conditions and samples were taken after 60, 90, 120,150 and 180 minutes(V3).

The experiment V3 also revealed chalcopyrite as the dominant crystal modification. The XRD patterns are distinct and show chalcopyrite. On that account it can be assumed that after a reaction time of 60 minutes chalcopyrite, which is the thermodynamically more stable modification, is formed.

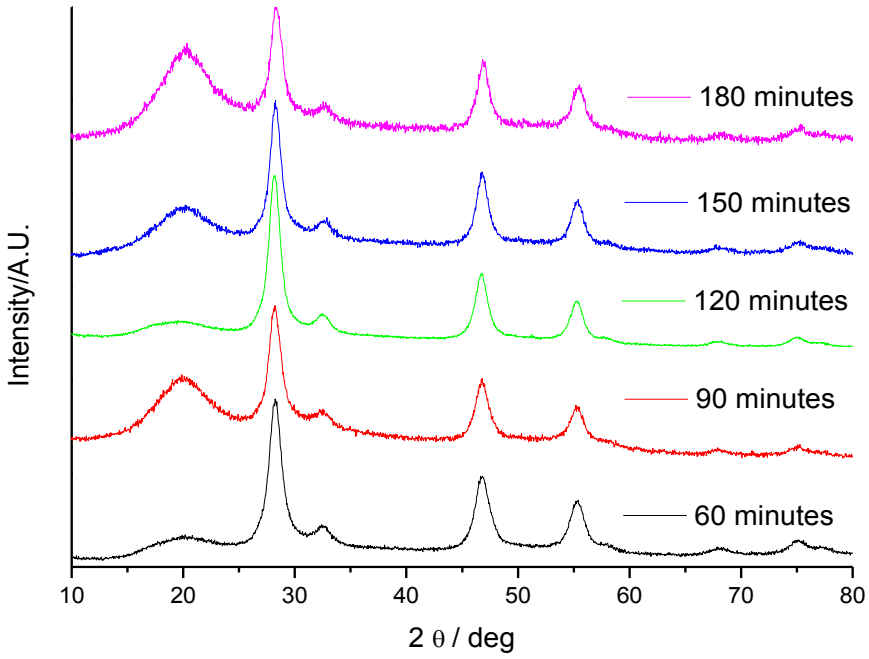

Figure 17 XRD patterns of experiment V3, $CuInS_2$ nanoparticles prepared under inert gas condition with different reaction times

Using the reflection peak at 2θ=46.3° the following particle sizes were calculated with the Scherrer equation:

Table 4 Sizes calculated for the $CuInS_2$ nanoparticles of experiment V3 under inert gas conditions and intermediate reaction time

Reaction time [minutes]	Particle Size [nm]
60	6
90	6.7
120	7.4
150	7.4
180	7.2

The shrinking of the calculated value for the nanoparticles observed after 180 minutes can be explained by the nature of calculation of the size with the Scherrer equation. The Scherrer equation is an estimation due to the compromise of using a shape factor K for spherical particles of 0.9 (Equation: (4)).

Conclusion of the experiments V1, V2, V3

All in all the results of the TEM images and the XRD measurements of the three sets of experiments it can be said that the shorter reaction time shows a tendency of wurtzite formation, whereas the prolonged reaction time favours chalcopyrite as crystal modification. This can be explained by the existence of the crystal structures of wurtzite and chalcopyrite, where chalcopyrite possesses the higher order and is thermodynamically more stable than wurtzite, which is the kinetically favoured phase.[49] However, in these experiments no significant influence of inert gas condition could be shown. Currently we have no explanation for this effect. It was assumed that working under inert gas condition prevents counter reactions, such as the oxidation process of Cu^{1+} to Cu^{2+} or the alternative incorporation of oxygen into the crystal lattice, but it could not be definitely determined. For the following experiments inert gas conditions were used in order to have reproducible reaction conditions.

UV/Vis and photoluminescence spectra

Absorption and emission spectra were recorded from the samples with a reaction time of 5, 15 and 40 minutes using chloroform as a solvent. Looking carefully at the absorption spectra it can be seen, that the onset of both reactions, prepared under inert gas condition or atmospheric oxygen condition, do not differ significantly. A possible explanation is that the particles are bigger than the found Bohr radius, which was found

[49] Qi, Y.;Liu, Q.; Tang, K.; Liang, Z; Ren, Z.;Liu, X. *J. Phys. Chem. C.* **2009**; 113,10; 3939-3944

to be 4.1 nm for a single $CuInS_2$ nanoparticle. [50] The nanoparticles of these samples exhibit a size between 10-22 nm, depending on their reaction time. If the nanoparticles are smaller than the Bohr radius the HOMO and LUMO level of the particles reveal a higher distance. As soon as the particles grow, the distance between the HOMO and LUMO level gets smaller. This occurs till the Bohr radius. As soon as nanoparticles exceed the Bohr radius the HOMO and LUMO level stay the same and as a consequence also the absorption spectra are not changing significantly.

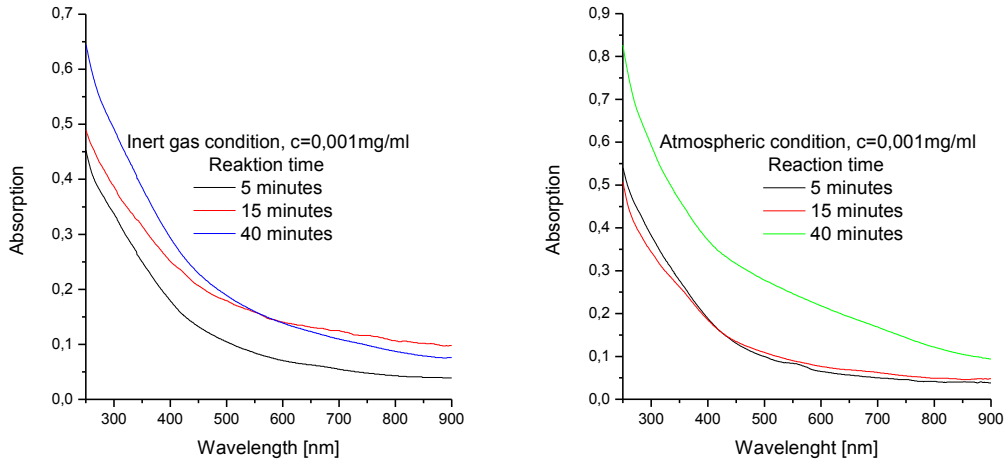

Figure 18 Absorption spectra of $CuInS_2$ nanoparticles with a reaction time of 5, 15 and 40 minutes, Inert gas condition (top), atmospheric oxygen condition (bottom)

As can be seen in Figure 18 the nanoparticles which were exposed to a longer reaction time exhibit a higher absorption intensity. This can be explained through taking their growing particle size into account. The bigger a particle grows the smaller gets their surface to volume ratio. As a result of that less oleylamine binds to their surface due to the fact that the ratio gets smaller and consequently due to more volume more absorbing mass is available. Therefore a higher intensity of the absorption spectra can be observed.

The emission spectrum shows the signal of oleylamine. The $CuInS_2$ nanoparticles themselves do not disclose an emission signal. Based on the emission spectra it can be said, that the oleylamine has coordinated onto the surface of the nanoparticles.

[50] Izquierdo-Roca, V.; Shavel, A.; Saucedo, E.; Jaime-Ferrer, S.; Ivarez-Garcı´a, J.A´; Cabot, A.; Pe´ rez-Rodrı´guez, A.; Bermudez, V.; Morante, J.R. *Solar Energy Materials & Solar Cells* **2010**, doi:10.1016/j.solmat.2010.11.014

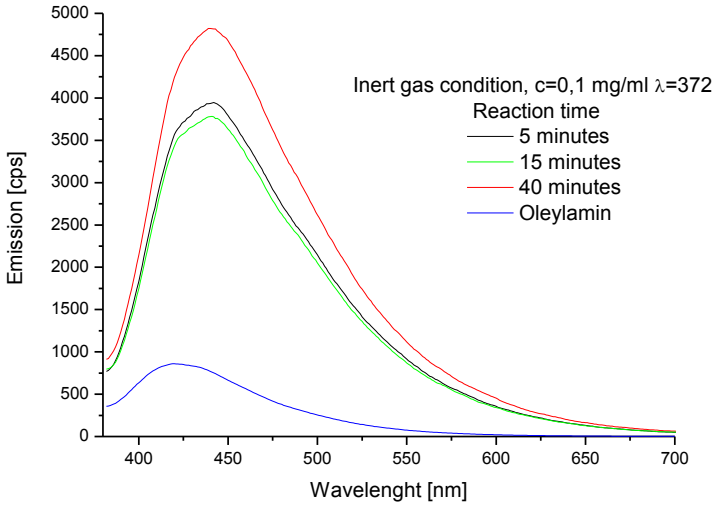

Figure 19 Emission spectra, $CuInS_2$ nanoparticles with different reaction times compared to pure oleylamine (blue line)

As can be seen in Figure 19 the oleylamine has coordinated to the surface of the nanoparticles. The signals are slightly red shifted in their maximum. This can be caused by the coordination of the oleylamine onto the surface of the nanoparticles. The oleylamine coordinates with the amine onto the surface of the nanoparticles. The two electrons from the amine group transfer to the traps on the surface of the particle. There the electrons have more room. This leads to the red shift. This theory correlated with the concept of the “particle in a box” principle.[51]

For all further experiments absorption and emission spectra were recorded. The onset of the absorption spectra did not change significantly, on the base that the particles exceed the Bohr radius. Changes in intensity showed an overall tendency of increasing with a larger particle size.

Looking at the emission spectra it could be shown that the oleylamine coordinated to the surface of all the nanoparticles, which were prepared in the different sets of experiments.

[51] Atkins, P.W.; Paula, de J. *Physikalische Chemie*, 4th ed. ; Wiley-VCH Verlag GmbH & Co KGaA; **2006**

3.1.2 Influence of purified oleylamine

It has been reported in the literature that by using oleylamine as a capping agent a preference exists of the formation of wurtzite crystal modification. Oleylamine has high capper strength, therefore normally only a few nuclei are formed during the nucleation. As a consequence there is still a lot of monomer concentration during the growing phase. This fact determines a fast growth rate, which promotes the formation of wurtzite as crystal modification.[39,49] As mentioned before wurtzite is the kinetically favoured modification. A reason why in experiments done before chalcopyrite as well as wurtzite modifications appeared, is that the oleylamine, which was used for the synthesis, could have contained certain impurities. Oleylamine with the technical grade of 70 percent was used, out of the reason that it was the only commercially available. As a result of that there are different impurities dissolved in the solvent, such as amines with different chain lengths.

In this experiment the oleylamine was distilled using a vacuum distillation. The resulting fractions were characterised with NMR. This time the metal salts were dissolved in purified oleylamine. Elementary sulfur served as sulfur source and was separately dissolved in the distilled oleylamine. Samples were taken every 10 minutes for the time frame of 1 hour.

TEM

In Figure 20, the TEM images of the nanoparticles prepared with the purified oleylamine for 30 minutes show nanoparticles with a diameter between 6 and 15 nm. In addition some larger particles of hexagonal shape with a size distribution between 35-50 nm and a thickness of 7-10 nm can be observed.

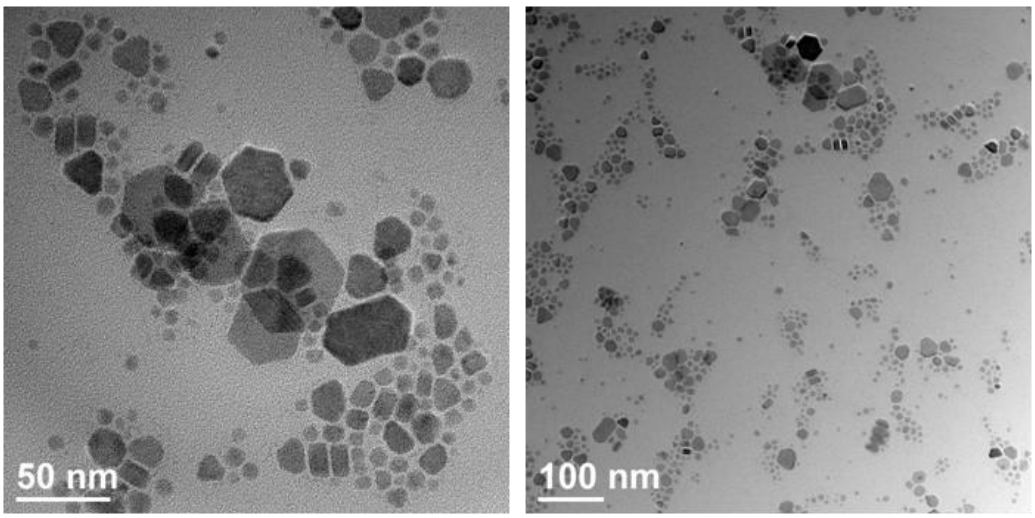

Figure 20 TEM images of $CuInS_2$ nanoparticles prepared with purified oleylamine after 30 minutes

The TEM image shows a representative overview of the nanoparticles. As can be seen in Figure 20 the particles are clearly defined and some well formed hexagons are visible. These hexagons are an indication of wurtzite, which is consistent with the results from XRD measurements. Furthermore some tetrahedrons are visible, which can be assigned to chalcopyrite. The hexagons, which do not have a regular shape, can be attributed to chalcopyrite as described in chapter 3.1.1. Moreover, it can be assumed, that wurtzite, which acts as the kinetically favoured modification, is probably built first which would explain the bigger size of the hexagons in comparison to the smaller tetrahedrons. [28,47]

Compared to the particles synthesized without distilled oleylamine the particles are more defined and the sizes are more regular, although the size distribution is still broad. This can be probably attributed either to Ostwald ripening, which could have already been started at that point of the reaction.

XRD

Figure 21 shows the XRD – patterns prepared from nanoparticles synthesized in distilled oleylamine. The experiment was performed under inert gas condition.

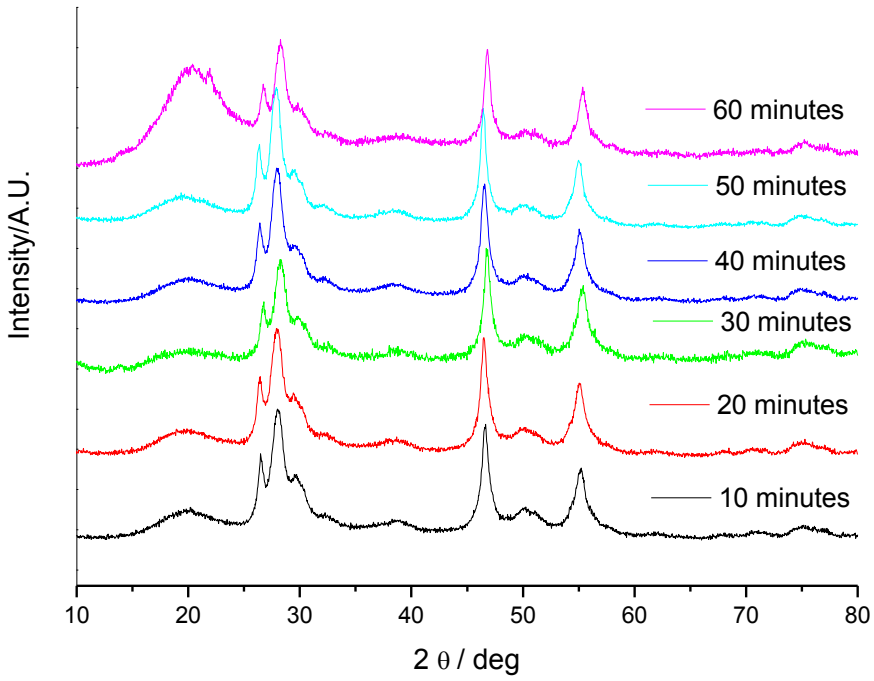

Figure 21 XRD – patterns of $CuInS_2$ nanoparticles prepared under inert gas conditions with purified oleylamine as solvent/capping agent

As can be seen the reflections of wurtzite are now clearly visible. The observed peaks at 2θ=26.3°(100), 27.7°(002), and 29.8°(101), 38.6°(102), 46.5°(110), 50.4°(103), 54.9°(112) are an indication of the crystal modification of wurtzite. However, it can also be observed that the XRD – patterns include chalcopyrite reflections. The peak at 2θ=27.7° (002) has the highest intensity, although compared to the reference data of the wurtzite (ICSD 163489) shown in Figure 12, it can be seen that the peak at 2θ=27.7° does not have the highest intensity. This indicates an overlay with the reflection peak of chalcopyrite at 2θ=27.8° (112). In addition to that, the reflection peak seen at 2θ= 32.4° (200) as well as the more intensive peaks at 54.8°(116) and 55.1°(312)[47] can be attributed to chalcopyrite. The peak at 2θ= 20° can be once again assigned to the oleylamine. In order to get further information about the fractions present in the reaction solution, a Rietveld analyse was performed. It reveals, that more wurtzite is present in the samples, with around 65% wurtzite and 35% chalcopyrite.
Overall if the XRD-patterns using distilled oleylamine are compared to the XRD-patterns of the experiment with the usage of oleylamine with technical grade of 70 percent shown in Figure 12, one can notice that the wurtzite reflections are more pronounced when using the distilled oleylamine, shown in Figure 21.

3.1.3 Influence of exchanging the sulfur source

Korgel et al. used a different sulfur source to generate particles with a low size distribution.[47] The idea was to use thiourea as a sulfur source, on the account that with this method the sulfur concentration as one of the monomers, which build up $CuInS_2$ nanoparticles, is low in the beginning of the reaction. Thiourea has to decompose before it can be assembled into the particles. As a consequence the monomer concentration of sulfur is low in the beginning. Referring to the theory of LaMer and Dinegar a low monomer concentration leads to a high critical size and a rather slow growth rate resulting in a small size distribution.[29]
The synthesis was preformed with distilled oleylamine. The metal salts and the thiourea were dissolved separately and mixed at room temperature.

TEM

In Figure 22 the nanoparticles prepared with distilled oleylamine and thiourea with a reaction time of 30 minutes are shown. The particles exhibit a size between 7-10 nm with some bigger particles with a diameter of 22 nm.

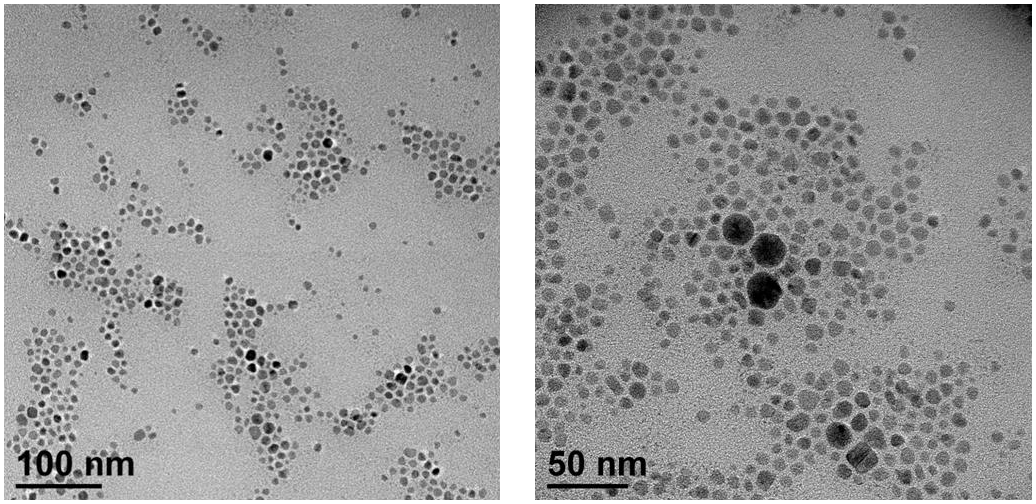

Figure 22 TEM images of $CuInS_2$ nanoparticles, prepared with thiourea and purified oleylamine after 30 minutes

As can be seen in Figure 22 the size distribution is narrower compared to the results of elementary sulfur source. The growth rate is slower resulting in more defined particles with narrow size distribution. In the TEM image above (Figure 22) hexagons are visible, which indicates wurtzite. The growth rate is low compared to a supersaturated solution such as it was the case with elementary sulfur. In the case of elementary sulfur the whole amount of sulfur is available from the start of the reaction and results in a high monomer concentration compared to thiourea. As a consequence the whole amount of sulfur can be incorporated into the nanoparticles. In the case of thiourea less monomer concentration is present. Therefore the particles are smaller and more regular.

XRD

The corresponding XRD patterns are displayed in Figure 23. The XRD patterns reveal that this sample involves wurtzite as well as a chalcopyrite. The characteristic peaks, fitting for both modifications are clearly visible at 2θ=~27.8°, ~46.4° and ~54.8°, compared to the reference data listed in Table 3. When having a close look at the XRD patterns characteristic peaks are slightly visible for both crystal modifications. The characteristic peak for chalcopyrite at 2θ=32° is visible as well as the broadening of the peak between 2θ=26° and 30° can be attributed to the characteristic 3 peaks at 26.3°(100), 27.7°(002) and 29.8°(101) for wurtzite. Furthermore, peaks arise at 2θ=~38° (38.6°, 102) and ~50° (50.4°, 103), which also can be attributed to wurtzite. Therefore, a mixture of chalcopyrite and wurtzite is present in this sample.

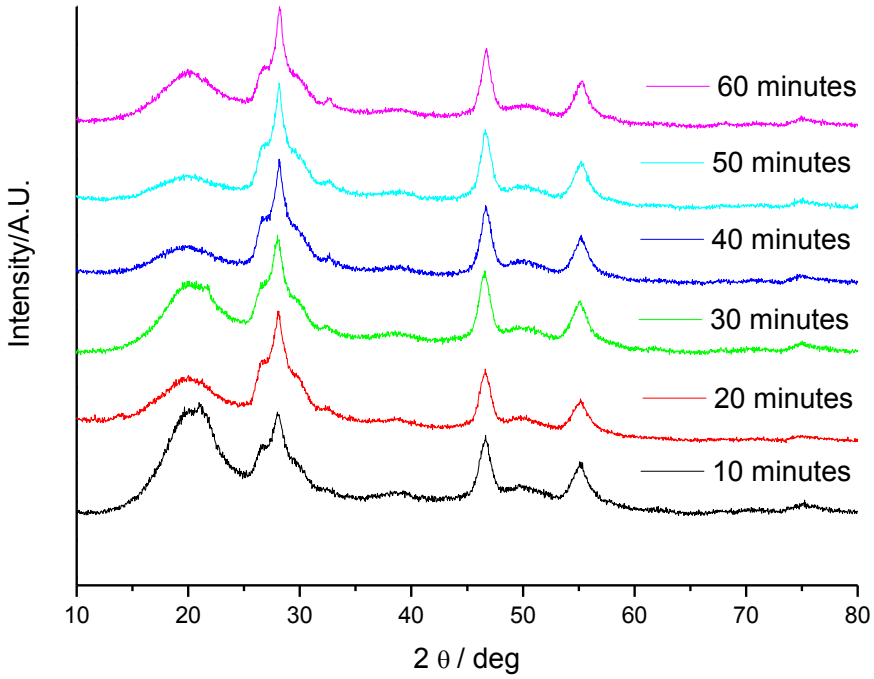

Figure 23 XRD patterns of $CuInS_2$ nanoparticles prepared with thiourea

In order to get more information Rietveld analysis was performed. It reveals, that more wurtzite is available in the samples, with approximately 70 % wurtzite and 30 % chalcopyrite. The sizes of both crystal modifications were calculated. The sizes are displayed in Table 5.

Table 5 Size calculated by Rietveld analysis for chalcopyrite and wurtzite

Reaction time (minutes)	Size: Chalcopyrite (nm)	Size: Wurtzite (nm)
10	6	4
20	7	3
30	7	3
40	7	4
50	7	4
60	8	4

However, the calculated particle size are in good agreement size read out of the TEM image, in which the bulk size is around 7-10 nm, with some exceptions of particles at a size of 22 nm.

3.1.4 $CuInS_2$ nanoparticles used for the preparation of solar cells

Due to the fact that the experiment with thiourea as a sulfur source revealed the features of a narrow size distribution and more wurtzite than chalcopyrite as crystal modification, this experiment was repeated to fabricate $CuInS_2$ nanoparticles with wurtzite as preferred crystal modification. On the account of the advantage described in 2.1.4. In order to have a sufficient amount of inorganic material for the preparation of solar cells, the synthesis was scaled up. (a reaction volume of 350 mL instead of 100 mL)

The reaction time was reduced, based on the findings that after 30 minutes big particles with a size of 22 nm were already visible in the TEM image (Figure 22), which was tried to avoid. Therefore the particles were precipitated in methanol after 20 minutes.

Moreover the addition of the sulfur source was changed. In the previous experiment the thiourea was dissolved in oleylamine and stirred at 50 °C for 30 minutes. Based on difficulties of dissolving thiourea beforehand, it was added as solid directly into the metal salt solution as soon as the mixture was cooled to room temperature. Afterwards the reaction solution was heated to 205°C.

TEM

In Figure 24 the nanoparticles prepared with thiourea and distilled oleylamine with a reaction time of 20 minutes are displayed. As can be seen the sample exhibits a narrow size distribution. Through the TEM images a size between 13-16 nm could be figured out for the nanoparticles.

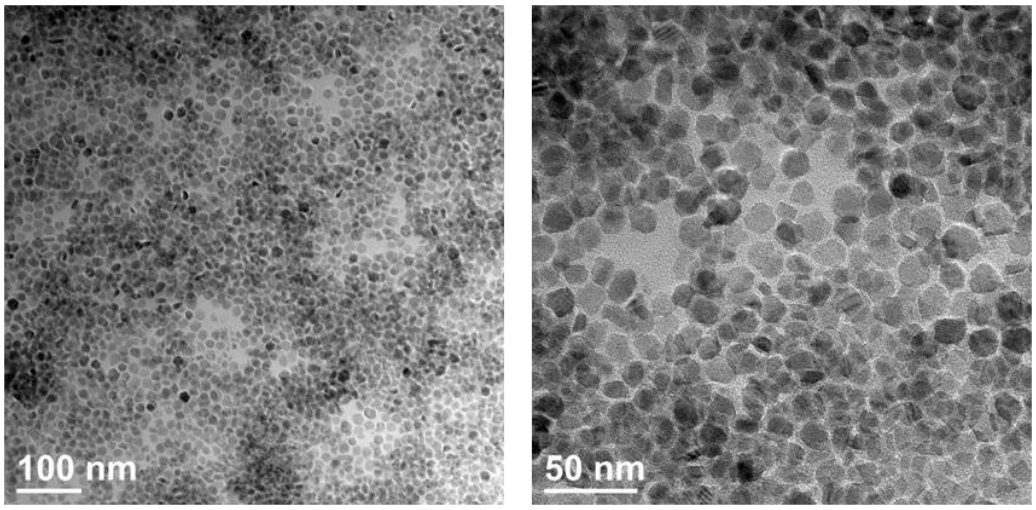

Figure 24 TEM images of $CuInS_2$ nanoparticles, narrow size distribution

Figure 24 shows that the particles are fairly uniform. The particles exhibit a disc shape with indicated wurtzite as a crystal modification. One reason for this uniformity could be either due to the shorter reaction time of 20 minutes and the stop of the reaction before Ostwald ripening could occur or in the way thiourea was added. The amount of thiourea was not dissolved before the addition to the metal salt solution. This could lead to a reduction of the monomer concentration, due to the fact that the thiourea had to dissolve in the reaction solution first. As a consequence less monomer concentration was available, which probably lead to uniform particles but a bigger crystal size. The particles gained after 30 minutes showed a bulk size between 7-10 nm whereas the particles attained after 20 minutes displayed a size between 13-16 nm.

XRD

Figure 25 shows the corresponding XRD patterns. Using the Scherrer equation a size of 13.1 nm was calculated.

The results of the XRD patterns are compared to the reference data (ISCD 163489). It reveals that pure wurtzite as crystal modification was obtained. The reflections of wurtzite are distinct and the intensities ob the reflection peaks are as well correlating with the intensity of the reference data. The results coincide to the results of the TEM images.

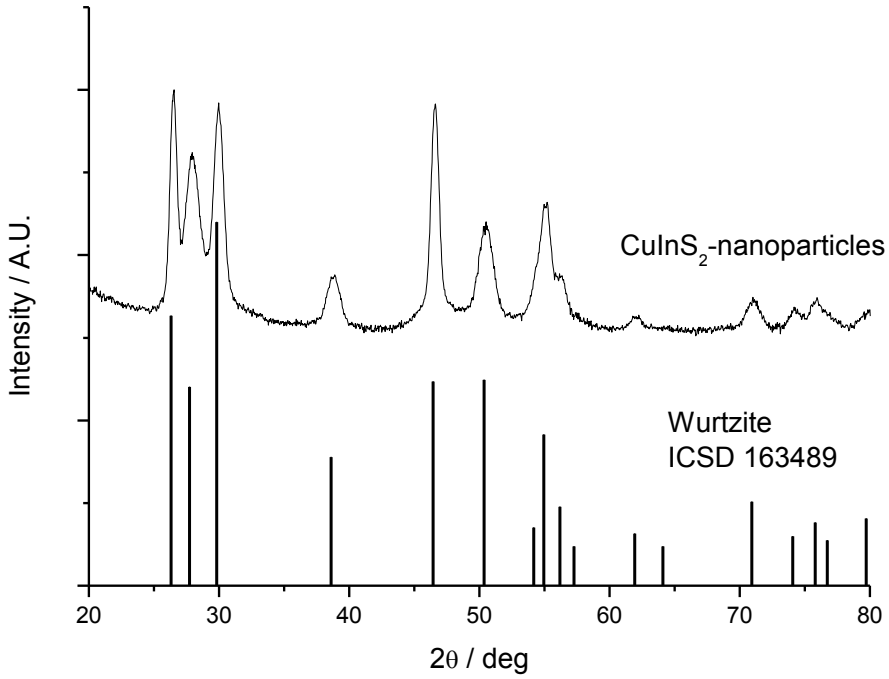

Figure 25 XRD patterns of $CuInS_2$ nanoparticles, wurtzite crystal modification

3.1.5 Conclusion

All in all it could be shown that nanoparticles with the favoured crystal modification and a low size distribution could be prepared. The first nanoparticles synthesized with oleylamine with a technical grade of 70 percent and elementary sulfur as a sulfur source lead to a high size distribution and polytype nanocrystals, but first defined $CuInS_2$ nanoparticles were observed. The dependence on the reaction time in relation to the growth of the nanoparticles and moreover the formation of the favoured crystal modification could be shown.
Further the positive influence of purified oleylamine on the growth of the nanoparticles was shown. The formation of wurtzite was clearly seen in the XRD patterns as well as in the TEM images. When looking at Figure 20 and Figure 22 both sets of experiment had a reaction time of 30 minutes, whereas it can be noted that in the case of elementary sulfur the size distribution was higher. The progressive decay of thiourea results in a lower size distribution and therefore has a positive influence on the formation of the nanoparticles.

3.2 Modifying $CuInS_2$ nanoparticles for the use in solar cells

Another aim of the thesis was the modification of the nanoparticles, before applying the inorganic material into a solar cell. In order to gain purer $CuInS_2$ nanoparticles, the particles underwent a washing process after the synthesis. The nanoparticles were precipitated in methanol[52], centrifuged and washed in methanol, if not noted differently. Therefore by this procedure, it can be ensured that by-products as well as surplus oleylamine were not longer present. All the nanoparticles that were previously been described in chapter 3.1 could be dissolved in chloroform after the synthesis and the precipitation process.
Based on the knowledge that the capping agent creates advantages as well as disadvantages, the aim of the experiments were to modify the surface of the nanoparticles towards a better performance when assembled in solar cells. The advantages and disadvantages have been shown in chapter 2.1.3, especially for their usage as an acceptor material. Remembering the fact that the capping agent occupies the traps on the surface of the nanoparticles and increases the voltage, it also behaves

[52] Czekelius, C.; Hilgendorff, M., Spanhel, L.; Bedja, I.; Lerch, M.; Müller, G.;Bloeck, U.; Su, D. S.; Giersig, M. *Advanced Materials* **1999**, 11, 643.

as an electric barrier and reduces the current. In order to reduce the electric barrier, different strategies were applied to optimize the nanoparticles for the usage in solar cells. In the first step the size-selective precipitation was performed to gain particles of a narrow size distribution. Next the nanoparticles underwent an acid treatment, with the goal to reduce the capper sphere around the nanoparticles. This could be possible due to the fact that not only a monolayer of capping agent could coordinate around the particle and as a consequence the capping sphere around the nanoparticles would get rather thick. The third strategy involved an exchange of the capping agent with more suitable molecules. Care had to be taken to find a compromise to exchange enough capping agent to reduce the isolating layer of the surface but not to remove too much of the long bulky capping agent to prevent particle agglomeration.

3.2.1 Size-selective precipitation

Regarding the broad size distribution, the first step to optimize the $CuInS_2$ nanoparticles for the assembly in the solar cells was a size-selective precipitation. The concept of this method is to precipitate the nanoparticles in a polar “nonsolvent”, such as methanol, in a controlled and size selective way. Hence the particles got gradually precipitated, based on the fact that larger particles preferentially precipitate before smaller particles do.[53]

These experiments started with the particles described in chapter 3.1.1, because the size distribution was the highest, which can be seen in the TEM images (Figure 10)

The residue, which originates from the reaction solution prepared under inert gas condition in experiment V1-IG-40, was precipitated with methanol in the first experiment SP1. More detailed information about the amount of methanol is described in chapter 4.3.1. The fractions were separated by centrifugation. Thereafter this procedure was repeated twice. By doing so, the fractions got separated by size. The size distribution of each fraction was analyzed by dynamic light scattering (DLS). DLS results also measure the capping sphere around the nanoparticles, which explains the higher nanoparticles size compared to XRD and TEM images.

The results of the first trial showed that the size-selective precipitation was successful.

[53] Klimov, V.I. *Semiconductor and Metal Nanocrystals*, Marcel Dekker, **2004**pg. 6-10

Table 6 Size-selective precipitation, addition methanol experiment SP1

Name	Average Value [nm] and Standard Deviation [nm]
Fraction 1	23 +/- 18
Fraction 2	12 +/- 11
Fraction 3	10 +/- 9
Fraction 4	3 +/- 4
Reference	20 +/- 17

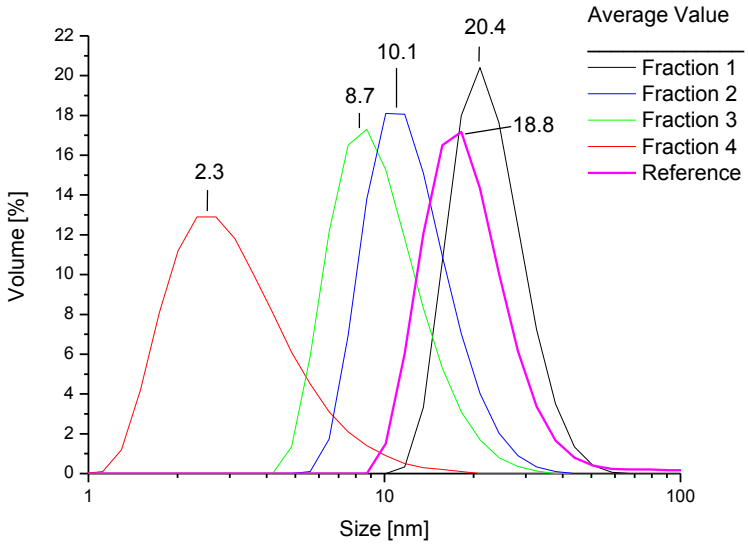

Figure 26 DLS Results of the size-selective precipitation, experiment SP1

As in Table 6 can be seen the sizes are getting gradually lower after each addition of methanol-treatment. The sizes read out of the TEM images (Figure 10) coincide with the results of the size-selective precipitation of the first fraction. It shows that the largest nanoparticles precipitate first. Moreover, the standard deviation increases with the amount of methanol addition. This can be attributed to the fact that larger particles, which did not precipitate within previously, became unstable after another addition of methanol. This can be observed at the DLS results in Figure 26. The peaks still overlap, although the maximum of the size is shrinking. By reference it is meant that the particles are precipitated once, as in the normal procedure after the synthesis.

Here it has to be mentioned that the results in the table are calculated and the average value as well as the standard deviation were received by the integrals of the DLS

results. In Figure 26 as well as in Figure 27 the DLS results show only the maximum values of the peak. That is the reason for the slight variance of the results.

In order to gain a lower size distribution and a smaller standard deviation, this experiment SP2 was repeated by adding smaller portion of methanol to precipitate the nanoparticles.

Table 7 Size-selective precipitation, less addition of methanol experiment SP2

Name	Average Value [nm] and Standard Deviation [nm]
Fraction 1	22 +/- 23
Fraction 2	13 +/- 9
Fraction 3	11 +/- 8
Residue	7 +/- 11

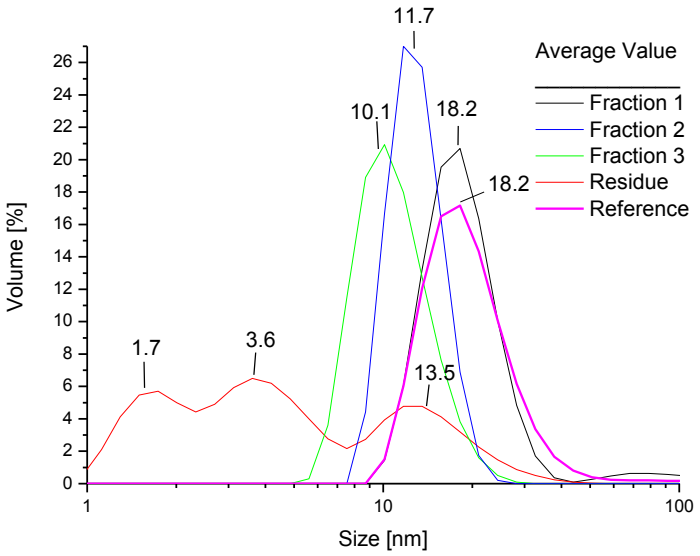

Figure 27 DLS results of the size-selective precipitation, less addition of methanol, experiment SP2

The size-selective precipitation worked based on the DLS results shown in Table 7. Moreover, the standard deviation slightly decreased as from the second fraction by adding a lower amount to the nanoparticles solution compared to the prior experiment. The label “residue” states that after adding three times a smaller portion of methanol for each fraction to precipitate, an excess of methanol was added, to precipitate all the

remaining particles in solution. As can be seen in Figure 27 it looks like a superposition of three size distribution peaks and display a large size distribution.

The first steps for a size-selective precipitation were successful and worked with the particles that exhibit a high size distribution. Therefore the experiment was applied to the particles with a minor size distribution, such as described in 3.1.4. Moreover the particles were already precipitated once with the normal precipitation procedure after the synthesis (described in chapter 4). On that account methanol was added 3 times with a rising amount. It was calculated with a percentage for the first addition of 10 percent, 50 percent and a large excess of methanol. When adding 10 and 50 percent to the nanoparticle solution, only a very small fraction precipitated. The effect was even too little to be measured with DLS. When adding the excess of methanol a large fraction of particles precipitate. Due to the fact that the nanoparticles were washed once, a part of the oleylamine was already removed. As a consequence the hydrophobic behavior is reduced and a bigger amount of polar solvent is necessary in order to cause the precipitation.

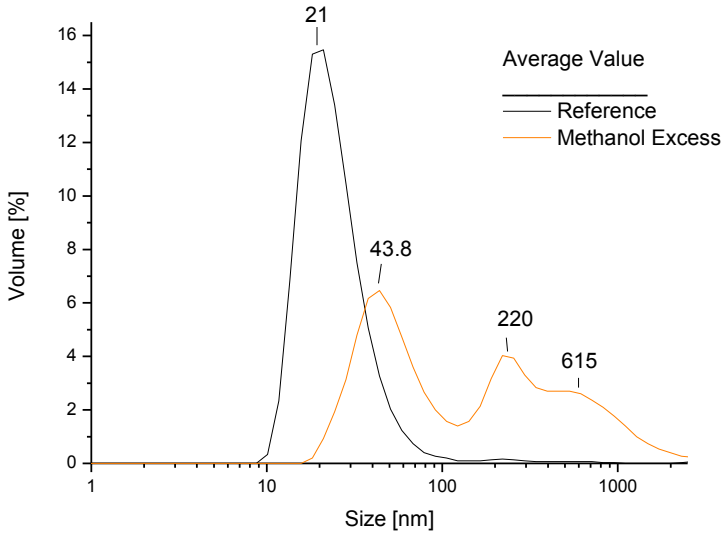

Figure 28 Size-dependent precipitation, low size distribution of the nanoparticles

The term “reference” in Figure 28 states that the nanoparticles were not precipitated once more with an excess. When comparing the reference to the particles after methanol treatment, it can be assumed that 3 peaks are overlapping (orange line). The measuring curve exhibits 3 maximums at ~43 nm, ~220 nm and ~615 nm. It can be assumed that these are agglomerated due to the fact that the oleylamine was washed away by the methanol treatment. As soon as the capping agent is not present the

nanoparticles tend to agglomerate, which is reflected by a bigger nanoparticle size in the DLS results.

Due to the results it can be noted that for the particles, which are mostly used during this work for the assembly in solar cells, described in chapter 3.1.4, a size-selective precipitation is not necessary. The size distribution is already low, which can be seen in Figure 24. In order to narrow the size distribution even more, further investigations would have to be done.

3.2.2 Reduction of the capper sphere

Based on the effects of a capping sphere around the nanoparticles, surface modification is considered as a crucial factor to improve the performance of solar cells by enhance the charge transfer from polymer to nanoparticles as well as the electron transfer between the nanoparticles. [54,] Therefore there are two ways of modifying the nanoparticles surface. One approach is the exchange of the capping agent, as described in the next chapters: on the other hand it was reported to reduce the capper sphere around the nanoparticles by an acid washing treatment. In the literature this acid treatment was described for CdSe nanoparticles with trioctylphosphine and oleic acid as capping agents. It was reported that the acid treatment reduced the average particle to particle distance significantly in comparison to untreated nanoparticles. Moreover the aggregation tendency of the nanoparticles is clearly visible after the acid treatment. [55, 56]

In the paper at hand the reduction in size of the oleylamine capper sphere by using acid treatment was performed.

The first tests for the acid treatment were done with the particles, described in chapter 3.1.1, with a reaction time of 40 minutes. The $CuInS_2$ nanoparticles, which were used for this experiment, were on the one hand untreated and on the other hand obtained after the size-selective precipitation (Fraction 3) with a size of 10.1 nm. The particles were dissolved in hexanoic acid then they were precipitated with methanol and separated by centrifugation.

Figure 29 shows the DLS results before and after the acid treatment.

---

[54]Zhou, Y. et al *Solar Energy Materials & Solar Cells* **2011**, 95, 1232-1237

[55]Zhou, Y.; Eck, M.; Krüger, M. *Energy and Environmental Science* **2010**, DOI:10.1039/c0ee00143k

[56]Zhou, Y.; Riehle, F.; Yuan, Y.; Schleiermacher, H.; Niggemann, M.; Urban, G.; Krüger, M. *Appl. Phys. Lett;* **2010**, 96, 013304

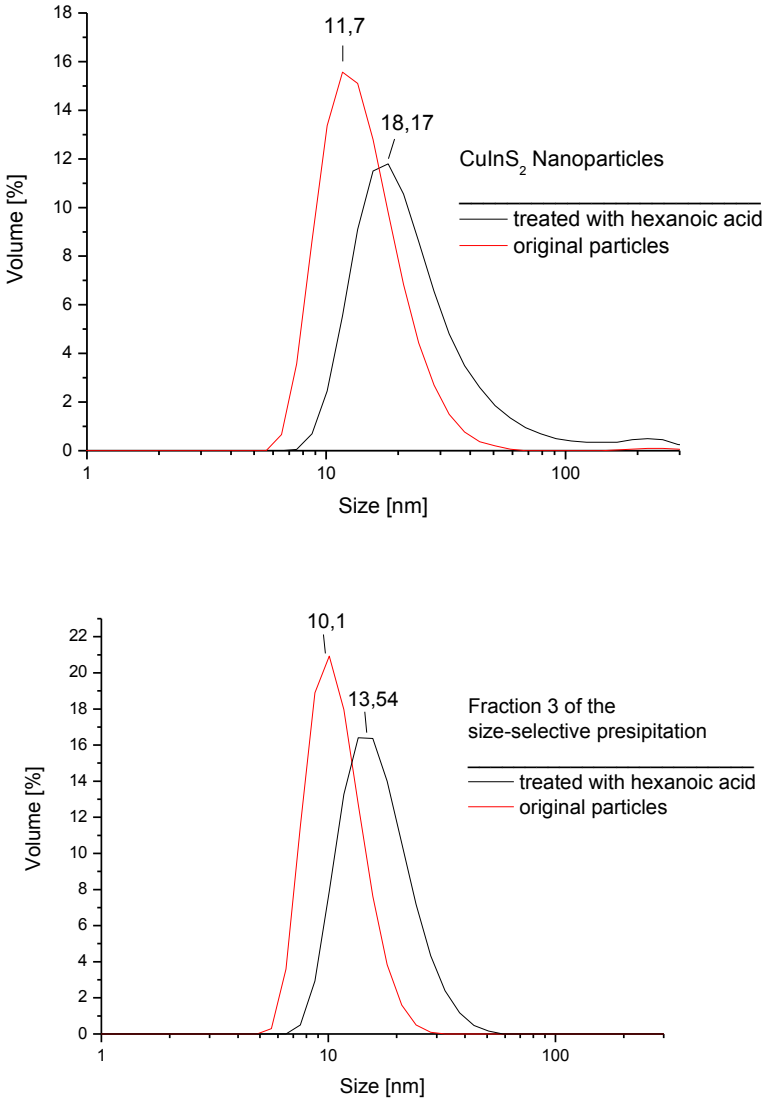

Figure 29 DLS results of $CuInS_2$ nanoparticles before and after acid treatment, particles obtained after synthesis (top), particles obtained after size-selective precipitation (bottom)

Figure 29 shows that in both cases an increase in size is notable. TGA measurements were performed. The untreated particles revealed a change in mass of 80.5 %, whereas the change in mass for the treated particles was 22.6 %. Considering the fact that the acid treatment should reduce the capper sphere around the nanoparticles it can be assumed that the particles started to agglomerate and therefore the acid treatment was successful although too much oleylamine was removed from the surface of the nanoparticles.

The treatment with hexanoic acid was repeated. Therefore the particles with a narrow size distribution, such as described in chapter 3.1.4, were dissolved in hexanoic acid and precipitated in methanol. The particles were dissolved in chloroform. As seen in the results before, the particles were soluble but some minor aggregates could be observed in the solution. The particles were incorporated into solar cells to see if an improvement of the efficiency occurred due to the reduced capper sphere. The corresponding results will be discussed in chapter 3.3.5.

3.2.3 Capper exchange with pyridine

Oleylamine is known as non conductive material. As a consequence a high amount of this capper can reduce the conductivity of the nanocomposite layer. On that account the capper can be exchanged, which is reported in a wide range of literature.[57,58] The capper can be exchanged with either smaller and/or electro-active capping agents. The reason why small electro-active molecules, which would clearly be an advantage for the assembly in solar cells, were not used directly during the synthesis, is based on the fact that the particles cannot be stabilized to a sufficient extent. Therefore the particles tend to agglomerate and so they are not soluble anymore. Using oleylamine, a long bulky molecule, the particles do not agglomerate. Nonetheless the capper exchange is quite difficult due to the fact that a compromise has to be found in how much oleylamine should be exchanged, so that the conductivity increases but the particles do not agglomerate.

In literature pyridine is most commonly used for capper exchange to improve the device efficiency[57,58] The successful pyridine capper exchange for cadmium chalcogenides, which lead to an improvement in performance in solar cells was reported in various papers.[59,60,61] This can be attributed to the fact that pyridine can act as coordinating molecule due to the electron pair of the nitrogen. Moreover it is a small molecule compared to oleylamine. However, care has to be taken when using pyridine, because it can mediate the precipitation of different polymers, by reason of their solubility in chloroform but insolubility in pyridine, as for example P3HT.[62] Olson et al. [63]

---

[57] Reiss, P.; Couderc, E.; Girolamo, J.; Pro, A. *Nanoscale* **2011**, 3, 446-489

[58] Sun, B.; Marx, E.; Greenham, N. *Nano Letters* **2003**, 3, 7, 961-963

[59] Sun, B.; Greenham, N. *Phys. Chem. Chem. Phys*. **2006**: 8; 3557-3560

[60] Huynh, W.; Peng, X.; Alivisatos, A. *Adv. Mater.* **1999**; 11; 923-926

[61] Huynh, W.; Dittmer, J.; Alivisatos, A. *Science* **2002**; 295; 2425-2427

[62] Huynh, W.; Dittmer, J.; Libby, W.; Whiting, G.; Alivisatos, P *Adv. Funct. Mater*. **2003**, 13, 1, 73-79

reported on a system of CdSe/P3HT devices, where the best efficiency of 1.77% was reached using butylamine as a shorter capping agent.

On the account to improve the performance of the devices, a pyridine capper exchange with the $CuInS_2$ nanoparticles, in detail described in chapter 4.2.5, was performed. The particles were dissolved in pyridine and refluxed.

After the treatment the particles were dissolved in pure chloroform and also in a mixture of 20:80 pyridine to chloroform. The particles were not soluble in chloroform nor in the solvent mixture. In general pyridine is miscible with chloroform, which would increase the possibility for the nanoparticles to dissolve.[62] It can be assumed that too much oleylamine was removed on the nanoparticles in this experiment. It has been tried to dissolve them in an excess of chloroform and with the help of ultra sonic bath, which did not influence the solubility though. In the solvent mixture the particles coloured the solution black but were still visible agglomerated and the particles deposited on the bottom of the vial over night. Because of the insolubility no further characterisations were done.

On the account of the solubility test it can be assumed that the capper exchange with pyridine was successful, because the long bulky oleylamine was removed. As a consequence the particles did agglomerate. Further investigations have to be made to ensure that only a certain amount of oleylamine is removed and replaced by pyridine.

3.2.4 Capper exchange with tetrahydrothiophene (THT)

Considering the literature of the pyridine capper exchange[58], another capping agent for the exchange was tried. Aldekov et al. reported on experiments using small sulfur containg conjugated heterocycles combined with CdSe nanorods. The working group could not see an improvement in the performance of the solar cells compared with solar cells, which underwent a pyridine capper exchange. This was attributed to an observed phase separation of the polymer and the nanoparticles.[64] In order to find out if an improvement occurs in the system used in this work, the idea of using a sulfur containing molecule for the capper exchange was adopted. Hence, it was decided to use tetrahydrothiophen (THT) due to the fact that it is a small sulfur containing molecule. Moreover, THT is also used in lithium batteries as an electrolyte[65].

---

[63] Olson, J.D.; Gray, G.P.; Carter, S.A. *Solar Energy Materials & Solar Cells* **2009**, 93, 519-523

[64] Aldekov, D.; Chandezon, F.; Bettignies, R.; Firon, M.; Reiss, P.; Pron, A. *Eur. Phys.J.: Appl. Phys.* **2006**; 36; 261-265

[65] http://www.lookchem.com/TETRAHYDROTHIOPHENE/, accessed on 22nd June 2011

The nanoparticles were dissolved in THT and refluxed for 24 hours. After the treatment the particles were precipitated on the one hand in methanol and on the other hand in hexane. The particles precipitated in both equally well, however, when using hexane as the precipitating agent the particles were relatively soluble without treatment in the ultra sonic bath. Therefore the particles were precipitated in hexane due to the fact that the particles were better soluble than after a precipitation with methanol and hexane is less toxic than methanol. All in all the particles were soluble, although some agglomerates were visible. Therefore it can be assumed that some of the oleylamine was removed. The particles were incorporated into solar cells to see if an improvement of the efficiency of the solar cell occurs. The corresponding results are described in chapter 3.3.5.

3.3 Solar Cells

In this study solar cells with a heterojunction assembly were built. $CuInS_2$ nanoparticles were used as an acceptor material, whereat the particles were used with and without further treatment. As a donor material a conjugated polymer was used, which was either poly[[9-(1-octylnonyl)-9H-carbazole-2,7-diyl]-2,5-thiophenediyl-2,1,3-benzothiadiazole-4,7-diyl-2,5-thiophenediyl] (PCDTBT) or poly[2,1,3-benzothiadiazole-4,7-diyl-2,5-thiophenediyl(9,9-dioctyl-9H-9-silafluorene-2,7-diyl)-2,5-thiophenediyl (PSiFDBT). The first solar cells were built with PCDTBT. The adjustment from PCDTBT to PSiFDBT as a donor material was done due to the fact that PSiFDBT possesses a better solubility and does not form clusters in the active layer.

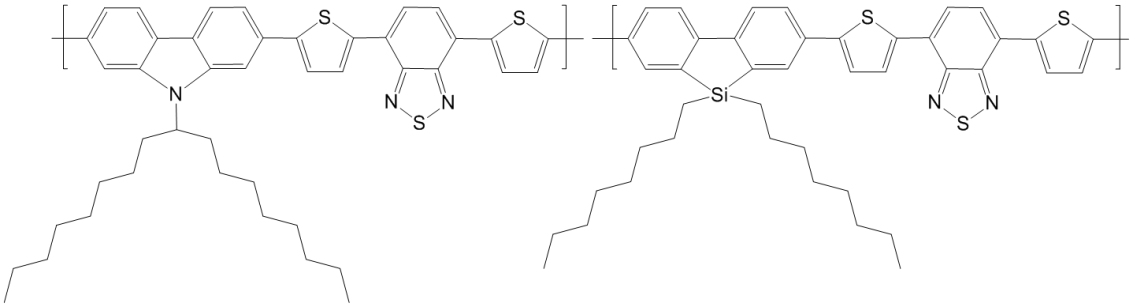

Figure 30 Structure of the polymers PCDTBT (left) and PSiFDBT (right)

The solutions of the active layer were filtered, if nothing differently noted, to eventually reduce existing agglomerates either of the polymer or the nanoparticles. The active layer was applied via spin coating. In order to investigate the reproducibility, two substrates with the same parameters were built.

The aim of this work was to optimize the efficiency of the solar cell. Therefore various polymer to nanoparticle concentrations were investigated. Moreover the influence of annealing was tested. The influence of treated nanoparticles when being incorporated into solar cells was traced as well as addition of additives or chemical vapour annealing. The reproducibility of the solar cells were rather high, since it is liable on temperature fluctuation and humidity.
Subsequently the results of the optimization work of the devices are shown. Due to the fact that in some cases the performance of the solar cells, which were built up with the same parameters, were quite different, the median was used to show a trend in the various performances. The median was used instead of the arithmetic average on the account of getting more realistic results. When using the arithmetic average outliers have a bigger influence on the result. The values of the current varied over one to two decimal powers. As a consequence it was difficult to work out which were the outliers. As a result it was not possible to erase the outliers, which then have more impact on the result. The standard deviation was added to show the distribution.
The current-voltage characteristic of the solar cells was recorded. Due to the fact that especially with not annealed solar cells a rather low current (around $1*10^{-5}$ mA/cm^2) was received, the problem of slightly waved current-voltage characteristics was observed. It is assumed that this effect can be attributed to contacting problem of the electrodes.

3.3.1 Solvents, filter and fabrication parameters

For the fabrication of solar cells certain parameters had to be tried before the preparation process could be started. In order to optimize the film formation, layers with different compositions were coated. Based on that, different polymer concentrations, various inorganic to organic ratios, two solvents and several spin coating parameters were tested. Moreover the solutions were applied on the solar cell in both filtered and unfiltered form. The layers prepared in this set of experiments were pre-test and no electrodes were evaporated and no I-V characteristics were recorded.
In conclusion it was discovered that spin coating parameters of a minimum of 2000 rpm with an acceleration of 300 rpm/s were necessary to obtain visual homogeneous layers with a minimum of error visible with the naked eye. Furthermore it was found that it was relevant to filter the solutions, due to the fact that the layers got branching cracks and less short circuits appeared. Non filtered solution revealed a higher tendency of patterns in the active layer. It can be assumed that these patterns were formed from non dissolved solids or agglomerates. Both solvents, chloroform and chlorobenzene, can be used; due to the solubility of the polymers (PCDTBT and PSiFDBT) as well as

the nanoparticles. Especially as soon as the solutions were filtered no inhomogenities were visible irrespectively of the solvent. Only with chloroform the layers seemed visibly thicker than using chlorobenzene as solvent. In order to identify the right polymer concentration and inorganic to organic ratio solar cells had to be produced and characterized.

Table 8 Overview of parameters of the pre-test

Parameters	Variations
Polymer concentration	5 mg/mL; 6 mg/mL
Inorganic:Organic ratio	5:1; 6:1; 7:1
Spin coating	1000 rpm, 2000 rpm, 3000 rpm
Solvents	Chloroform, Chlorobenzene

3.3.2 Influence of the capping agent on the solar cell performance

For the purpose of investigating the influence of the capping agent on the performance of the solar cell, devices were built out of nanoparticles with a high amount of about 80% of capping agent and a rather low amount of about 21% of capping agent, respectively. The amount of capping agent was measured by TGA. PCDTBT was used as a polymer.

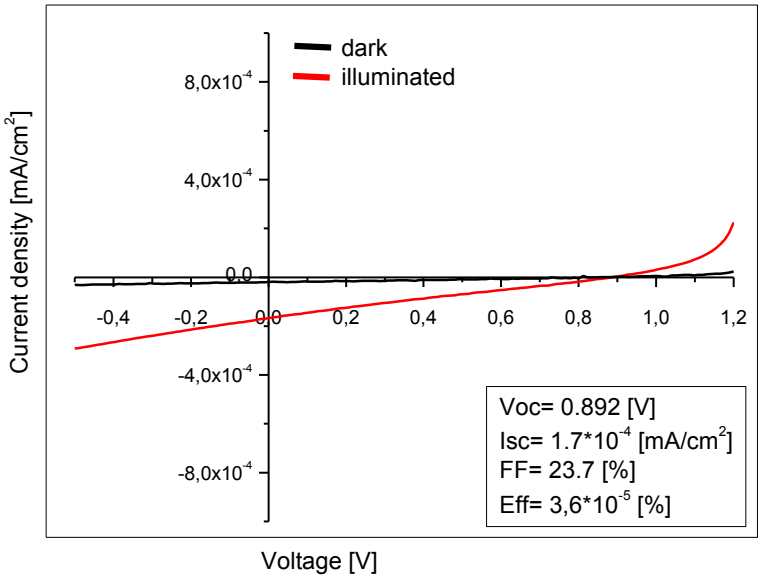

Figure 31 I-V characteristic of solar cells with 80% oleylamine on the nanoparticles

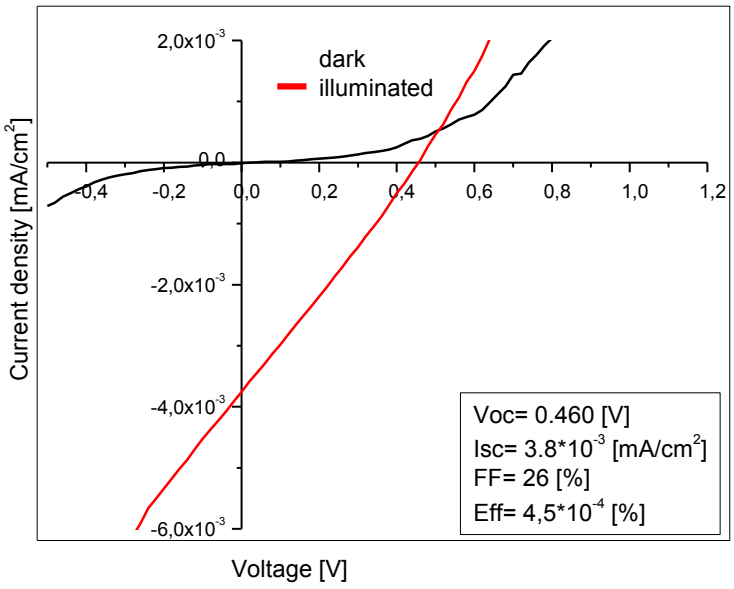

Figure 32 I-V characteristic of solar cell with 21% oleylamine on the nanoparticles

In Figure 31 and Figure 32 the I-V characteristics are shown of both sets of experiments. The results revealed significant differences between the solar cells prepared with nanoparticles surrounded by 80% or by 21% of capping agent. When looking on the V_{oc} it can be seen that with the particles with 80% of capping agent it is situated at around 890 mV whereas it decreases to 460 mV with the nanoparticles with

21% of capping agent. This can be explained by the capping agent, oleylamine, which coordinates to the surface of the nanoparticles and occupies the traps on the surface. As a result if more capping agent is available on the surface of the nanoparticles less traps are on the surface leading to higher values for the effective band gap, known as the main factor governing the open circuit voltage in hybrid solar cells.[39]

However, the current increases with less capping agent around the nanoparticles. In this experiment the current increased from 0.17 µA/cm^2 to 3.8 µA/cm^2. If less capping agent is coordinated to the surface of the nanoparticles the electric barrier around them is smaller and therefore the charge transport is more preferential. This electric barrier exists through the long bulky organic tail of the capping agent, oleylamine.

In conclusion it can be said that the capping agent has a big influence on the performance of the solar cell. A compromise of the amounts of capping agent on the surface of the nanoparticles has to be found, due to the fact that little capping agent reduces the voltage significantly and a high amount of capping agent decreases the current substantially.

3.3.3 Optimal ratio of inorganic to organic materials

Out of the motivation to find an optimal nanoparticles to polymer ratio for the active layer in the solar cells, some ratios and polymer concentrations were tried. First the experiment started with ratios of 5:1, 7.5:1 and 10:1 $CuInS_2$ nanoparticles to PSiFDBT as a polymer were tested, with a polymer concentration of 5, 10 and 15 mg/mL. I-V characteristics were recorded in order to work out a tendency for the best composition of inorganic to organic material. The median was calculated from each substrate with the same ratios and polymer concentration.

Based on the resulting data no correlation between the optimal amounts of inorganic to organic material could be drawn. The results are fluctuating and no significant tendency could be found. The solar cells were tested in terms of V_{oc}, I_{sc}, fill factor and efficiency, but no clear trend could be observed. However, the best efficiencies were found with a ratio of 5:1 nanoparticles to polymer with a polymer concentration of 10 mg/mL and additionally with a ratio of 7.5 inorganic to organic and polymer concentration of 5 mg/mL, which can be seen in Figure 33. As a consequence it was decided to use ratios of 5:1 and 7.5:1 nanoparticles to polymer with polymer concentrations of either 5 or 10 mg/mL for the further experiments to fabricate devices.

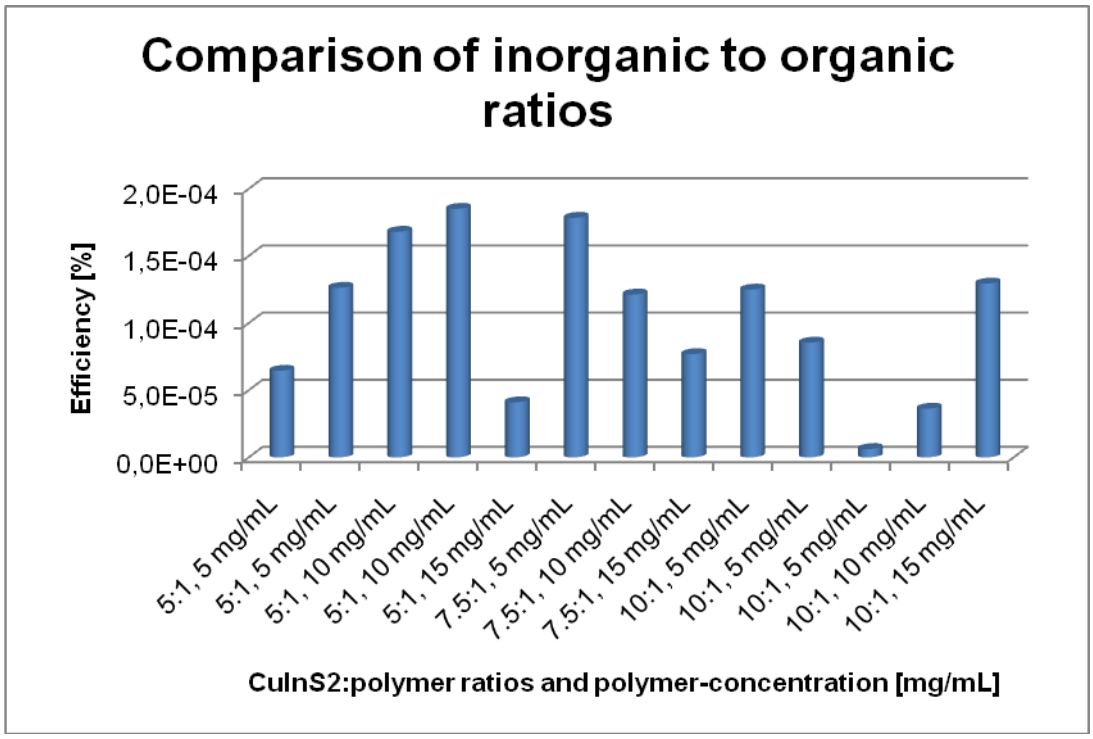

Figure 33 Comparison of solar cells prepared with various $CuInS_2$:polymer ratios and varying polymer concentrations

The performance of solar cells can vary for different reasons. For example solubility or the nanoparticles and polymer[56,66], layer thickness[67], size of the nanoparticles[53], dispersion within the solar cell[67]. Additionally temperature variations as well as humidity can have a major impact on the performance. One main aspect could be the layer thickness of the solar cell, which is also slightly fluctuating. A tendency can be seen when looking at the polymer concentration. The higher the polymer concentration was the thicker the layer became and the worse the efficiency turned out. For example with a nanoparticle to polymer ratio of 5:1 and a polymer concentration of 15 mg/mL the profilometer measurement showed a thickness of 800 nm. Generally the typical thickness of the total solar cell is less than 500 nm whereas the PEDOT:PSS is usually 40-80 nm, followed by the active layer with approximately 60-200 nm and an electrode of 100-150 nm.[67] The solar cells which revealed a better performance, exhibited a layer thickness between 200 and 300 nm.

Some polymer concentrations and also inorganic to organic ratios were repeated. In case of efficiency the reproducibility with a ratio of 5:1 nanoparticles to polymer and a

[66] Brandrup, J.; Immergut, E.; Grulke, E. *Polymer Handbook*, 4th ed. New York: John Wiley and Sons, **1999**

[67] Saunders, B.; Turner, M. *Advances in Colloid and interface science* **2008**, 138, 1-23

polymer concentration of 10 mg/mL is the most stable one. Each experiment consisted out of 6-9 solar cells and the median was calculated for both sets. With a standard deviation of $1.2*10^{-5}$ (median value of the two sets of experiments: 1st set:$1.7*10^{-4}$ %, 2nd set:$1.9*10^{-4}$ %) it has the least variance compared to $4.6*10^{-5}$ (1st set: $6.4*10^{-5}$ %, 2nd set: $1.3*10^{-4}$ %) in case of a ratio of 5:1 nanoparticles to polymer and a polymer concentration of 5 mg/mL and even $6.0*10^{-5}$ (1st set: $1.2*10^{-4}$ %, 2nd set: $8.5*10^{-5}$ %, 3rd set: $6.2*10^{-6}$ %) of solar cells with a ratio of 10:1 nanoparticles to polymer and a polymer concentration of 5 mg/mL.

In this experiment the best performing solar cell of all concentrations and ratios under investigations was a solar cell with a ratio of 7.5:1 nanoparticles to polymer and a polymer concentration 5 mg/mL. This cell obtained a V_{oc} of 820 mV, an I_{sc} of $1.0 *10^{-3}$ mA/cm^2, a fill factor of 22.7 % and an efficiency of $1.9*10^{-4}$ %.

All in all it has been discovered that ratios of 5:1 and 7.5:1 are the most stable and best working ratios. The nanoparticle to polymer ratio of 10:1 did not perform as well compared to the other ratios. A possible explanation could be that the volume of both materials were not balanced anymore and too much nanoparticles were present in the active layer.

The polymer concentration should vary between 5 and 10 mg/mL because everything higher did not work.

3.3.4 Effect of thermal treatment

In order to improve the performance of the solar cells and due to the fact that no thermal treatments were used in experiments before, different annealing processes were tested. First a post annealing step was tried, in which the solar cells were put on a hot plate after the fabrication. Therefore an immediate effect could be seen, due to the direct comparison of the solar cells when measured once before the annealing step.

Furthermore two different annealing steps in a tube furnace were tried out. First the solar cells were heated to 200 °C in 7 minutes with a following period of 15 minutes at 200 °C on the one hand and on the other hand 30 minutes at 200 °C under vacuum in a tube furnace.

As mentioned in the literature annealing is found to be an effective method to enhance the performance of the solar cell. Annealing can cause different effects within the solar cell. It can improve the hole mobility due to the increase of crystallinity of the polymer, which is the case with P3HT[68], but it can also enhance the electron mobility in the

[68] Zhao, Y.; Yuan, G.; Roche, P.; Leclerc, M. *Polymer* **1995**, 36, 2211

acceptor phase[69]. The polymers tend to crystallize at temperatures above the glass transition temperature. As a consequence an enhancement of the mobility can be observed as well as the influence of the morphology resulting from the thermal treatment. Moreover it was reported in the literature that an improvement of the performance was observed, when eliminating the capping agent by a thermal treatment. This was shown for CdSe nanoparticles.[62]

Considering the fact that the $CuInS_2$ nanoparticles are capped with oleylamine, it was tried to enhance the performance of the solar cell by annealing.

The following paragraph shows the results of the hot plate annealing. The post thermal treatment, when the solar cells are annealed after the evaporation of the Al electrodes, did not reveal a distinct improvement of the performance of the solar cell. The results show a tendency of decreasing efficiency. Because of that, fluctuating results can be observed for the open circuit voltage. This fluctuation can be caused by the evaporation of oleylamine from the nanoparticles out of the active layer. This argument can be reinforced by the fact that some microscopy pictures revealed bumps in the Al electrode after the post thermal treatment. (Figure 34) This can be attributed to the escape of oleylamine out of the active layer.

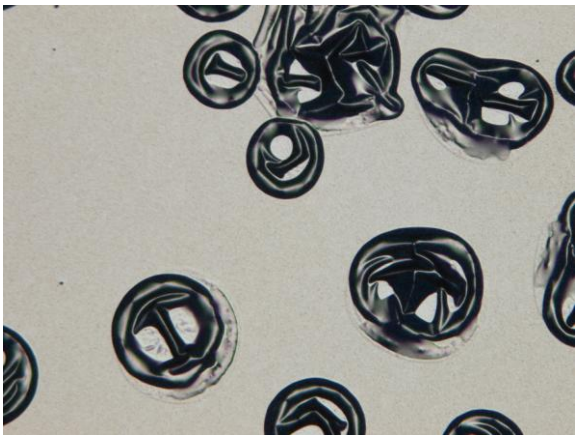

Figure 34 Aluminium electrode after post thermal treatment

Summarizing the hot plate annealing did not reveal a significant enhancement of the performance, overall it even decreased the efficiency of the solar cell. This could be caused by loosing contact area between the electrode and the active layer, due to lift of the Al.

[69] Dittmer, J.; Marseglia, E.; Friend, R. *Adv. Mater*. **2000**, 12, 17, 1270-1274

Considering the results and the literature another approach of annealing was tried out. The solar cells underwent annealing steps in a tube furnace under vacuum at 200 °C for either 15 or 30 minutes.

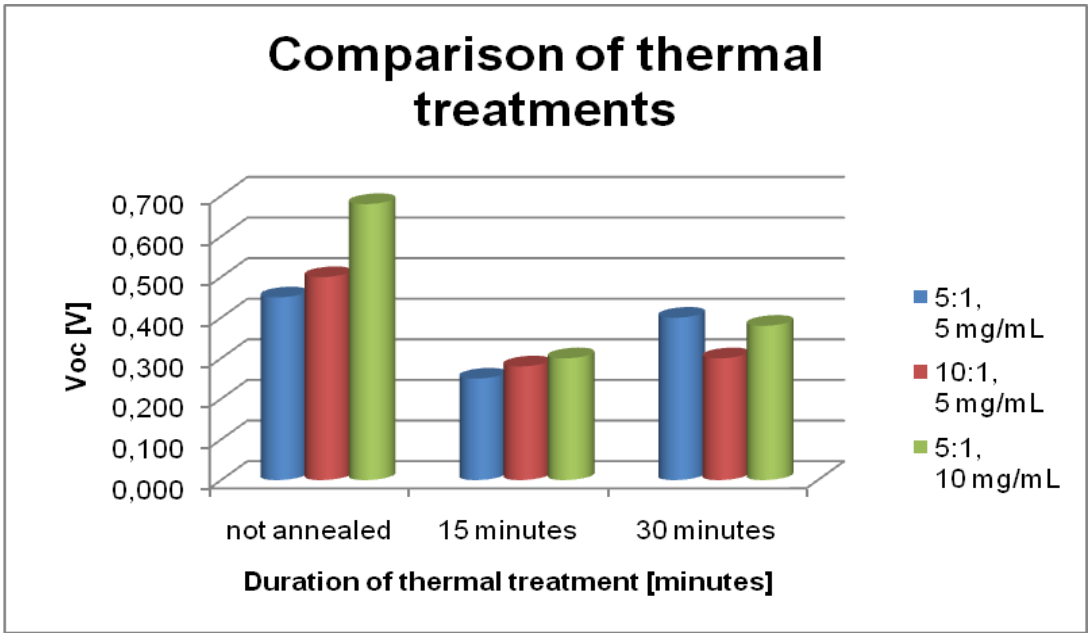

Figure 35 Open circuit voltage, comparison of thermal treatments

Figure 35 shows a comparison in the open circuit voltages of either 15 or 30 minutes of thermal treatments and no annealing. The data is shown for three different $CuInS_2$ nanoparticles:PSiFDBT ratios and polymer concentrations. In all cases a decrease of the V_{oc} from the not annealed solar cells to both thermal treatments can be observed. It can be assumed that it is attributable to the loss of oleylamine from the surface of the nanoparticles. Since the devices were annealed in a tube furnace under vacuum condition of 2.1 mbar. This circumstance leads to a decrease of the V_{oc} with more traps appearing on the surface of the solar cell and the effective band gap is smaller because of the additional energy levels of the traps.

However, simultaneously it can be seen that the short circuit current increases. (Figure 36)

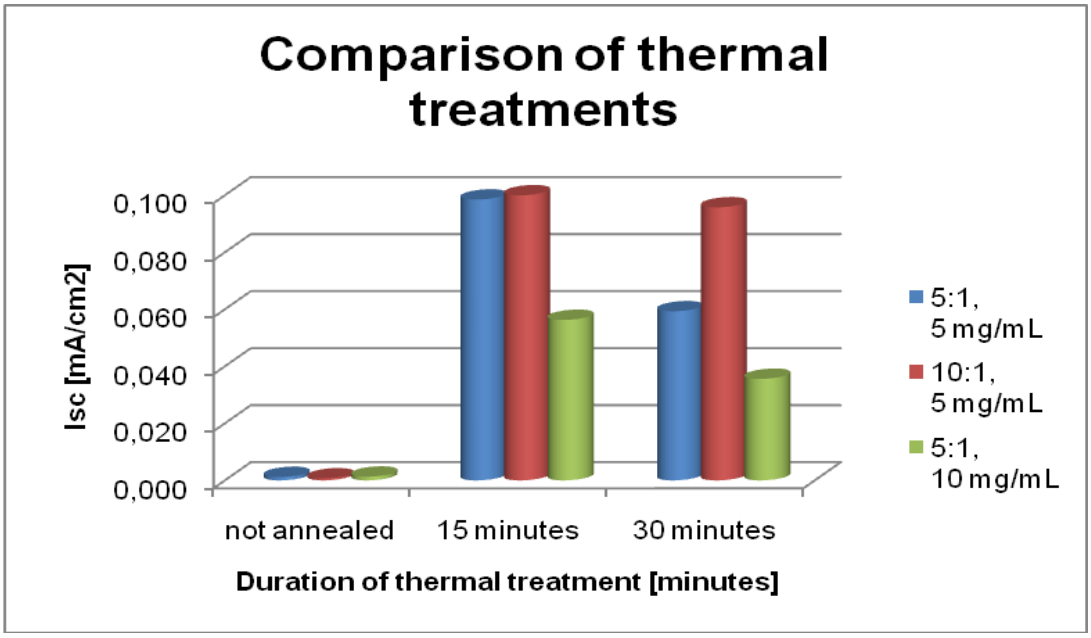

Figure 36 Short circuit current, comparison of thermal treatments

The data shows an increase of the I_{sc} from the not annealed solar cells to the solar cells, which underwent a thermal treatment. In all three mix ratios the increase can be seen. This can be explained by the reduced capper sphere around the particles. As a consequence the charge transfer is facilitated and an increase of the short circuit current is the result.

Due to these facts the annealing step has a positive effect on the efficiency, as it can be seen in Figure 37.

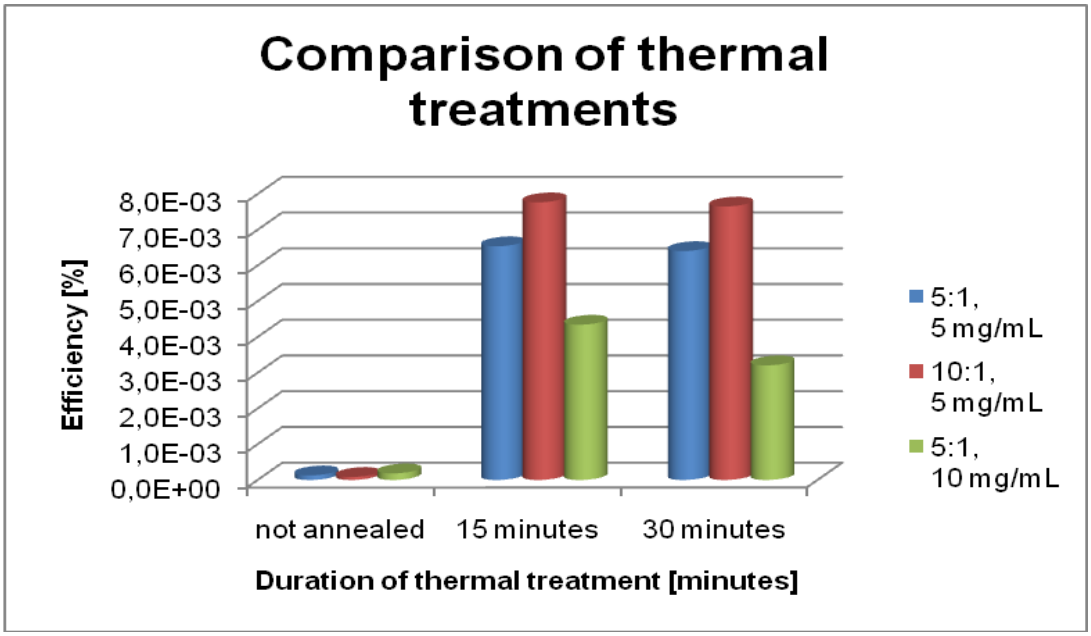

Figure 37 Efficiency, comparison of thermal treatments

All in all it can be said that an annealing step in the tube furnace has positive effects on the performance of the solar cell.

Having a close look on the data of the thermal treatment with durations of 15 minutes and 30 minutes differences between the annealing times can be observed. Once more three mix ratios of the two materials are compared. Each of the solar cells was annealed 15 and 30 minutes.

The comparison of the annealing times reveals an increase of the open circuit voltage after 30 minutes Figure 35, whereas the comparison of short circuit current of the solar cells exhibits a decrease after 30 minutes (Figure 36).
A possible explanation for the increase of the open circuit voltage after 30 minutes of annealing time is that due to the annealing less oleylamine is coordinated to the surface of the nanoparticles. Additionally the nanoparticles have more time to diffuse through the active layer. As a consequence the agglomeration cannot be prevented entirely. It could come to a depletion region of inorganic material due to a increase of the size of the agglomerates.[70] This agglomeration leads to a more defined surface with fewer traps and therefore to an increase of the open circuit voltage. A further indication for this assumption is found in the decrease of the short circuit current. Based on the possible agglomeration of the nanoparticles the contact area decreases between the donor and the acceptor phase. Due to the increased diffusion lengths in the active layer the competing recombination becomes more dominant.[67] The higher recombination rate can also be seen in the fill factor, which decreases with the longer annealing time of 30 minutes. (Figure 38) A further explanation for the decrease in efficiency after 30 minutes could lie in the starting decomposition of the polymer.

[70] Chang, L.; Lademann, H.; Bonekamp, J.; Meerholz, K.; Moule, A. *Adv. Funct. Mater.* **2011**; 21; 1779-1787

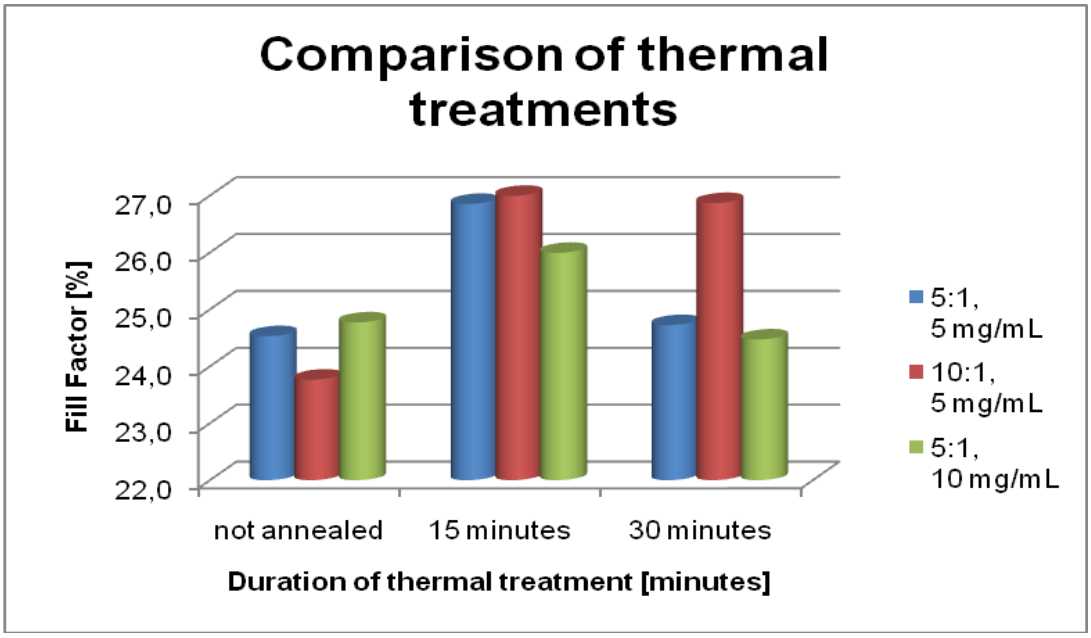

Figure 38 Fill Factor, comparison of thermal treatments

Due to the fact that the efficiency decreases after 30 minutes, it has been decided to continue on with an annealing time of 15 minutes.

In this experiment the best solar cell was prepared with an annealing time of 15 minutes and a $CuInS_2$ to PSiFDBT ratio of 10:1 with a polymer concentration of 5 mg/mL. The V_{oc} of this solar cell was 280 mV, the I_{sc} was $1.1*10^{-1}$ mA/cm^2, a fill factor of 27.3 % and an efficiency of $8.5*10^{-3}$ % were measured.

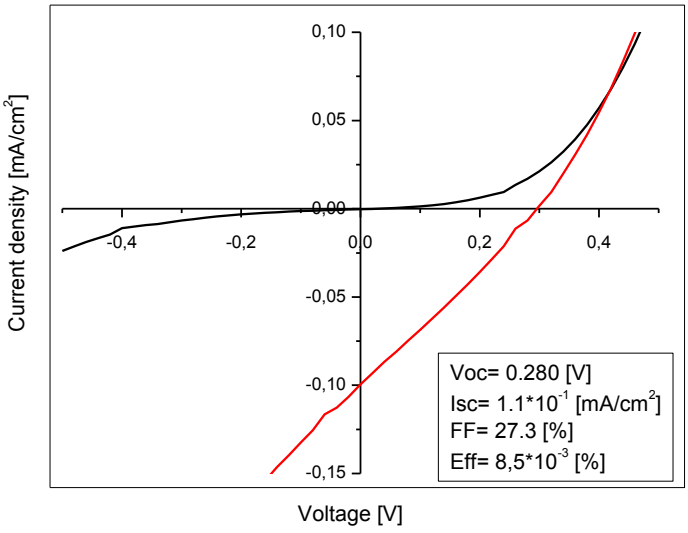

Figure 39 I-V characteristic of the best performing solar cell after an annealing time of 15 minutes

In recapitulation it can be noticed that annealing increases the efficiency of the solar cell due to the further remove of oleylamine on the surface from the nanoparticles and therefore a reduction of the electric barrier, which was caused by the long bulky organic tail of the oleylamine. As a consequence the charge transfer is facilitated and the short circuit current increases.
Moreover it was found that an annealing time of 30 minutes was worse compared to an annealing time of 15 minutes in case of the efficiency.

3.3.5 Modified nanoparticles

Surface modification of nanoparticles is a crucial factor to enhance the performance of solar cells, as it has already been described in chapter 3.2. The modified particles described in 3.2.2 and 3.2.4 were used for the fabrication of solar cells. For the reason that the particles treated with pyridine were not soluble, they could not be incorporated on the devices.
Devices fabricated with non-treated particles, particles with a ligand exchange treatment of tetrahydrothiophen (THT) and a reduced capping sphere, obtained after washing with hexanoic acid, were compared. All of them were prepared with a nanoparticle to polymer ratio of 10:1 and a polymer concentration of 5 mg/mL. In order to see if annealing also has a positive effect on the performance of the solar cells, as it was shown in chapter 3.3.4, the substrates were both not annealed and annealed for 15 minutes.
The reference device was measured and calculated. All the results are shown in Table 9. Looking at the results of the reference device, it can be observed that with the annealing step of 15 minutes, all parameters of the IV-characteristic increased, which is not the case when the modified nanoparticles are incorporated into the devices.

Table 9 **V_{oc}, I_{sc}, fill factor and efficiency values of the solar cells build with THT and HS modified nanoparticles and the reference**

	V_{oc} (mV)	I_{sc} (mA/cm^2)	Fill factor (%)	Efficiency (%)
Reference-Not annealed	250	$1.0*10^{-4}$	24	$6.2*10^{-6}$
Reference- 15 minutes	260	$2.8*10^{-1}$	30	$2.2*10^{-2}$
THT- not annealed	270	$8.3*10^{-2}$	27	$6.1*10^{-3}$
THT- 15 minutes	230	$2.8*10^{-1}$	28	$1.9*10^{-2}$
HS- not annealed	60	$3.1*10^{-2}$	23	$4.8*10^{-4}$
HS- 15 minutes	20	$7.2*10^{-2}$	18	$3.0*10^{-4}$

Comparing the reference solar cell with the devices prepared with the modified nanoparticles a trend in their performance is visible. The solar cell with the modified nanoparticles applied, which did not undergo a thermal treatment, show an enhancement in the performance, whereas after the annealing both the solar cells with THT treated nanoparticles and the substrates with hexanoic acid (HS) treated nanoparticles reveal a decline in their performance compared to the reference cell. Still the solar cells prepared with the THT treated nanoparticles after the annealing were in the same range in the efficiency as the reference cell.

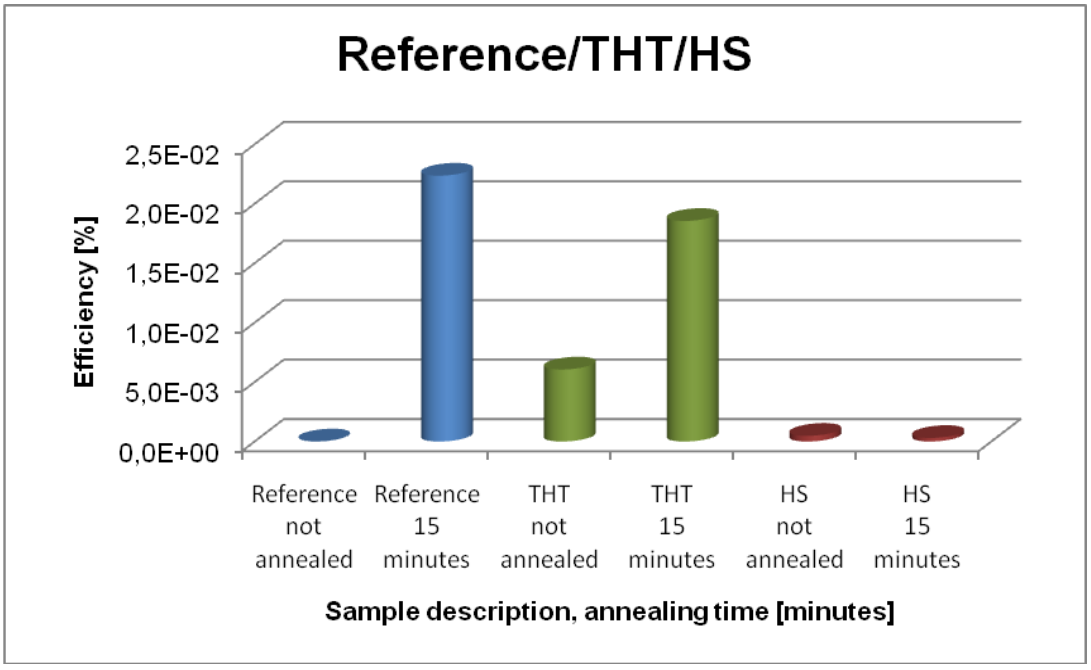

Figure 40 **Comparison of the efficiency of a reference solar cell (blue), a solar cell prepared with modified nanoparticles with tetrahydrothiophen (green, THT) and a solar cell with nanoparticles which underwent an hexanoic acid treatment (red, HS)**

These results show that the modification of the nanoparticles did work and even caused a positive effect on the performance, since the efficiency of the not annealed devices increased approximately three decimal powers (efficiency: $6.1*10^{-3}$ %) in the case of THT nanoparticles. For the HS nanoparticles the efficiency showed an improvement of less than 2 decimal powers (efficiency: $4.8*10^{-4}$ %). As already proven, the exchange with THT as wells as the minimization of the capper sphere worked (chapter 3.2.2 and 3.2.4). Although it was noticed that these particles tend to agglomerate and were not as soluble as their counterparts covered in oleylamine, it can be assumed that the treatment had an influence on the charge transfer behaviour, due to an increase in the I_{sc}. The loss of the non conductive oleylamine had a positive effect.

It is noticeable that the annealing of 15 minutes enhanced the performance of the solar cells in the case of oleylamine capped nanoparticles and THT treated nanoparticles (efficiency after annealing:$1.9*10^{-2}$ %). Only the HS treated nanoparticles (efficiency after annealing: $3.0*10^{-4}$ %) revealed a decrease after the thermal treatment. This results lead to the speculation that with the annealing step a good amount of oleylamine is removed from the surface. Therefore in the case of the HS nanoparticles it is assumed that it leads to a bigger tendency of agglomeration. In the case of THT and oleylamine capped nanoparticles fewer loss of the capping agent improves the performance. Nevertheless in the case of the modified nanoparticles the oleylamine was already reduced and with the thermal treatment even more oleylamine and even exchange molecules are removed (boiling point of tetrahydrothiophene: 119 °C), which leads at the same time to agglomerates of the nanoparticles in the active layer and hence, reduces the efficiency of the devices, because of less acceptor/donor interface. These results show how delicate the optimization of nanoparticles is, in order to find the balance between capping agent and modification process.

All results considered, it can be said that the modification of the nanoparticles had advantageous and disadvantageous effects on the performance of the solar cell. With no thermal treatment the efficiency increased, which lead to the assumption that both the capper exchange as well as the minimization of the capper sphere were successful. In the case of an annealing step it looks as the modified particles did not contributed to the performance of the solar cell compared to the reference solar cell, but the solar cells prepared with the THT nanoparticles were in the same value range. However, it is assumed that it correlated with the fact that the nanoparticles were already less soluble after the experiment, described in chapter 3.2.2 and 3.2.4 and probably agglomerate in the active layer, due to the further loss of oleylamine, which lead to a decrease of contact area of acceptor/donor and thus a decrease in the performance.

As mentioned before in chapter 3.2, the modification of the nanoparticles worked. It was successful to incorporate the nanoparticles into the solar cell and obtain working devices, but more optimization work would have to be done, particularly to find the right compromise of how much capping agent get removed to improve the conductibility but still prevent agglomeration.

3.3.6 Additional treatment with benzene-1,2-dithiol

Wu et al. reported a way to improve the efficiency in CdSe/P3HT solar cells through a chemical vapour annealing. While it is mainly reported that the use of capper exchange reactions to enhance the charge transfer of the nanoparticles, Wu et al. found a way to improve the performance of a solar cell during solar cell fabrication.[71] On the account that modifying the surface of the nanoparticles was already realized by acid treatment and capper exchange with pyridine and tetrahydrothiophen, a different approach was adopted. Wu et al. prepared hybrid solar cells composed of CdSe nanoparticles as the acceptor phase and the polymer P3HT as the donor phase. The samples, which were treated with the benzene-1,2-dithiol, underwent the vapour annealing right after the spin coating. It was reported on an enhancement of 66% in I_{sc} and 70% in efficiency. The improvement of the short circuit current and the efficiency was explained by two reasons. First it could be possible that the benzene-1,2-dithiol molecules diffuse into the layer react with the CdSe nanoparticles and replace the capping molecule, which results in an increase of charge transfer. Secondly when benzene-1,2-dithiol vapour interacts with the nanoparticles it effects the morphology in a different way as it can be done by a regular annealing process.

On the basis of this research the approach of chemical vapour annealing was applied to the system used in this work. Hence, solar cells with a nanoparticle to polymer ratio of 5:1 and a polymer concentration of 10 mg/mL were produced. In order to cover all possibilities of chemical vapour annealing, the benzene-1,2-dithiol treatment was applied after spin coating the active layer, after the solar cells were annealed either 15 or 30 minutes and after the evaporation of the aluminium electrode. Furthermore, in one additional experiment it was tried to see the influence of benzene-1,2-dithiol as an additive in the solution for the active layer. The working group of Peet et al.[72] as well as the review by Saunders and Turner[67] reported on an increase of the performance of the

[71] Wu, Y.; Zhang, G. *Nano Lett*. **2010**, 10, 1628-1631

[72] Peet, J.; Kim, J.; Coates, N.; Ma, W.; Moses, D.; Heeger, A. *Nature Mater.* **2007**; doi:10.1038/nmat1928

solar cell, when adding an alkanedithiol to the active solution. The improvement was explained by a better morphology of the active layer caused by the alkanedithiol. During every experiment a reference solar cell was prepared, which was not treated with benzene-1,2-dithiol, so that the performance of the solar cell could be compared to the used system.

I-V characteristics were recorded. Looking at the experiment in which the benzene-1,2-dithiol treatment was applied after the evaporation of the electrode when the devices were not annealed, the results of the devices revealed an increase in the efficiency of 2.5% additionally in the V_{oc} of 30% and 31% of the fill factor can be observed, whereas a decrease of 52% of the I_{sc} can be noticed. Before the treatment the devices were characterized with an efficiency about $1.86*10^{-4}$ %, a V_{oc} of approximately 690 mV, an I_{sc} around $1.4*10^{-3}$ mA/cm^2, a fill factor near 24.9%. After the treatment with the benzene-1,2-dithiol the efficiency increased to a value of approximately $1.91*10^{-4}$, a V_{oc} of around 900 mV, and a fill factor around 32.7%, but a decrease in the Isc with a value around $6.6*10^{-4}$ mA/cm^2. This increase in the efficiency can be ascribed to the increase of the V_{oc}. Overall there is a slight improvement in the efficiency of the solar cell.

When comparing the results of the I-V characteristics of all the experiments described in the beginning of this chapter, it can be seen that no increase in the efficiency occurred. The results of the experiments are summarized by the calculated median of the efficiencies of the different sets of experiments shown in Table 10.

Table 10 Efficiencies of the solar cells gained from the different sets of benzene-1,2-dithiol experiments

Moment of applying benzene-1,2-dithiol	Efficiencies [%]	Reference efficiency [%]
After spin coating	$1.3*10^{-4}$	$1.8*10^{-4}$
After annealing 15 minutes	$1,7*10^{-3}$	$4.3*10^{-3}$
After annealing 30 minutes	$1.6*10^{-3}$,	$3.2*10^{-3}$
After 15 minutes annealing and evaporation of the electrodes	$1.2*10^{-3}$ %	$4.3*10^{-3}$
After 30 minutes annealing and evaporation of the electrodes	$1.6*10^{-4}$	$3.2*10^{-3}$
As additive and no annealing	$5.3*10^{-5}$ %	$1.2*10^{-4}$
As additive and 15 minutes annealing	$1.8*10^{-3}$	$2.0*10^{-3}$
As additive and 30 minutes annealing	$8.4*10^{-4}$	$6.6*10^{-3}$

Although in the case of adding the benzene-1,2-dithiol into the active layer solution seemed to be better dissolved and the layers looked smoother, which would in principle indicate an improvement in the morphology of the active layer[72], no enhancement could be seen. Possible explanations why the desirable results were not observed could be that the oleylamine showed stronger ligand strength and therefore coordinated stronger to the surface of the nanoparticles, so that the benzene-1,2-dithiol could not replace the capper contrary to the case of alkylphosphonic acid, which was used by Wu et al. Another assumption is that the spin coated films were already to dry when the vapour annealing treatment took place. Therefore the active layer was already settled and the benzene-1,2-dithiol could not diffuse through the active layer or react with the nanoparticles and introduce a different morphology. However, this is quite speculative, since benzene-1,2-dithiol is a rather small molecule.

In conclusion it can be said that the chemical vapour annealing is an interesting and adoptable method for capper exchange of nanoparticles within a device. In this work the method by Wu et al was applied on $CuInS_2$ nanoparticles. Solar cells with PSiFDBT as donor material were fabricated, but did not show the desired enhancement of the solar cells. On that account further optimization work should be done to see the improvement of the performance of the devices.

3.3.7 Solvent mixtures

When looking at the top layer of the solar cell, it could be noticed that the surface revealed a rather rough surface, due to the fact that the evaporated Al electrodes did not feature the typical metallic shine. The more inorganic material was mixed into the solution for the active layer the less metal shine was displayed by the electrodes. On that account microscopy pictures were recorded. The pictures displayed that in the active layer some bigger agglomerates are present. It could not be determined if those agglomerates came from the nanoparticles or from the polymer. In order to overcome this process different approaches were tried out. It was tried to improve the solubility of the polymer as well as of the nanoparticles. Out of previous results it was known that the polymer as well as the nanoparticles were soluble in both chloroform and chlorobenzene. (chapter 3.3.1) On that account solvent mixtures of chloroform and chlorobenzene were tested. In order to cover an acceptable range three chloroform to chlorobenzene ratios were used: 5:1, 3:1 and 1:1.

I-V characteristics were recorded. For the fabrication of the solar cell a nanoparticles to polymer ratio of 7.5:1 with a polymer concentration of 5 mg/mL was used. All the solar cells underwent a thermal treatment of heating to 200 °C in 7 minutes and holding the

temperature at 200 °C for 15 minutes. In order to determine a variation in the performance of the solar cell, a reference was prepared with chloroform as solvent.

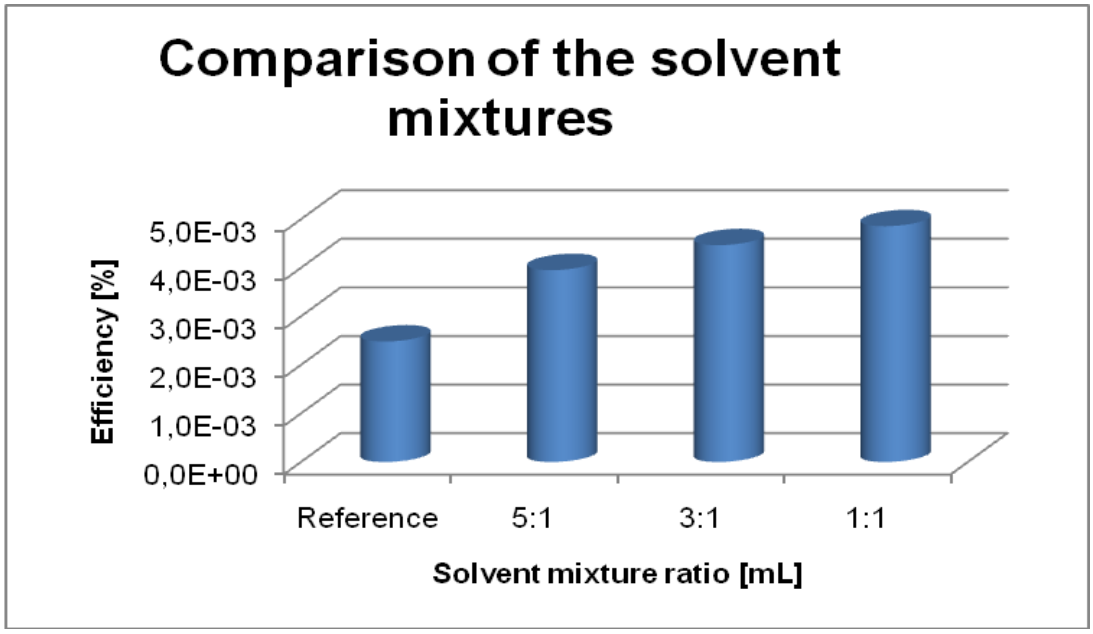

Figure 41 Efficiency of the solar cell as a function of solvent mixture ratios

In Figure 41 the efficiency as a function of the ratio of the solvent mixture is displayed. It can be observed, that with the increase of the chlorobenzene content an improvement in the efficiency of the solar cell can be observed. Moreover, the short circuit current increased from $3.2*10^{-2}$ mA/cm^2 of the reference to $5.9*10^{-2}$ mA/cm^2 for the 1:1 mixture. Simultaneously the fill factor increased from a value of 24.7 % of the reference to 27.0 % at the highest amount of chlorobenzene. Only the V_{oc} of the reference solar cell decreased from 340 mV to 280 mV of the solvent ratio of 1:1. The overall enhancement can be explained by two effects: first the solubility of the polymer increased by using chlorobenzene, thus it can lead to a better morphology and a higher mobility within the polymer. When producing the solar cell it was observed that the electrodes revealed more metallic shine the higher the amount of chlorobenzene was in the solvent mixture. That indicates that the layers became smoother, which indicated a better morphology within the layers. This could have lead to a better contact of the active layer and the Al electrode. The working group of Janssen[73] demonstrated that although the charge transfer decreases in PCBM/P3HT solar cells prepared in chlorobenzene solutions, the increase of the efficiency is based on an improvement of the morphology in the active layer. One possibility to explain this circumstance is that

[73] Janssen, G.; Aguirre, A.; Goovaerts, E.; Vanlaeke, P.; Poortmans, J.; Manca, J. *Eur. Phys. J. Appl. Phys*. **2007**; 37; 287-290

chlorobenzene has a higher boiling point than chloroform, thus it evaporates slower and as a consequence the nanoparticles have more time to diffuse and disperse through the polymer network. The polymer chains can undergo the crystallisation process and arrange themselves in the active layer. The crystallisation leads to a higher degree of order and a low series resistance, which again can enhance the performance of the devices. Li et al. investigated chloroform and chlorobenzene as solvent for their devices using a system of PCBM and P3HT. An increase of the efficiency was seen by using chlorobenzene, due to the higher boiling point and a reduction in the solution evaporation rate.[74] Secondly due to the observations in chapter 3.3.1 it was noticed that the layer thickness was thinner when using chlorobenzene as a solvent. It is possible that a thinner layer has positive effects on the performance. As described by Moule et al, if the thickness of the active layer is too thin it results in a poorer efficiency.[75] This can be explained due to a greater total absorption of light if the layers are thicker. Contrary to this the recombination of the excitons in the polymer is more likely, caused by an increase in the distance, which the electrons have to diffuse to reach the electrode.[67] A thickness between 100-225 nm was suggested to be most efficient.[75] In order to get more information about the layer thickness profilometer measurements can be made.

Altogether it can be said that the solvent mixture has a positive influence on the performance of the solar cell. With increased content of chlorobenzene the layers appeared smoother. This can imply an improvement in the morphology of the layer, which can lead to an enhancement of the efficiency of the solar cell. Chlorobenzene can even affect the layer thickness and as a consequence the performance of the solar cell increased.

[74] Li, W., Guo, J., Sun, X.; Zhou, B. *Proc. SPIE 7847* **2010**; 784709; doi:10.1117/12.868374

[75] Moule, A.; Bonekamp, J.; Meerholz, K, *J Appl. Phys* **2006**; 100:094503

4 Experimental Work

4.1 Used chemicals, materials and solvents

All chemicals, materials and solvents used for the synthesis of nanoparticles and preparation of solar cells, are listed with purity and source of supply in the following Table 11. If not noted differently all chemicals are used without further purification.

Table 11: List of chemicals, materials and solvents used for the experimental work

Chemicals / materials/solvents	Purity / properties	Source of supply
2 – propanol	puriss.	Sigma Aldrich
Acetone	puriss.	Sigma Aldrich
Aluminium	wire, 1.0mm diam., 99.98 percent	Umicore
Benzene-1,2-dithiol	96 percent	Aldrich
Chlorobenzene	99.8 percent	Aldrich
Chloroform	CHROMASOLV, ≥ 99.999 percent	Sigma Aldrich
Chloroform	puriss. p.a.	Sigma Aldrich
Copper (I) iodide	purum, ≥ 99.0 percent	Riedel-de Haën
Hexanoic acid	99.5 percent	Aldrich
Hydrochlorid Acid	37 percent - 38 percent, fuming	J. T. Baker
Indium (III) chloride	98 percent	Aldrich
Indium (III) chloride	99.999 percent	Aldrich
ITO-covered glass substrates	15 x 15 mm, R_S 15 – 25 Ω	Delta technologies
Methanol	99.8 percent	Aldrich
Oleylamine	≥70 percent	Fluka
PEDOT:PSS	Baytron P VPAI4083	HC. Starck

Pyridine	CHROMASOLV, ≥ 99.9 percent	Sigma Aldrich
Sulfur	Sublimed, 100 mesh powder	Aldrich
Thiourea	puriss. p.a., ≥ 99.0 percent	Fluka
Tetrahydrothiphene	99 percent	Aldrich
Zinc powder	< 10 µm, ≥ 98 percent	Aldrich

4.1.1 Indiumtinoxide (ITO)

In this study Indiumtinoxide (ITO) covered glass substrates with the dimensions of 15 x 15 mm were mainly used, if not differently stated.
The ITO layer is a conductive electrode material. The advantages of the ITO layer are has a high transparency of over 78 percent in the visual spectra and additionally a good electric conductivity.[76]

4.1.2 PEDOT:PSS

Polyethylendioxythiophene (PEDOT), which is doped with Polystyrenesulfonate (PSS) to increase the conductivity, smooths the surface of the ITO electrode. The advantages of this material are that it possesses a higher work function of 5.1 eV in comparison to the ITO electrode (4.7 eV). This causes a higher open circuit voltage between the anode and cathode. Another positive aspect is that it operates as a diffusion barrier to oxygen, which would otherwise spread into the active layer and reduce the efficiency. Moreover, it is not vulnerable towards UV light or heat and is transparent. [76]

[76] Rath T. *Diploma thesis* **2005**, 23-24

4.2 Synthesis of $CuInS_2$ nanoparticles

The syntheses of $CuInS_2$ nanoparticles were accomplished under variable conditions. All of these synthesis methods are carried out in an oil bath. The parameters for the centrifugation were 3500 rpm for 10 minutes. The used characterization techniques are mentioned and described in chapter 4.2.6.
In the reactions described below, toxic and low volatile thiols can be evolved. All reactions were carried out under a fume hood and protection clothing was worn.

4.2.1 Influence of inert gas

100 mL oleylamine were degassed by argon for 25 minutes. 1.526 g (8 mmol, 1 eq.) CuI and 1.773 g (8 mmol, 1 eq.) $InCl_3$ were dissolved in 80 mL oleylamine. While the metal salt solution was heated, 20 mL degassed oleylamine were transferred into a Schlenk vessel and 1.540 g (48 mmol, 6 eq.) sulfur was added. Both flasks were heated to 170 °C for 40 minutes to assure that all the metal salts were dissolved. Afterwards 35 mL of the metal salt solution were given into a Schlenk vessel, one filled under atmospheric condition and the other one with argon as an inert gas. The two flasks were heated to 220 °C. As soon as the oil bath reached 220 °C, 8.75 mL of the sulfur solution were added. Henceforth the time was measured and samples were taken after 5, 15 and 40 minutes. The residue of the reaction was stored in the fridge and not precipitated.

After the certain reaction time, 2 mL of the nanoparticles solution were poured into 8 mL of cold methanol. Black $CuInS_2$ nanoparticles were precipitated and separated from the solution by centrifugation. The nanoparticles were re-suspended in methanol and once again centrifuged. The product was dried over night in the fume hood.
The particles were characterized by UV/Vis spectroscopy, photoluminescence spectroscopy, transmission electron microscopy (TEM) and x-ray diffraction (XRD).

4.2.2 Influence of inert gas and a prolonged reaction time

40 mL oleylamine and 10 mL oleylamine were filled into two separate flasks and degasified for 25 minutes. 0.764 g (4 mmol,1 eq.) CuI and 0.886 g (4 mmol, 1 eq.) $InCl_3$ were added to the 40 mL degassed oleylamine. The solution was heated to 170 °C for 40 minutes. 0.770 g (24 mmol, 6 eq.) sulfur was given into the 10 mL of degassed

oleylamine. As with the metal salt solution, the sulfur solution was heated to 170 °C for 40 minutes. For the second set the same procedure was applied but this time the oleylamine was not degassed. All of the samples were given into separate flasks but the same oil bath was used to assure the same temperature and time frame. The initial masses of the second set were 0.763 g (4 mmol, 1 eq) CuI and 0.886 g (4 mmol, 1 eq.) $InCl_3$, which were added into 40 mL of oleylamine and 0.770 g (24 mmol, 6 eq.) sulfur were added to 10 mL.
Immediately after the 40 minutes the reaction solution was heated up to 220 °C. When the reaction solution reached the final temperature, 8.75 mL sulfur solution was added. Samples were taken after 60, 180 and 300 minutes.

In order to separate the black $CuInS_2$ particles, 2 mL of the solution was precipitated in 8 mL of cold methanol. The nanoparticles were separated by centrifugation. This process was carried out 3 times. The product was dried over night in the fume hood.

The residue of the reaction was stored. The particles were characterized by UV/Vis and photoluminescence spectroscopy, transmission electron microscopy (TEM) and x-ray diffraction (XRD).

This experiment was repeated with the same ratio and concentration of the chemicals and the same temperatures under inert gas conditions as described in chapter 4.2.2. Samples were taken after 60, 90, 120, 150 and 180 minutes.

4.2.3 Influence of purified oleylamine

For this reaction the oleylamine was distilled. The distillation was carried out under a vacuum of 2.1 mbar in an oil bath of 230 °C. Three fractions were gained. The first fraction was separated at a temperature of 60-120 °C with a yield of roughly 15 percent of volume. The second fraction, which was also the fraction which was used in the reaction, was split off at a temperature of 150 °C with a yield of about 60 percent of volume. The final fraction was separated at a temperature of 160 °C-170 °C with a yield of approximately 25 percent of volume. The fractions were characterized by NMR. Subsequent the fraction 2 of the purified oleylamine was then degassed for 30 minutes.

0.229 g (1.2 mmol, 1 eq.) CuI and 0.266 g (1.2 mmol, 1 eq.) $InCl_3$ were added into 12 mL distilled oleylamine. The solution was heated up to 170 °C for 40 minutes. At the same time 0.269 g (8 mmol, 6.7 eq.) were added into 3.5 mL of distilled oleylamine and

heated up to 170 °C for 40 minutes. Next 3 mL (0.231 g, 7 mmol, 6 equ.) of the sulfur mixture was added to the metal salt solution.

Into a centrifugation vial 2 mL of the solution were transferred every 10 minutes and cooled off for 5 minutes. Then 8 mL of methanol were added and centrifuged in order to isolate the particles. This procedure was repeated 3 times. In the fume hood the samples were dried over night.
The particles were characterized by UV/Vis spectroscopy, photoluminescence spectroscopy, transmission electron microscopy (TEM), IR spectroscopy and x-ray diffraction (XRD).

The residue of the solution was precipitated in 10 mL methanol and centrifuged once.

NMR: distilled oleylamine

^{1}H NMR: 5.34 ppm (m, 4H, *NH_2, CH=CH*), 2.67 ppm (t, NH_2-*CH_2*-CH_2), 2.0 ppm (m, 4H, *CH_2*-CH=CH-*CH_2*), 1.42 ppm (t, 2H, NH_2-CH_2-*CH_2*), 1.28 ppm (m, 20H, CH_3-CH_2-*CH_2*-*CH_2*-*CH_2*-*CH_2*-*CH_2*-CH_2, NH_2-CH_2-CH_2-*CH_2*-*CH_2*-*CH_2*-*CH_2*-CH_2, CH_3-*CH_2*), 0.87 ppm (t, 3H, CH_3)

^{13}C NMR: 129,9 ppm (*CH=CH*), 42,29 ppm (NH_2-*CH_2*), 33,90 ppm (*CH_2*-CH=CH-*CH_2*), 32,58 ppm (NH_2-CH_2-*CH_2*), 31,89 ppm (CH_3-CH_2-*CH_2*), 29,23-29,73 ppm (CH_3-CH_2-CH_2-*CH_2*-*CH_2*-*CH_2*-*CH_2*,CH-CH-CH_2-*CH_2*-*CH_2*-*CH_2*), 26,87 ppm (NH_2-CH_2-CH_2-*CH_2*), 14,09 ppm (*CH_3*), 22,65 ppm (CH_3-*CH_2*)

4.2.4 Influence of exchanging the sulfur source

The purified oleylamine, as described in chapter 4.2.3, was used in this reaction. 0.229 g (1.2 mmol, 1 eq.) CuI and 0.265 g (1.2 mmol, 1 eq.) $InCl_3$ was mixed into 12 mL distilled oleylamine. The solution was heated up to 170 °C for 40 minutes. While the metal salts were dissolved, 0.267 g (3.5 mmol, 3 eq.) thiourea was added into 3.5 mL of oleylamine. The solution was stirred at 50 °C for 30 minutes. Meanwhile the metal salt solution was cooled to room temperature. 3 mL of the thiourea solution (0.229 g, 3 mmol, 2.5 eq.) were added to the metal salt solution and immediately heated up to 220 °C in the preheated oil bath.

With a thermometer the temperature was controlled. As soon as the solution reached 220 °C time measurement for taking the samples were started. The heating rate was 13 °C/min. Every 10 minutes a sample was taken for a timeframe of 60 minutes.

In order to separate the $CuInS_2$ nanoparticles the solution was precipitated. 2 mL of the solution were put into a centrifugation vial and cooled down for 5 minutes. Next 8 mL of methanol were added and for separation the solution was centrifuged. The product was dried in the fume hood over night.
The particles were characterized by UV/Vis spectroscopy, photoluminescence spectroscopy, transmission electron microscopy (TEM), IR spectroscopy and x-ray diffraction (XRD).

4.2.5 Synthesis of $CuInS_2$ nanoparticles for the usage in solar cells

CuI (6.681 g, 35 mol, 1 eq.) and $InCl_3$ (7.753 g, 35 mol, 1 eq.) were dissolved in 350 mL of distilled oleylamine. Subsequent the oleylamine was degassed for 30 minutes. The solution was heated to 170 °C for 30 minutes resulting in a clear solution. Afterwards the solution was cooled down to room temperature, followed by adding of 6.676 g (87.5 mol, 2.5 eq.) thiourea to the metal salt solution. After stirring the solution for 5 minutes the solution was heated up to 220 °C in a preheated oil bath. The temperature of the solution was monitored with a thermometer. As soon as the solution reached 205 °C the time was taken. A heating rate of 4.3 °C/min was reached. After 20 minutes the reaction was stopped and the resulting solution was cooled down and precipitated in 1.4 L of methanol and separated by centrifugation. The particles were washed by suspending in methanol and separated by centrifugation then they were dried under a fume hood. A yield of 94.98 percent was received, after drying the particles under vacuum for 2 days.
The particles were characterized by UV/Vis spectroscopy, photoluminescence spectroscopy, transmission microscopy (TEM), IR spectroscopy and x-ray diffraction (XRD).

4.2.6 Characterization techniques

4.2.6.1 Powder X-ray diffraction (PXRD)

In order to gain further information on the crystallographic structure of the nanoparticles, powder X-ray diffraction (PXRD) was carried out. The particles were characterized on a PANalytical, Expert PW3710 operated at 40 kV and 35 mA, using CuK α-radiation (λ= 154.06 pm) at a step scan modus of 0.035° / step with 12-16

seconds / step a 2 θ – range of 5.00 - 95.00°. By analysing the X-ray diffraction patterns it was possible to estimate the average particle size of the $CuInS_2$ nanoparticles. Hence the Scherrer equation was used, which is based on the broadening of the diffraction peak. (Equation: (4))

$$D_{XRD} \approx \frac{K * \lambda}{\Delta(2\theta) * \cos(\theta)} \quad \textbf{(4)}$$

K...shape factor, which is 0.9 for spherical particles

λ....wavelength of the x-rays

Δ(2θ)...full width at half maximum (FWHM) for the peak radians

Θ...half of the scattering angle 2θ.

This equation is only a good approximation for spherical particles. For the calculation of the particles size, the (204) reflection at 2θ=46.5° was used. The calculated sizes of the Scherrer equation are listed in the corresponding tables in the corresponding chapters.

4.2.6.2 Transmission electron miscroscopy (TEM)

Transmission electron microscopy (TEM)-images were done on a Tecnai F 20 microscope (FEI Company) with a Schottky emitter, an UltraScanCCD camera and a Gatan GIF Quantum energy filter system. Selected area electron diffraction measurements were evaluated by determination of the diffraction center and measurement of the ring radii using the method and software plug-in described by Mitchell.[77] TEM-samples for imaging were prepared from a dispersion of 0.04 mg/mL particles in chloroform by putting a drop of the dispersion on a Nickel-TEM-grid with a carbon film and evaporation of the solvent. With the help of the computer program “DigitalMicrograph” by the company Gatan values for the sizes of the nanoparticles can be read out of the TEM images.

4.2.6.3 UV/Vis spectroscopy

A Shimadzu UV-1800 UV-Spectrophotometer in combination with the software UVProbe 2.31 was used for measuring UV-Vis spectra. The particles were dissolved in chloroform with a concentration of 0.1 mg/mL, if not noted differently.

---

[77] Mitchell, D.R.G. *Ultramicroscopy* **2008**, 108, 367-374

4.2.6.4 Photoluminescence spectroscopy

Photoluminescence spectroscopy was performed on the spectrofluorimeter RF-5301PC from Shimadzu.

4.2.6.5 Dynamic light scattering (DLS)

The size of the particles was determined by dynamic light scattering (DLS) using a Malvern Zeta Sizer ZEN 3600 from Malvern Instruments (He-Ne laser with a wavelength of 633 nm and a power of 4.0 mW) in chloroform solutions. The concentration of the solutions was 3 mg/mL. The data were evaluated by the computer program origin 8.5.

4.2.6.6 Thermogravimetric analysis (TGA)

Thermogravimetric analysis (TGA) measurements were performed with a simultaneous thermal analyzer STA 449 C Jupiter from Netsch-Gerätebau gmbH (crucibles: aluminium) with a heating rate of 10 °C/min in a flow of He (50mL/min).

4.2.6.7 Fourier transform infrared spectroscopy (FTIR)

FTIR-spectroscopy was carried out on a Perkin Elmer FT-IR-spectrometer Spectrum One. For all measurements CaF_2-substrates were used.

4.2.6.8 Nuclear magnetic resonance (NMR)

The ^{1}H NMR spectra was analyzed with a Bruker Avance III 300 MHz spectrometer. All the samples were dissolved in deuterated chloroform. The measuring was carried out with 32 scans and a delay of 2 seconds.
The ^{13}C NMR was also analyzed with a Bruker Avance III 300 MHz spectrometer with 256 scans and a delay of 2 seconds.

4.3 Optimizing the capper sphere

The used characterization techniques are described in chapter 4.2.6.

4.3.1 Size-selective precipitation

The size selective precipitation was done by stepwise addition of methanol (experiment SP1). 2 mL methanol were added to 3 mL of the residue of the particles described in chapter 4.2.1. The precipitates and the supernatant were separated by centrifugation. Then the next portion of methanol was added to the supernatant. This procedure was repeated 3 times. The product was characterized through DLS and UV/Vis spectroscopy.[78]

This experiment (SP2) was repeated by using a smaller portion of methanol. Therefore 1.25 mL of methanol were added to 5 mL of the turbid $CuInS_2$ nanoparticles solution. This procedure was repeated 3 times and at last a big excess of methanol was added to precipitate all remaining particles in the reaction solution. Over night the particles were dried in the oven at 40 °C. The fractions were characterized by DLS.[53]

For the experiment (SP3) 1 g of the particles, described in chapter 4.2.5, were dissolved in 5.5 mL chloroform. 550 µL methanol were added to this resulting solution. The precipitates and the supernatant were separated by centrifugation. Then another 2.75 mL methanol were added to the supernatant obtained from this procedure and another centrifugation was performed. The last fraction was gained by adding methanol abundantly. The product was dried over night in the fume hood followed by a drying process in the oven at 40 °C for 15 hours. For the first fraction 4.9 percent were obtained, the second fraction yielded 7 percent and the last fraction hold 87.9 percent.

4.3.2 Minimizing the capper sphere

In order to reduce the capper sphere around the $CuInS_2$ nanoparticles hexanoic acid was used. [54,55]

---

[78] Ferreira, D.L.; Silva, F.O.; Viol, L.C.S.; Schiavon, M.A.; Licinio, P.; Valadares, M.; Cury, L.A.; Alves, J.L.A. *29th International Conference on the Physics of Semiconductors* **2009**,CP1199

For the pre-testing two different fractions of particles were used. First $CuInS_2$ nanoparticles, which were obtained after the synthesis described in chapter 4.2.1, were used. The particles were mixed with the hexanoic acid in a weight ratio of 1:12. The suspension was heated to 80 °C for 10 minutes. Then the solution was cooled to room temperature and separated by precipitation in methanol.
Secondly on fraction 3 of the size-selective precipitation, described in chapter 4.3.1, the acid treatment was applied. 50 mg of the nanoparticles were dissolved in 600 mg of hexanoic acid and heated to 80 °C for 10 minutes. Then the mixture was cooled to room temperature and precipitated in 1 mL of methanol.

The particles, which were used for the assembly in the solar cells, also underwent the acid treatment. 204 mg (0.8 mmol) $CuInS_2$ nanoparticles as described in chapter 4.2.5 were dissolved in 500 µL chloroform. 30 mL of hexanoic acid were supplemented to the solution. After stirring the obtained mixture for 10 minutes at 70 °C, 50 mL of methanol were added. The reagents were combined in a ratio of nanoparticles to hexanoic acid to methanol 1:15:25 in terms of volume. For separating the precipitates from the supernatant the solution was centrifuged. The precipitates were suspended in 3 mL chloroform and 6 mL of methanol were added. This solution was stirred for 5 minutes and heated to 45 °C. Then the product was separated by centrifugation and dried over night in the fume hood. [54]

4.3.3 Capper exchange with pyridine

200 mg (0.8 mmol) of the $CuInS_2$ nanoparticles as described in chapter 4.2.5 were dissolved in 50 mL pyridine. The resulting solution was heated to 118 °C and held on this temperature under reflux for approximately 15 hours. The temperature was chosen because of the boiling point of 115 °C of pyridine. Next the particles were precipitated at room temperature in 40 mL hexane. It was tried to recover the product by centrifugation, but the supernatant was turbid after the centrifugation. The centrifugation was repeated twice, with no significant improvement. Afterwards 3 mL of the supernatant were mixed with another 8 mL hexane but the particles still could not be recovered. 1 mL of the supernatant was supplemented with 5 mL of methanol and once again the particles could not get separated by centrifugation. The supernatant was split into half and 40 mL hexane were added to one half and centrifuged again. At last 20 mL hexane were added. This provides a ratio of 1:2 in case of pyridine:hexane. The product was separated by centrifugation and the supernatant was stored. The particles, that precipitated, were dried over night in the fume hood. The particles could

not be resuspended. The solvents applied were chloroform, pyridine, a solvent mixture of 20:80 pyridine:chloroform and chlorobenzene. IR-measurements were performed.

4.3.4 Capper exchange with tetrahydrothiophen (THT)

Tetrahydrothiophene (THT) was used to exchange the capper of the $CuInS_2$ nanoparticles. 202 mg (0.8 mmol) $CuInS_2$ nanoparticles were dissolved in 50 mL THT and the reaction was heated to 124 °C under reflux for 24 hours. This temperature was chosen due to a boiling point of 121 °C of THT. The reaction solution was cooled to room temperature and stirred for another day. In order to identify the right precipitation solvent, methanol and hexane were tried. The product was separated by centrifugation and dried in the fume hood under argon. Subsequently both precipitates were suspended in the same amount of chloroform. The particles that precipitated in methanol were less soluble than the particles precipitated in hexane. In addition FTIR spectroscopy was done where no differences were detected. Therefore hexane was used as a precipitation solvent and 96 mL were inserted to 48 mL of the reaction solution. The precipitates were separated from the supernatant by centrifugation and dried over night in the fume hood.

4.4 Production of nanocomposite solar cells

Figure 42 shows the flow diagram of the fabrication steps for the solar cells. Detailed information are described in the following chapters.

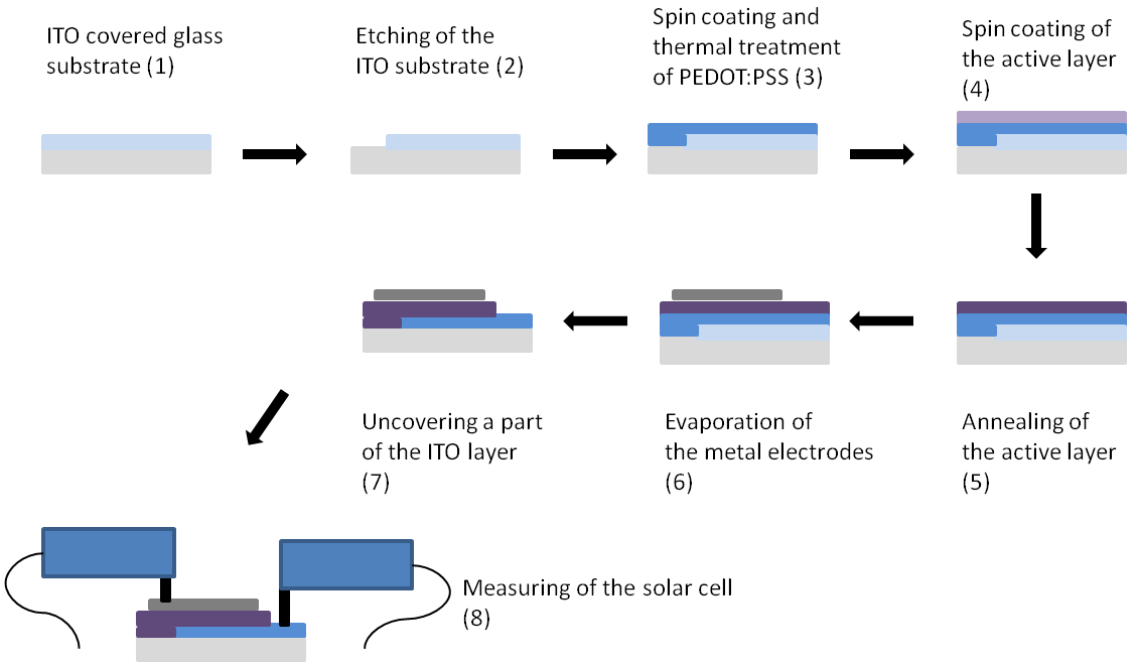

Figure 42 Flow diagram for the fabrication of a solar cell

4.4.1 Pre –treatment of the substrate

The substrates for the solar cell have to be pre-treated beforehand in order to optimize the conditions for applying the layers. The pre-treatment consisted of chemical etching and of cleaning the substrates in the right way.

4.4.1.1 Chemical etching

This process was necessary due to the way how the I-V characterizations of the solar cells were recorded. The upper electrode got contacted with test tips. As the measurement tip can transfix the electrode and the active layer both, the upper and lower electrodes could be in contact. If chemical etching was not applied a short circuit would occur.

In the first step of the process adhesive tape was put on the main part of the substrate in order to protect the ITO layer on the substrate against etching. Next the ITO covered glass substrate was dipped into water and put into zinc powder. In order to

remove the ITO layer the substrate was put into fuming hydrochloride acid. In a final step the substrate was washed with water. Afterwards the substrate was washed with acetone to take off the residues of the tape. It was of utmost importance to be careful that the etching edge was a straight line and that it had almost no indentations.

4.4.1.2 Cleaning of the substrate

The cleaning process had to be done very carefully due to the fact that there should be no dust or other residues which could disturb the performance of the solar cell. The procedure consisted of 4 steps.

The first step started with acetone as described in chapter 4.4.1.1 by removing the residues of the tape. Next the substrates were washed with water and cleaned in an ultrasonic bath for 20 minutes at 30 °C. Afterwards they were transferred into an isopropanol bath and left again for 20 minutes at 30 °C.

Before starting the preparation of the layers of the solar cells, the substrates were cleaned with a non-fuzzing tissue to remove all sticky residues and dust and in addition acetone was dropped on the substrate and taken off with a stream of nitrogen.

4.4.2 General preparation techniques and equipment

4.4.2.1 Spin coating

During this work the layers were applied by spin coating on a spin coater CT62 produced by the company Karl Suss Technique. The schematic illustration of the principal working steps is shown in Figure 43. Two layers were applied by spin coating. For the PEDOT:PSS layer a standard procedure was used. Therefore a speed of 2500 rpm was reached with an acceleration of 300 rpm/s and kept constant for 30 seconds. For the active layer a speed of 2000 rpm was reached with an acceleration of 300 rpm/s and held for 20 seconds. As not stated otherwise all the layers were applied via spin coating with the parameters described above.

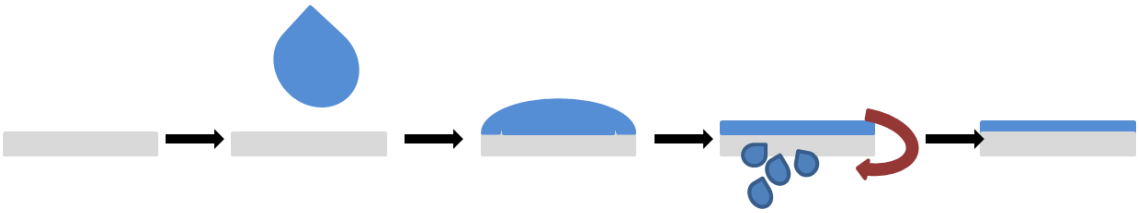

Figure 43 Schematic illustration of spin coating

4.4.2.2 Thermal treatment

For the thermal treatment a MR Hei-Standard magnetic stirrer combined with an EKT Hei-Con external control unit and a temperature sensor was used. This magnetic stirrer was used to dry the PEDOT:PSS layer at 150 °C for 10 minutes as well as for the experiments to anneal the active layer after measuring the solar cells without thermal treatment. In this case a temperature of 200 °C for 15 minutes was applied.
The annealing step for the solar cells was carried out in inert gas atmosphere and had taken place in a tube furnace from Heraeus (RO 4/25 in combination with a controller RE 1.1).

4.4.2.3 Evaporation of metal electrodes

The metal electrodes were made of Al and were applied by evaporation. For this an evaporation unit MED 10 Baltec was used. Before the solar cells were put into the evaporation unit, a shadow mask was taped on the substrate in order to get a structured and a well defined area of the electrodes. The evaporation of the metal was done under a vacuum higher than $5*10^{-5}$. The evaporation unit MED 10 used a top down evaporation with a tungsten coil.

4.4.3 Fabrication of solar cells with $CuInS_2$ nanoparticles

The first steps for the preparation of the solar cells were the chemical etching and cleaning process. Next the solutions were prepared in variable concentrations and inorganic to organic ratios. This will be described in detail in the following chapters. If not mentioned differently the $CuInS_2$ nanoparticles described in chapter 4.2.5 were used for the fabrication of the solar cells. Moreover if not noted otherwise, the polymer PSiFDBT was used as donor material. Also all the solutions were dissolved in chloroform and filtered with a 1.2 µm nylon filter as not stated otherwise. The PEDOT:PSS (Baytron P VPAI 4083) was diluted with water in a ratio of 3:7 and afterwards spin coated as described in chapter 4.4.2.1. The PEDOT:PSS layer was dried in the glove box for 10 minutes at 150 °C. Afterwards the active layer was spin coated on the substrate as described in chapter 4.4.2.1. There were two different annealing programs used for the thermal treatment in the oven. Under vacuum the substrates were once heated to 200 °C in 7 minutes and held at 200 °C for 15 minutes in the one case and for 30 minutes in the other case in the tube furnace of Hereaus. This corresponds to step 5 in the flow diagram of Figure 42. If this annealing step was applied it is mentioned in the following chapters. The last step before measuring the solar cells was to deposit the Al metal electrodes by evaporation. In some cases the

solar cells underwent another thermal treatment. After measuring the I-V characteristic the solar cells were put on the magnetic stirrer to be heated to 200 °C for 15 minutes as described in chapter 4.4.2.2. If this step was applied it is mentioned as step 9 in the following chapters.
All in all, the assembly of the solar cells built during this work was glass/ITO/PEDOT:PSS/active layer/Al.

4.4.3.1 Effect of solvent, polymer to nanoparticles ratio and filtered solutions

The residue of the $CuInS_2$ nanoparticles, described in chapter 4.2.1, was precipitated in methanol and used for this experiment. The nanoparticles were mixed with the polymer PCDTBT in the ratios of 5:1, 6:1 and 7:1 with a polymer concentration of 5 mg/mL. Those solids were dissolved once in chloroform and the other time with chlorobenzene and stirred for 1 hour at room temperature. In each case two solutions of each concentration was prepared and on the one hand the solutions were filtered and on the other hand they were not filtered. In this experiment the solar cells got annealed as described in chapter 4.4.3 as step 9.

4.4.3.2 Effect of the amount of capping agent

The $CuInS_2$ nanoparticles were mixed with the polymer PCDTBT in a ratio of 6:1 and 7:1 for the polymer concentration of 6 mg/mL and in a ratio 6:1 with a polymer concentration of 5 mg/mL. Consecutively the solutions were stirred for 1 hour at room temperature.

4.4.3.3 Variation of polymer to nanoparticles ratio plus different polymer concentrations and additional thermal treatment

The CIS/polymer suspension was prepared with polymer concentrations of 5 mg/mL, 10 mg/mL and 15 mg/mL. The ratios of the inorganic to organic were for each concentration 5:1, 7.5:1 and 10:1. The solutions were stirred for 2 hours at room temperature. The solar cells got annealed as described in chapter 4.4.3 as step 9.

4.4.3.4 Comparison between non thermal treatment and an annealing step

The suspensions of $CuInS_2$ nanoparticles and polymer were prepared with ratios of 5:1 and 10:1 with a polymer concentration of 5 mg/mL. The $CuInS_2$ nanoparticles were dried under vacuum over night. The solutions were stirred for 2 hours on the magnetic stirrer at room temperature and were put into the ultrasonic bath for 20 minutes.

4.4.3.5 Additional treatment with benzene-1,2-dithiol

For this fabrication of solar cells a solution was prepared with a ratio of 5:1 $CuInS_2$ nanoparticles to polymer and a polymer concentration of 10 mg/mL. The solution were stirred for 15 minutes, then it was put into the ultrasonic bath for 25 minutes and finally were stirred again for 3 minutes. The particles were dried under vacuum conditions over night.

For this experiment solar cells were produced, which underwent a benzene-1,2-dithiol vapour annealing step at different stages in the fabrication process.
The first solar cell was prepared as in chapter 4.4.3 described but without the annealing step number 5. Then the solar cell was measured. After the measurement the solar cell was given into a closed 250 mL glass flask. 30 µL of benzene-1,2-dithiol were put on a little desk, which was placed on the bottom of the vessel. This was necessary in order to avoid the direct contact of the solar cells with the liquid phase. The whole glass vessel was placed on a hot plate, which was pre-heated to 120 °C and the reaction flask was left on there for 20 minutes.[79] Then another I-V characteristic curve was recorded.
The production process of the second solar cell was the same but after the spin coating of the active layer the substrate was given into the glass vessel and underwent the benzene-1,2-dithiol vapour annealing, as described above. Then the evaporation of the Al contacts followed and an I-V characteristic curve was recorded.
Next solar cells were fabricated as described in chapter 4.4.3, in addition with the annealing steps 5. The first solar cell was produced and measured and underwent the benzene-1,2-dithiol treatment as written in the paragraph 3 in this chapter.
Then another solar cell was fabricated but before the benzene-1,2-dithiol treatment the annealing of the active layer was done. Next the I-V characteristic curve was recorded.

4.4.3.6 Addition of benzene-1,2-dithiol

The solution used for the active layer in this experiment, was prepared with a ratio of 5:1 $CuInS_2$ nanoparticles to polymer and a polymer concentration of 10 mg/mL. For this purpose 0.75 mg $CuInS_2$ nanoparticles were dissolved in 720 µL chloroform and stirred over night. 15 mg PSiFDBT polymer were given into 750 µL chloroform and stirred over night. The next day a solution of 1 per mille benzene-1,2-dithiol was prepared. 30 µL of

[79] Wu, Y.; Zhang, G. *Nano Letters* **2010**, 10, 1628-1631

this solution were added to the nanoparticles solution and stirred for further 15 minutes. Then the solutions were combined.
Afterwards with this solution solar cells, which underwent no thermal treatment or the annealing steps, a described in chapter 4.4.3 and indicated as step 5,were fabricated.
For the comparison solar cells were fabricated without the addition of benzene-1,2-dithiol in the solution for the active layer.

4.4.3.7 Modified nanoparticles

The CIS/Polymer solution was prepared with a ratio of 10:1 and a polymer concentration of 5 mg/mL. The calculated amounts of $CuInS_2$ nanoparticles as well as the polymer were put into a vial. Then half of the total solution volume was given to the nanoparticles and the other half to the polymer. The solutions were stirred over night and the next day they were combined.
In this experiment the nanoparticles, which were treated with the hexanoic acid as mentioned in chapter 4.3.2, were used for the preparation of the solution for the active layer. In addition the nanoparticles which were modified by tetrahydrothiophen as described in chapter 4.3.4, were applied for the other set of solar cells. For the comparison solar cells with the nanoparticles, which were not modified, were produced.

4.4.3.8 Solvent mixtures

A ratio of 7.5:1 $CuInS_2$ nanoparticles to polymer was used with a polymer concentration of 5 mg/mL. The solutions were prepared with solvent mixture consisting of chloroform and chlorobenzene, whereby the polymer was stirred over night with the right amount of chlorobenzene and the nanoparticles were stirred with the correct amount of chloroform, which was used to create the mixtures. The implemented ratios for this experiment were 1:1, 3:1 and 5:1 of chloroform to chlorobenzene. The next day the solutions were combined and stirred for further 30 minutes. Moreover, a solution, which can serve as reference was prepared with the same ratio and polymer concentration as mentioned and chloroform as a solvent.
The solar cells only underwent the annealing step of heating to 200 °C in 7 minutes and holding of 200 °C for 15 minutes.

4.4.4 Measuring and characterization

4.4.4.1 I-V characterization

In order to characterize the solar cells generally the first step is to record an I-V curve. The solar cells were measured under argon atmosphere in the glove box. A Keithley

2400 source meter was used. While working on this master thesis the lamps were modernized and so two different lamps were used for measuring. The illumination was provided through a borosilicate glass window at the bottom of the glove box by either a halogen lamp (250W, 24V) or a Dedolight 400D. The light had an intensity of 100 mW/cm^2. For the characterization and the resulting calculations the I-V characteristics were recorded under illuminated and dark conditions. The analysis was done by a MS Excel evaluation programm written by Christopher Fradler.

4.4.4.2 Profilometer

The profilometer was a Veeco Dektak 150+ Surface. It was used to measure the film thickness and roughness.

4.4.4.3 Light microscopy

The microscope pictures were taken with an Olympus BX60F5 light microscope in combination with an Olympus E520 digital camera.

5 Conclusion

Within this work the synthesis of $CuInS_2$ nanoparticles was optimized, the surface of the particles was modified and the effects on the performance of nanocomposite solar cells were investigated. This type of solar cell consists of a material combination of organic, conjugated polymers and inorganic nanoparticles, which reveals several advantages. The optical and electronic properties of the nanoparticles, which act as the acceptor phase, can be tuned by the size and shape. In addition the nanoparticles contribute to the absorption of light and higher current densities are expected compared to fullerene/polymer solar cells. $CuInS_2$ nanoparticles provide a high absorption coefficient and a band gap of 1.5 eV, which made this material so interesting as acceptor material.

In the first part the focus was set on the synthesis of $CuInS_2$ nanoparticles, a promising material for the incorporation into solar cells. The emphasis was put on the fabrication of nanoparticles with a narrow size distribution and a homogenous crystal modification, in order to see their influence on the performance when they were incorporated into a solar cell. For all nanoparticles fabricated for this work one main procedure was applied. The particles were prepared with a colloidal solvent reaction. As to produce $CuInS_2$ nanoparticles, with the desired properties, various reaction times as well as different sulfur sources were tested. Moreover the influence of purity of the solvent/capping agent oleylamine was investigated.

When comparing the synthesises of the $CuInS_2$ nanoparticles it is notable, that the use of oleylamine with a technical grade of 70%, as it is commercially available, and elementary sulfur with reaction times under 1 hour lead to mixture of the crystal modifications chalcopyrite and wurtzite. Additionally a broad size distribution was observed. In further experiments the influence of the reaction time was tested. XRD measurements showed that prolonged reaction times lead favourably to chalcopyrite as crystal modification, due to its thermodynamically stability. The size distribution was narrowed as well.

However, out of the reason that Cu and In are randomly distributed in the plane lattice of the wurtzite which would provide the possibility to tune the bandgab, it was tried to synthesis $CuInS_2$ nanoparticles with the wurtzite modification. Therefore a different the reaction times were shortened in order to obtain wurtzite as it is the kinetically favoured crystal modification.

Finally it was found that the use of purified oleylamine as a capping agent similarly thiourea as a sulfur source lead to a narrow size distribution and primarily to wurtzite as crystal modification. After 20 minutes particles with a size between 13-16 nm were obtained. The positive influence on the formation of the particles was attributed to the progressively decomposition of thiourea and the purity of the distilled oleylamine. Figure 44 shows the TEM image of these $CuInS_2$ nanoparticles. The particles obtained from this synthesis were mainly used for the incorporation into solar cells as well as for the experiments of the surface modification.

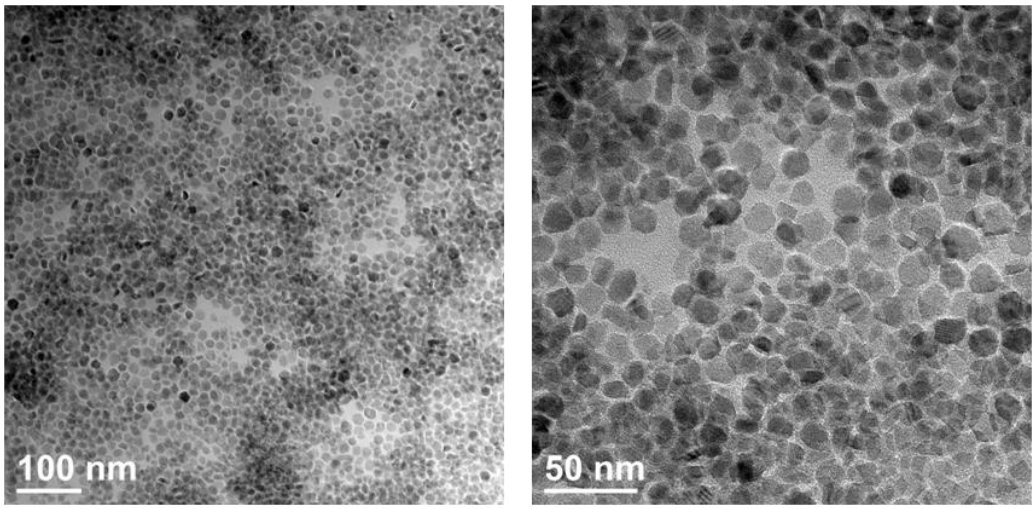

Figure 44 TEM images of $CuInS_2$ nanoparticles with pure wurtzite as crystal modification, prepared with distilled oleylamine and thiourea, obtained after 20 minutes reaction time,

In the following part the surface of the nanoparticles was modified. Based on the knowledge that with the use of a capping agent advantages and disadvantages come along, the aim of the experiment was to modify the surface of the nanoparticles towards a better performance when incorporated in solar cells.

In the first step size selective precipitation was used as a powerful tool to decrease the initially broad size distribution of the nanoparticles. In order to reduce the electrical isolating capper sphere, necessary to prevent the agglomeration of the particles, an acid treatment was applied. DLS and TGA measurements revealed the successful use of this strategy as the amount of capping agent was significantly reduced. However, this procedure also leads to the formation of agglomerates, indicating the need for the right balance. The third strategy involved an exchange of the capping agent with more suitable molecules in this case pyridine and tetrahydrothiophene. Most important was to find a compromise between exchaniging enough capping agent to improve the properties of the surface but nevertheless not to remove too much of the long bulky capping agent to prevent the particles from agglomeration. Unfortunately, in the case of

pyridine the balance for the exchange of the oleylamine could not be found. For further optimization, the amount of pyridine as well as the reaction time can be reconsidered.

A major part of the $CuInS_2$ nanoparticles were used for the fabrication of the solar cells. Poly[[9-(1-octylnonyl)-9H-carbazole-2,7-diyl]-2,5-thiophenediyl-2,1,3-benzothiadiazole-4,7-diyl-2,5-thiophenediyl] (PCDTBT) and poly[2,1,3-benzothiadiazole-4,7-diyl-2,5-thiophenediyl(9,9-dioctyl-9H-9-silafluorene-2,7-diyl)-2,5-thiophenediyl (PSiFDBT) served as donor materials. In order to optimize the performance of the solar cells various inorganic and organic concentrations, annealing steps and solvent mixtures were investigated. The impact of various parameters was observed such as capper, solvent, temperature, modified surfaces of nanoparticles and chemical vapour annealing. The most promising results were obtained when treating the substrates with an annealing step of 15 minutes in the tube furnace and using solvent mixtures of chloroform and chlorobenzene.

It was shown that annealing of the solar cells resulted in an increase of the efficiency due to the removal of oleylamine from the surface of the nanoparticles and consequently a reduction of the electric barrier took place. As a consequence the charge transfer is facilitated and the short circuit current increased.

Moreover it was found that an annealing time of 30 minutes did not enhance the performance compared to an annealing time of 15 minutes regarding the efficiency. This could be a result of an agglomeration of the nanoparticles due to a longer time for diffusion of the nanoparticles and a reduced capping sphere, which cannot interfere with the tendency of agglomeration. Additionally the decline in performance can also be caused by the starting decomposition of the polymer.

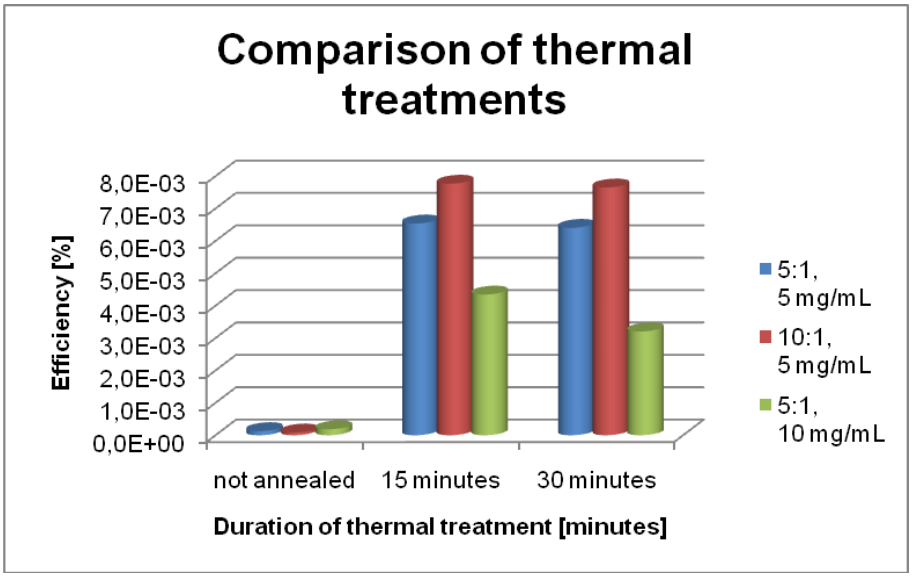

Figure 45 Influence of the annealing time on the efficiency of solar cells

The improvement seen when using the solvent mixture of chloroform and chlorobenzene can be based on enhancing the morphology in the active layer. One possibility to explain this circumstance is that chlorobenzene has a higher boiling point than chloroform, thus it vaporizes slower and as a consequence the nanoparticles have more time to diffuse and disperse through the polymer network. The polymer chains undergo further crystallization and arrange themselves in the active layer. This effect can go hand in hand with the possibility that the layer thickness was more suitable for the solar cells. In order to optimize the performance of the solar cell further investigations of the optimization of the layer thickness as well as the morphology have to be made.

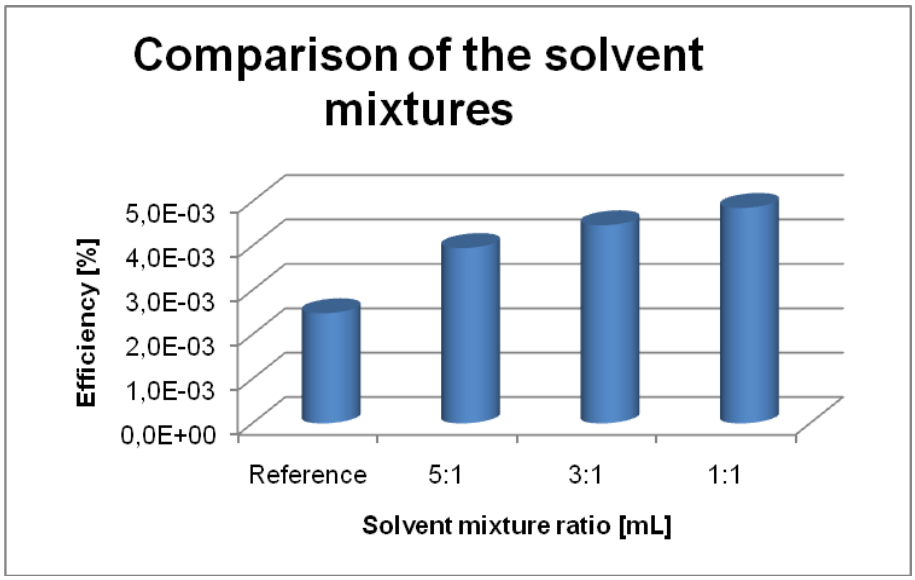

Figure 46 Efficiency of the solar cell as a function of solvent mixture ratios

6 Appendix

6.1 List of abbreviations

a.u.	Arbitrary units
BHJ	Bulk heterojunction
CIS	Copper indium disulfide
d	Film thickness
DLS	Dynamic light scattering
E_{ex}	Exciton energy
eq.	Equivalents
EQE	External quantum efficiency
eV	Electron volt
FF	Fill factor
FTIR	Fourier transform infrared spectroscopy
HOMO	Highest occupied molecule orbital
HS	Hexanoic acid
I	Current
I_{mpp}	Circuit at the maximum power point
IPCE	Incident photon to current efficiency
I_{SC}	Short circuit current
ITO	Indium tin oxide
K	Shape factor
LUMO	Lowest unoccupied molecule orbital
P3HT	Poly(3-hexylthiophene-2,5-diyl)
PCBM	[6,6]-Phenyl C61 butyric acid methyl ester
PCDTBT	Poly[[9-(1-octylnonyl)-9H-carbazole-2,7-diyl]-2,5-thiophenediyl-2,1,3-benzothiadiazole-4,7-diyl-2,5-thiophenediyl]
PSiFDBT	Poly[2,1,3-benzothiadiazole-4,7-diyl-2,5-thiophenediyl(9,9-dioctyl-9H-9-silafluorene-2,7-diyl)-2,5-thiophenediyl

PEDOT:PSS	Poly(3,4-ethylenedioxythiophene) : poly(styrenesulfonate)
P_{in}	Incident light power
P_{max}	Maximum power point
T	Temperature
TAA	Thioacetamide
TEM	Transmission electron microscopy
THT	Tetrahydrothiophene
V	Voltage
V_{mpp}	Voltage at the maximum power point
V_{OC}	Open circuit voltage
XRD	X-ray diffraction
η	Efficiency
η_e	Power conversion efficiency
η_A	Photon absorption efficiency
$\eta_{dif}f$	Exciton diffusion yield
η_{diss}	Exciton dissociation yield
η_{tr}	Charge carrier transport yield
η_{cc}	Charge carrier yield
θ	Angle (X-ray diffraction)
λ	Wavelength
σ	Standard deviation

6.2 List of Tables

6.3 List of Figures